



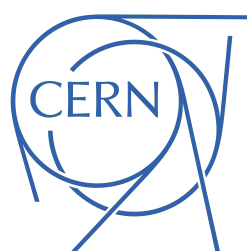
Monte Carlo Study of TeV-Scale String Resonances in Photon-Jet Scattering Events at the LHC

by

Kyle Drury

Supervised by Dr. Douglas Gingrich

A research report presented for NSERC 2023



Department of Physics and Astronomy
The University of Alberta
Canada
2023/08/09

Abstract

We conduct a Monte Carlo study with STRINGS and Pythia for evidence of low TeV-scale string resonances in $gg \rightarrow g\gamma$ and $gq \rightarrow q\gamma$ subprocesses on the order of a few TeV. If the extra compacted spatial dimensions predicted by string theory are sufficiently large, then the fundamental string scale M_s will also be on the order of a few TeV, energy levels attainable by the Large Hadron Collider (LHC) at CERN. Proton-proton (pp) collisions producing string resonances are simulated with STRINGS and Pythia using center-of-mass energies $\sqrt{s} = 13.0$ and 13.6 TeV. We probe string scales $M_s = [5.0, 7.0]$ TeV in 0.5-TeV steps. The Monte Carlo samples produced in this study can be used for photon-jet scattering resonance searches with ATLAS at the LHC.

Contents

1	Introduction	3
2	STRINGS Validation	4
2.1	Differential Cross Sections	4
2.2	Cross-section as a Function of M_s	6
3	STRINGS MC Sample Generation	9
3.1	String Scale Selection	9
3.2	Sample Generation & Validity Testing	12
4	Analysis	12
4.1	Kinematic Data	12
4.2	Angular Distribution Study	16
4.3	Pythia Samples	17
5	Conclusions	20
6	Sources	21
7	Appendices	22
7.1	Strong Coupling Testing	22
7.2	Differential Cross-sections	23
7.2.1	$M_s = [1, 4]$ TeV (gg scattering only)	23
7.2.2	$M_s = [7, 9]$ TeV	24
7.2.3	$M_s = [5, 7]$ TeV	26
7.3	Kinematic Data Histograms	28
7.3.1	$\sqrt{s} = 13$ TeV, $M_s = 5$ TeV	28
7.3.2	$\sqrt{s} = 13$ TeV, $M_s = 5.5$ TeV	31
7.3.3	$\sqrt{s} = 13$ TeV, $M_s = 6.0$ TeV	34
7.3.4	$\sqrt{s} = 13$ TeV, $M_s = 6.5$ TeV	37
7.3.5	$\sqrt{s} = 13$ TeV, $M_s = 7.0$ TeV	40
7.3.6	$\sqrt{s} = 13.6$ TeV, $M_s = 5.0$ TeV	43
7.3.7	$\sqrt{s} = 13.6$ TeV, $M_s = 5.5$ TeV	46
7.3.8	$\sqrt{s} = 13.6$ TeV, $M_s = 6.0$ TeV	49
7.3.9	$\sqrt{s} = 13.6$ TeV, $M_s = 6.5$ TeV	52
7.3.10	$\sqrt{s} = 13.6$ TeV, $M_s = 7.0$ TeV	55
7.4	Pythia Kinematic Data	58
7.4.1	$M_s = 5$ TeV, $\sqrt{s} = 13$ TeV	58
7.4.2	$M_s = 5.5$ TeV, $\sqrt{s} = 13$ TeV	59
7.4.3	$M_s = 6$ TeV, $\sqrt{s} = 13$ TeV	60
7.4.4	$M_s = 6.5$ TeV, $\sqrt{s} = 13$ TeV	61
7.4.5	$M_s = 7$ TeV, $\sqrt{s} = 13$ TeV	62
7.4.6	$M_s = 5$ TeV, $\sqrt{s} = 13.6$ TeV	63
7.4.7	$M_s = 5.5$ TeV, $\sqrt{s} = 13.6$ TeV	64
7.4.8	$M_s = 6$ TeV, $\sqrt{s} = 13.6$ TeV	65
7.4.9	$M_s = 6.5$ TeV, $\sqrt{s} = 13.6$ TeV	66
7.4.10	$M_s = 7$ TeV, $\sqrt{s} = 13.6$ TeV	67
7.5	Figures & File Organization on Local Cluster	68

1 Introduction

The Standard Model (SM) of particle physics is the most successful theory explaining observed phenomena in the universe. According to the SM, all fundamental particles are zero-dimensional points that can be broken into several categories according to their characteristics. Fermions (quarks or leptons) constitute ‘matter,’ Bosons, which can be scalar or vectorial in nature, are responsible for mediating the interactions between the fermions.

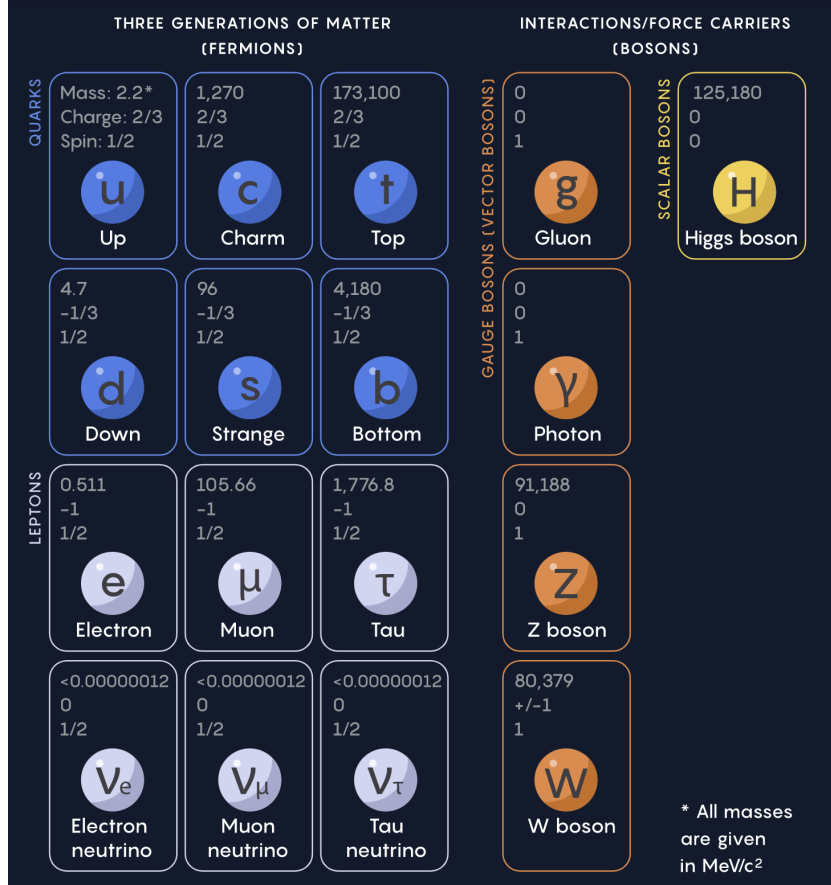


Figure 1: The current standard model [1]

The SM is lacking in some areas and fails to satisfy outstanding issues such as the Hierarchy problem [2]. String theory is a proposed framework that grapples with these issues by describing the fundamental particles of the SM in terms of one-dimensional strings. These strings may be open or closed, and interact with each other in ten-dimensional spacetime.

If the six unperceived spatial dimensions are sufficiently large, the scale of the interactions between strings (the string scale) M_s should be on the order of a few TeV. By using the Large Hadron Collider (LHC) at CERN to study pp collisions and the generated string resonances, we can determine if these interactions are being driven by theories predicted by the SM or low-scale string theory. For this project, we focus on observing single-parton scattering processes, which can either be $gg \rightarrow g\gamma$, or $gq \rightarrow q\gamma$. These interactions manifest at the LHC as $\gamma + \text{jet}$.

In section 2, we derive the fundamental string scale M_s and show that it may be on the order of a few TeV. We validate the STRINGS Monte Carlo Event generator in section 3 by comparing some generated data to previously established literature. In section 4, we make our string scale selection by plotting the number of events produced in LHC runs at CERN. We generate STRINGS samples and analyze the data, and then generate Pythia samples in section 5. Conclusions are made in section 6. Sources are in section 7, and appendices can be found in section 8.

2 STRINGS Validation

2.1 Differential Cross Sections

We would like to compare the cross-sections of dijet scattering processes with photon-jet scattering events produced by STRINGS. For this, we refer to [3]:

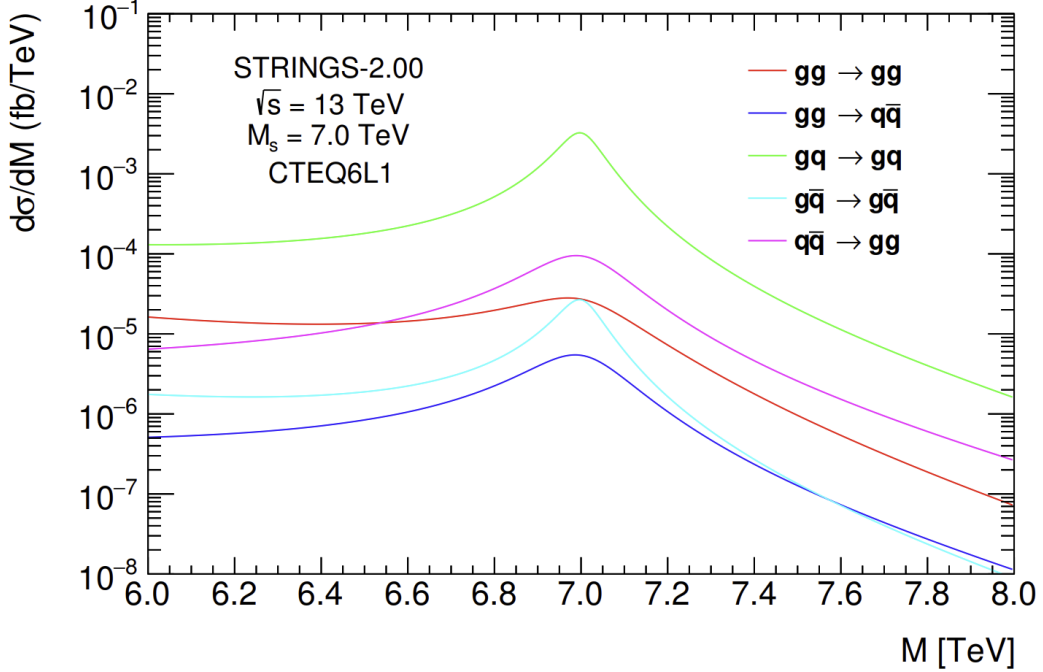


Figure 2: Differential cross-sections for diparton (below) scattering events for $M = [6,8]$ TeV

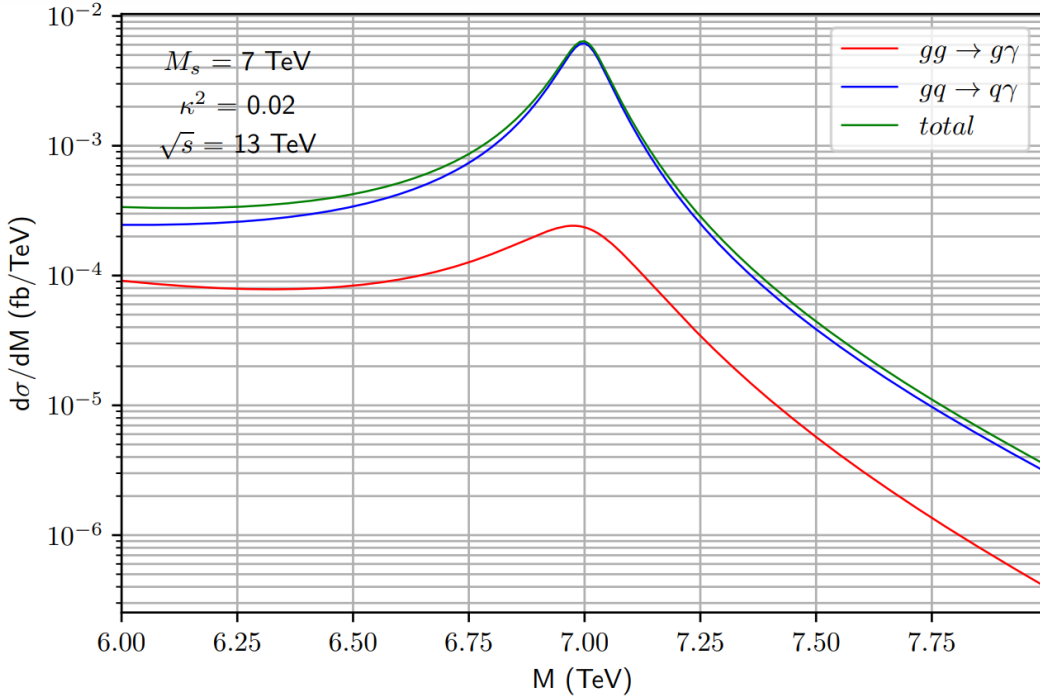


Figure 3: Differential cross-sections for single parton (above) scattering events for $M = [6,8]$ TeV

To validate the differential cross-section curve we have produced, we refer to [4]:

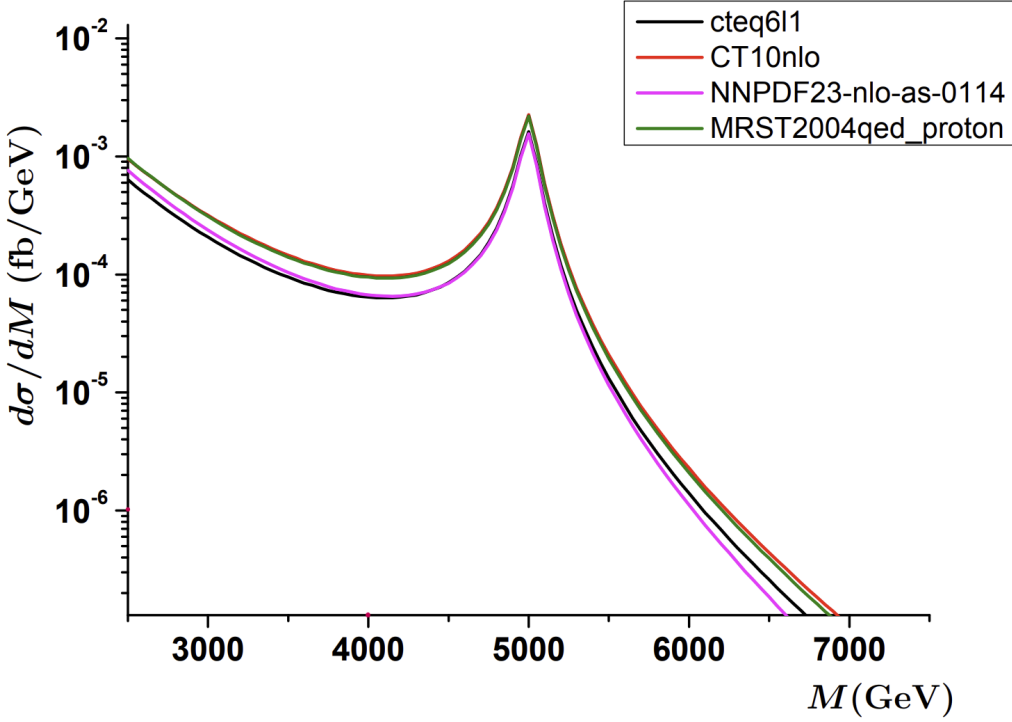


Figure 4: Differential cross-sections of single parton scattering events at $M_s = 5$ TeV

[4] uses some parameters that are different than ours. They have $\sqrt{s} = 14$ TeV, $\alpha_s = 0.1$, and concatenated widths rather than functions of g_s and M_s . They use $M = [2500, 6720]$ GeV.

$$\Gamma_{g^*}^{J=0} = 75 \frac{M_s}{\text{TeV}} \text{GeV} \quad \Gamma_{g^*}^{J=2} = 45 \frac{M_s}{\text{TeV}} \text{GeV} \quad \Gamma_{q^*}^{J=\frac{1}{2}} = 37 \frac{M_s}{\text{TeV}} \text{GeV} \quad \Gamma_{q^*}^{J=\frac{3}{2}} = 19 \frac{M_s}{\text{TeV}} \text{GeV} \quad (1)$$

Various attempts were made at reproducing these results. The plots are located on the CERN UofA Local Cluster and have the following filenames:

	Cross-section Plot	Ratio Plot
running coupling, pre-fix	runCoup_preFix_cross.png	runCoup_preFix_ratio.png
running coupling, post-fix	runCoup_postFix_cross.png	runCoup_postFix_ratio.png
coupling = 0.1, pre-fix	01Coup_preFix_cross.png	01Coup_preFix_ratio.png
coupling = 0.1, post-fix	01Coup_postFix_cross.png	01Coup_postFix_ratio.png
running coupling, concatenated, pre-fix	concat_preFix_cross.png	concat_preFix_ratio.png
running coupling, concatenated, post-fix	concat_postFix_cross.png	concat_postFix_ratio.png

Table 1: Cross-section Validation Plot File Names

By using small dots in the last two plots, we observe that the $\pm \sim 0.05$ fluctuations on either side of the peak are due to the data collected from Anchordoqui et al (pink) moving in a step-like fashion. This is a result of linear interpolation of the original points. Agreement at the peak is the best when concatenated widths are used

To see if a better agreement may be reached, we will attempt to recreate the curve using several different α_s coupling values, and then scaling by an appropriate factor to get the peaks to match. These plots are shown in Appendix 7.1.

The best results were achieved using a coupling of 0.1, and scaling the data by a factor of exactly 0.5278861221857577. On the left side of the peak, the error is about -15%, and on the right, +15%;

an even spread. Going lower than 0.1 causes the left side of the ratio plot to fall below the 0.85 mark, and going above causes the right side to rise above the 1.15 mark. Using coupling=0.1 is a 'happy medium,' and also demands a scale factor closest to $\frac{1}{2}$ than all the options.

Due to the scale factor, in strings.py we divide `Msq` by ~ 2 in order to adhere as closely as possible to Achordoqui et al.

2.2 Cross-section as a Function of M_s

We would also like to reproduce the results in [5], which communicates the gg cross-section for $M_s = [1,4]$ TeV:

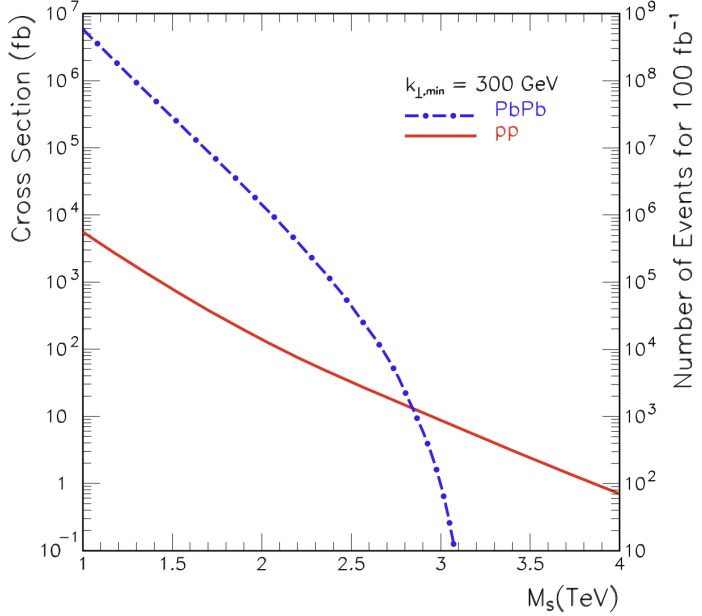


Figure 5: Cross-section vs. M_s from Anchordoqui et al

The only problem is that the region of integration is unknown. In other words, the minimum and maximum mass are not known. If $k_{\perp,\min} = 300$ GeV, then the minimum invariant mass can be derived from the following equation:

$$k_{\perp} = \frac{M}{2 \cosh y} \quad (2)$$

This equation gives $M_{low, cut} \sim 3334$ GeV. If we plot the cross-sections for string scales [1, 4] TeV by integrating over $M = [3334, 14000]$ GeV, the following plot is generated:

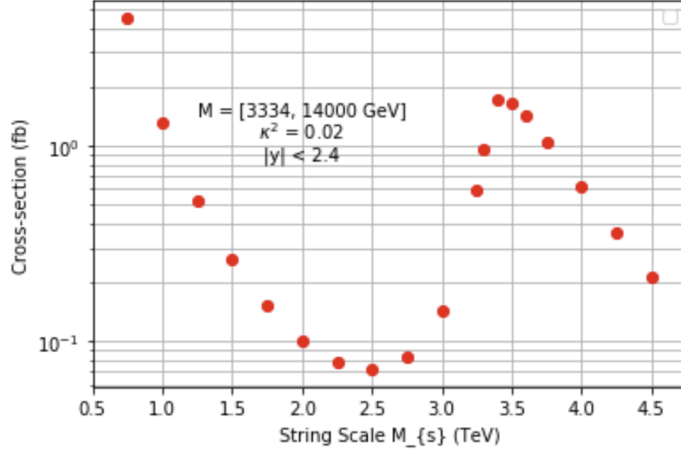


Figure 6: Cross-section of the gg subprocess (red) as a function of string scale M_s for $M = [3334, 14000]$ GeV.

This plot is problematic because there is a spike at $M_s = 3334$ GeV, due to the lower cut on the invariant mass also being 3334 GeV. As such, we ignore the parameter $k_\perp = 300$ GeV. We plot cross-sections of string scales from 1 TeV to 14 TeV in 1-TeV-steps over an invariant mass interval of $[1, 14]$ TeV. The following plot is generated:

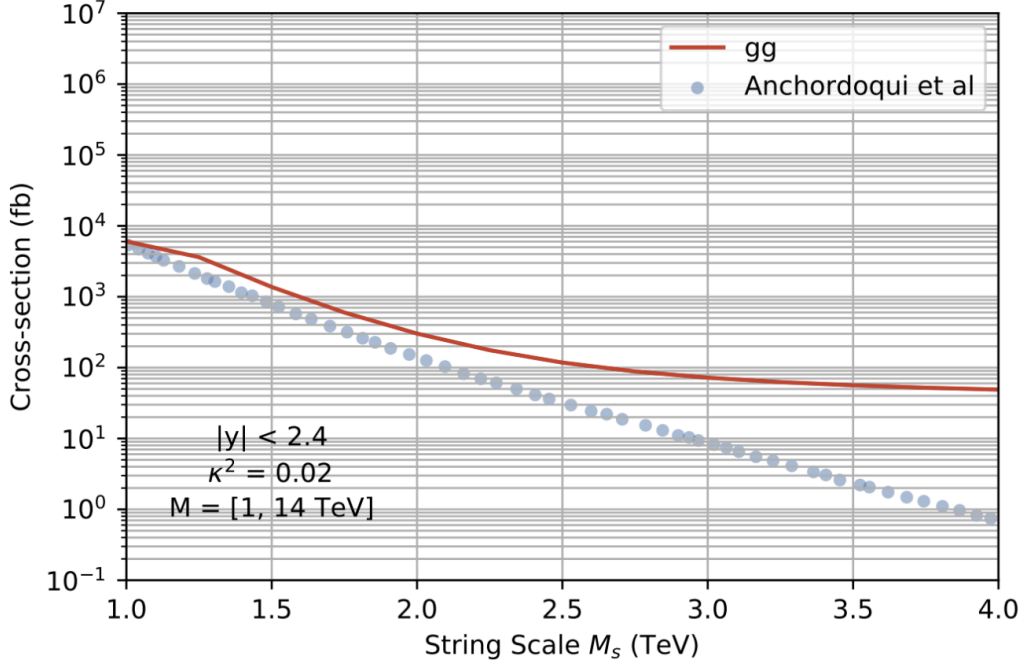


Figure 7: Cross-section of the gg subprocess (red) as a function of string scale M_s .

The plot from Fig 14 doesn't drop quickly enough; the region of integration is too large. It appears that we must choose an alternative for the invariant mass window that isn't as broad as $[1, 14]$ TeV (see Appendix 7.2.1).

Using $M = [M_{lowcut}, 14\text{TeV}]$ produces the most desirable results:

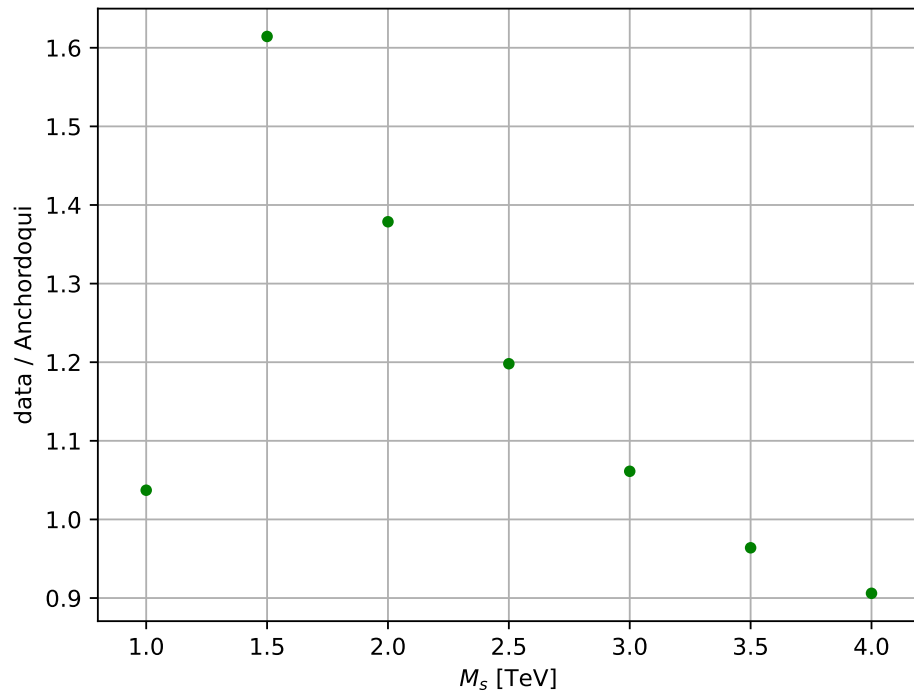
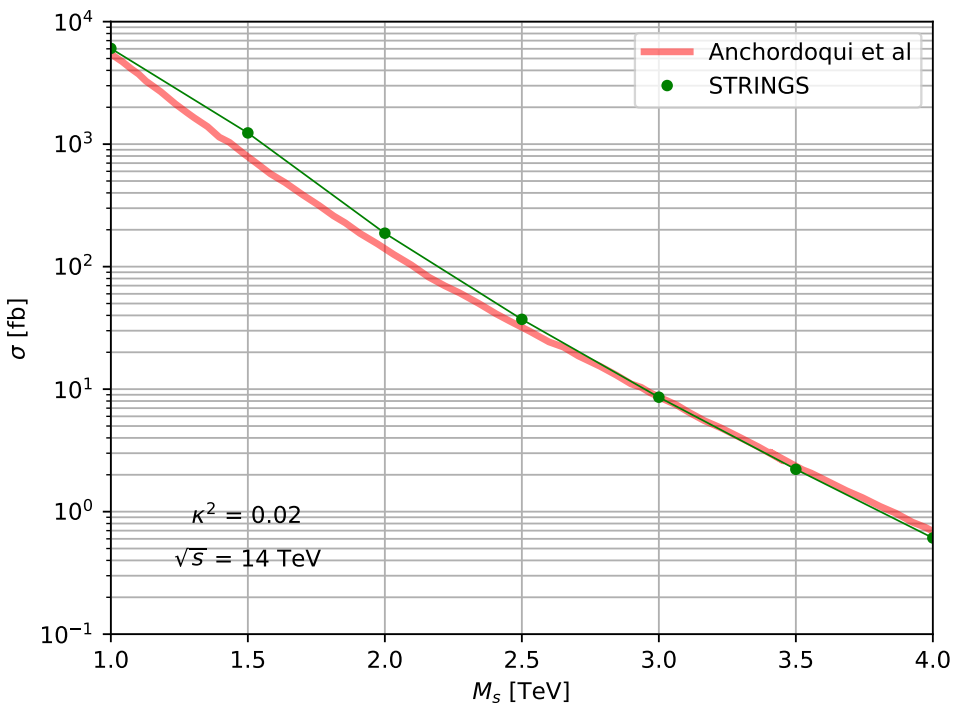


Figure 9: Ratio plot for M_s vs σ

All of the data points fall within 20% error with the exception of $M_s = 1.5, 2$. However, it appears that at higher string scales, the error is poised to reach an asymptote in the low negative percentages. This is acceptable.

3 STRINGS MC Sample Generation

3.1 String Scale Selection

On the order of a few TeV, it is important that our choice of string scales provides enough events for us to analyze. We begin by looking at the differential cross-sections for $M_s = [7, 9]$ TeV (Appendix 8.3.1). For $\sqrt{s} = 13$ TeV, and another for $\sqrt{s} = 13.6$ TeV, separate plots will be made. The region of integration is $M = [M_{cut}, \sqrt{s}]$

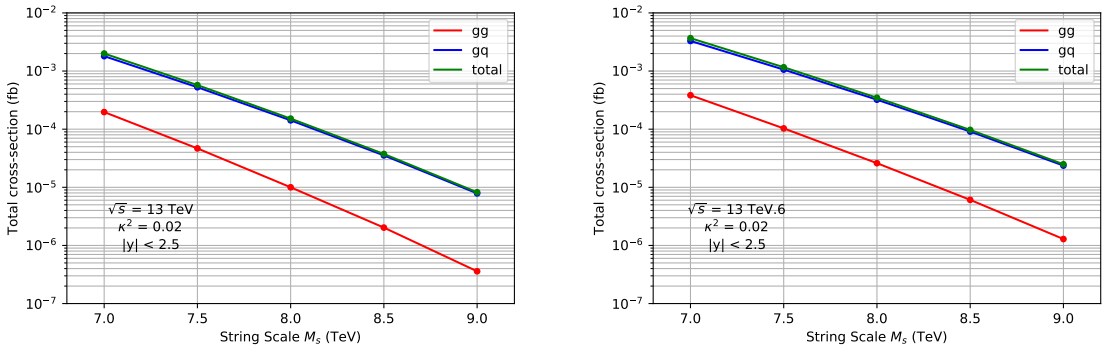


Figure 10: σ vs M_s , $M = [M_{cut}, \sqrt{s}]$

We can plot the number of events as a function of the string scale with the following formula:

$$N = 140\sigma_{13} + 115\sigma_{13.6} \quad (3)$$

where σ_i represents the cross-section for $M_s = i$ TeV.

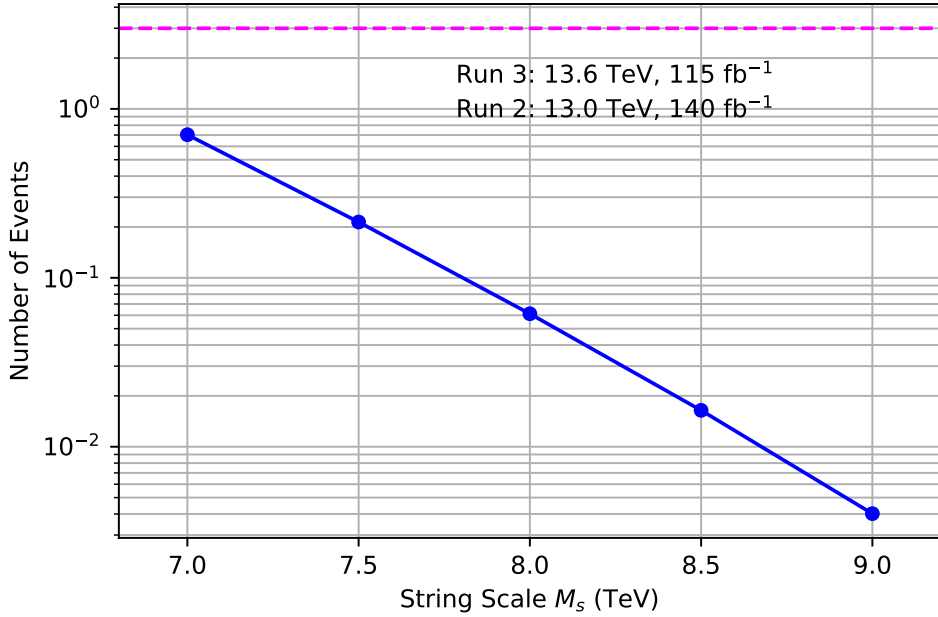


Figure 11: Number of events vs. M_s , $M_s = [7, 9]$ TeV

All the data points are far too low on the y-axis, so more events will need to be produced. The same process but for $M_s = [5, 7]$ TeV rather than $[7, 9]$, the σ plots for which are in Appendix 8.3.2.

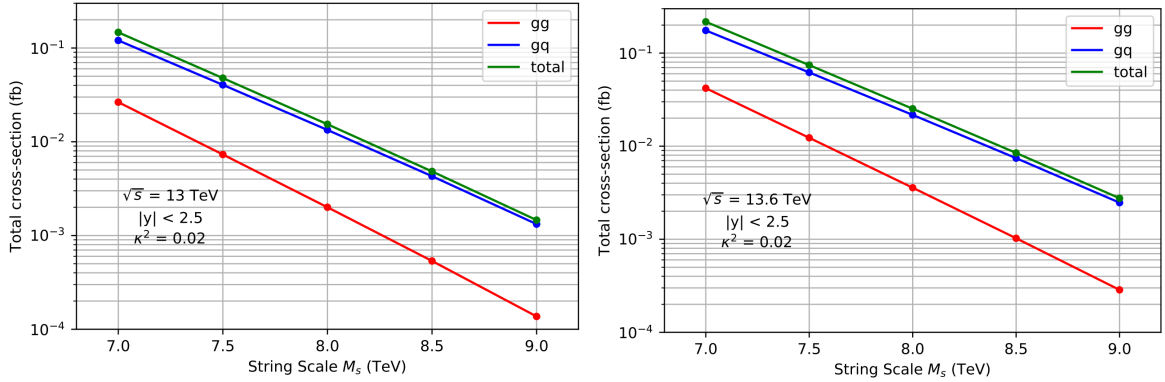


Figure 12: σ vs M_s , $M = [M_{cut}, \sqrt{s}]$

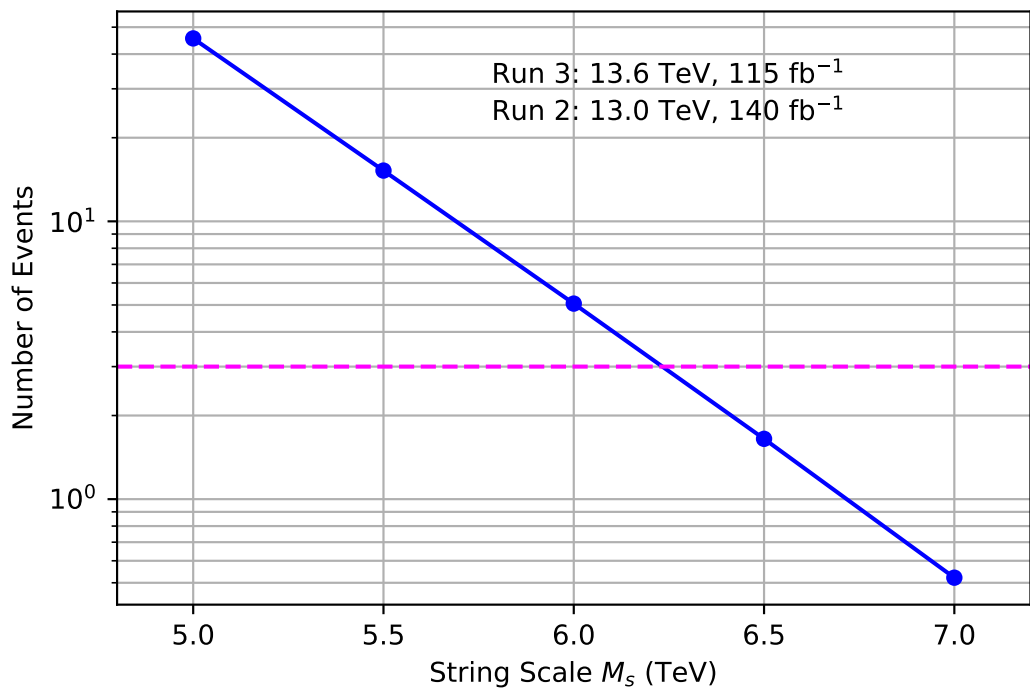


Figure 13: Number of events vs. M_s , $M_s = [5, 7]$ TeV. Note that 3 data points are located above $y=3$.

We now have 3 data points above the $y = 3$ line, meaning that we will be able to observe 95% of the scattering events at the LHC at these string scales.

3.2 Sample Generation & Validity Testing

The events generated in these MC samples are either gg or gq jet + photon scattering events. At different string scales and \sqrt{s} , the portions of scattering events that are gg and gq change:

	$M_s = 5 \text{ TeV}$	$M_s = 5.5 \text{ TeV}$	$M_s = 6 \text{ TeV}$	$M_s = 6.5 \text{ TeV}$	$M_s = 7 \text{ TeV}$
$gg \rightarrow g\gamma$	18.010%	15.310%	13.028%	11.737%	9.3811%
$gq \rightarrow q\gamma$	81.990%	84.680%	86.972%	88.263%	90.618%

Table 2: Event fractions for $\sqrt{s} = 13 \text{ TeV}$

	$M_s = 5 \text{ TeV}$	$M_s = 5.5 \text{ TeV}$	$M_s = 6 \text{ TeV}$	$M_s = 6.5 \text{ TeV}$	$M_s = 7 \text{ TeV}$
$gg \rightarrow g\gamma$	19.319%	16.564%	14.172%	12.128%	10.367%
$gq \rightarrow q\gamma$	80.681%	83.436%	85.828%	87.872%	89.633%

Table 3: Event fractions for $\sqrt{s} = 13.6 \text{ TeV}$

It is important to be confident that the actual number of gg and gq events being generated are proportional to the cross-sections of the two processes. For example, if the gg cross-section makes up 30% of the total cross-section for a certain invariant mass window, then 30% of the events generated should be gg . The differential cross-section is integrated in quadrature and with Monte Carlo integration.

Events Generated	Quadrature (gg, gq)	MC (gg, gq)	Event Fraction (gg, gq)
11,000	17.999%, 82.001%	17.931%, 82.069%	18.010%, 81.990%
150,000	—	17.981%, 82.019%	18.006%, 81.994%

Table 4: Proportion of cross-section and generated events for the gg and gq processes. Cross-section integrated over $M = [M_{cut}, \sqrt{s}]$, $\sqrt{s} = 13 \text{ TeV}$, $M_s = 5 \text{ TeV}$

4 Analysis

4.1 Kinematic Data

In the produced $\gamma + \text{jet}$ events, there are several kinematic quantities the outgoing partons possess that are of interest. In no particular order, they are; the 4-vectors of each outgoing particle, the transverse momentum p_T , the radial and azimuthal coordinates θ and ϕ , and the invariant mass. When the parton and photon quantities are summed, we get the characteristics of the string resonance. Histograms that convey this data are shown in Appendix 7.3.

On the next pages are histograms that have been created by superimposing each $\gamma + \text{jet}$ invariant mass histogram for $\sqrt{s} = 13 \text{ TeV}$ and 13.6 TeV .

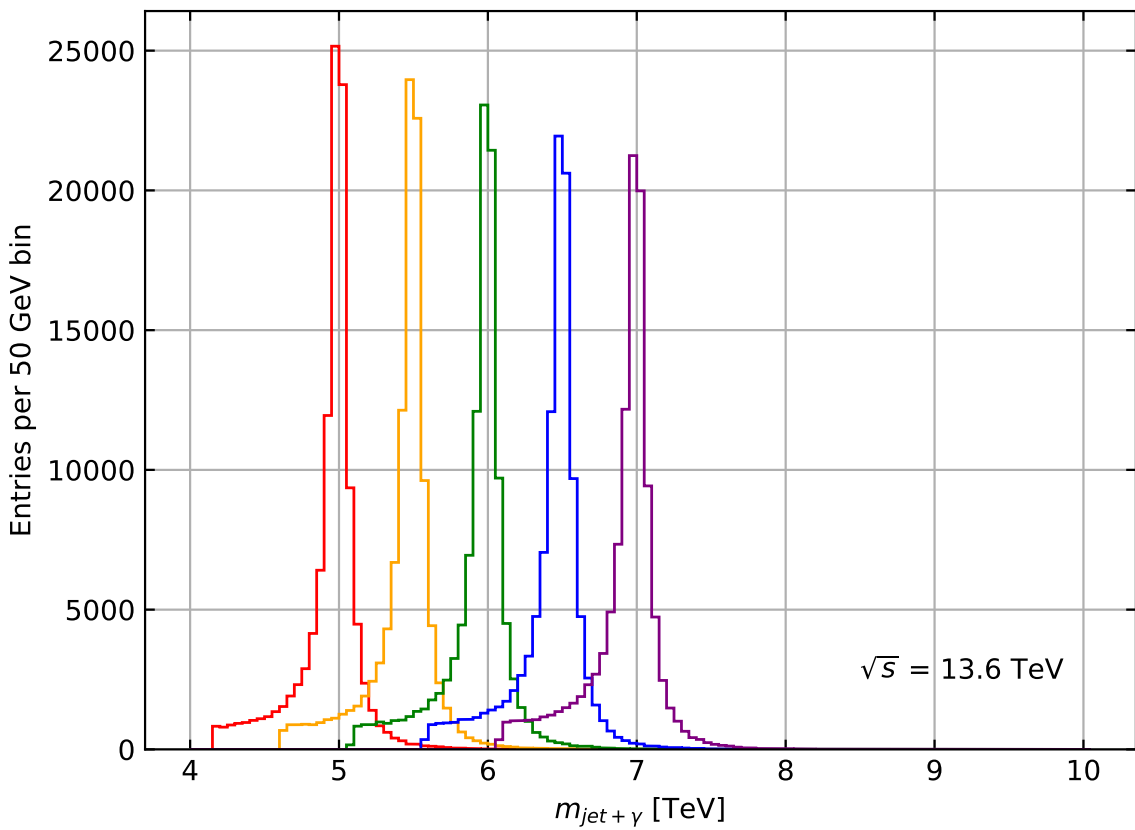
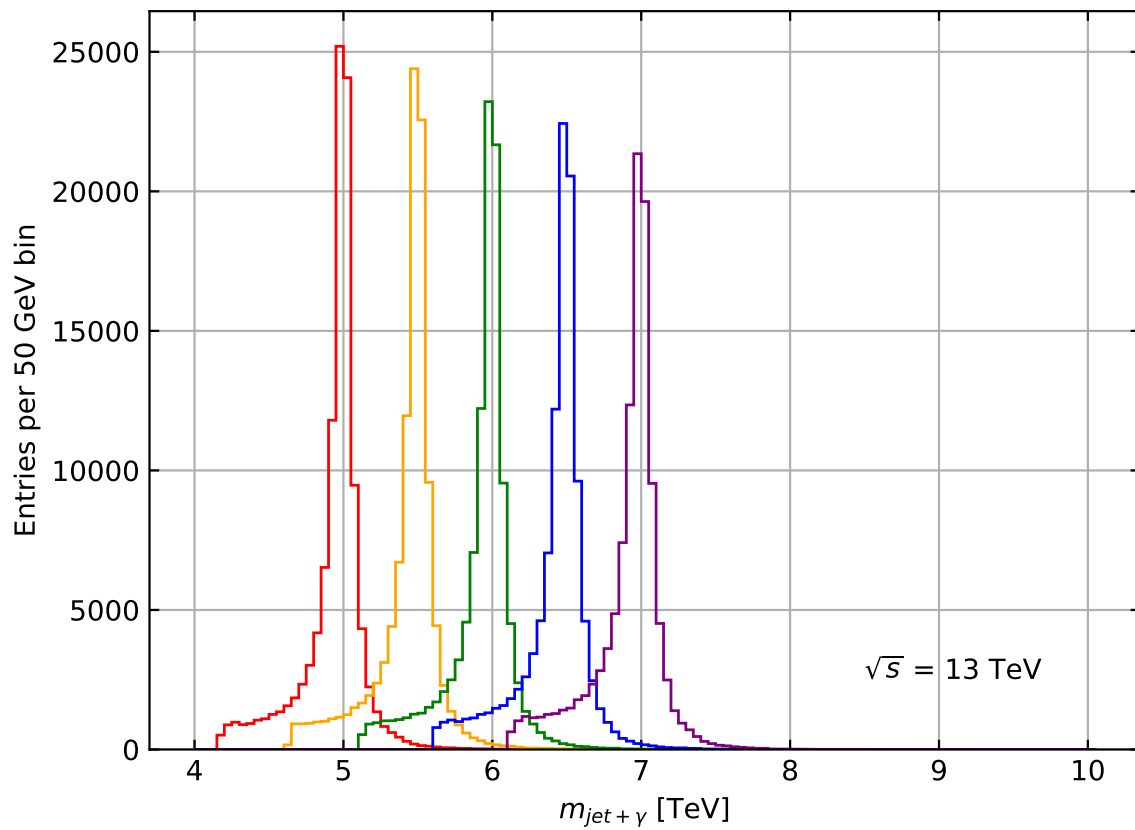


Figure 14: (Linear Axis)

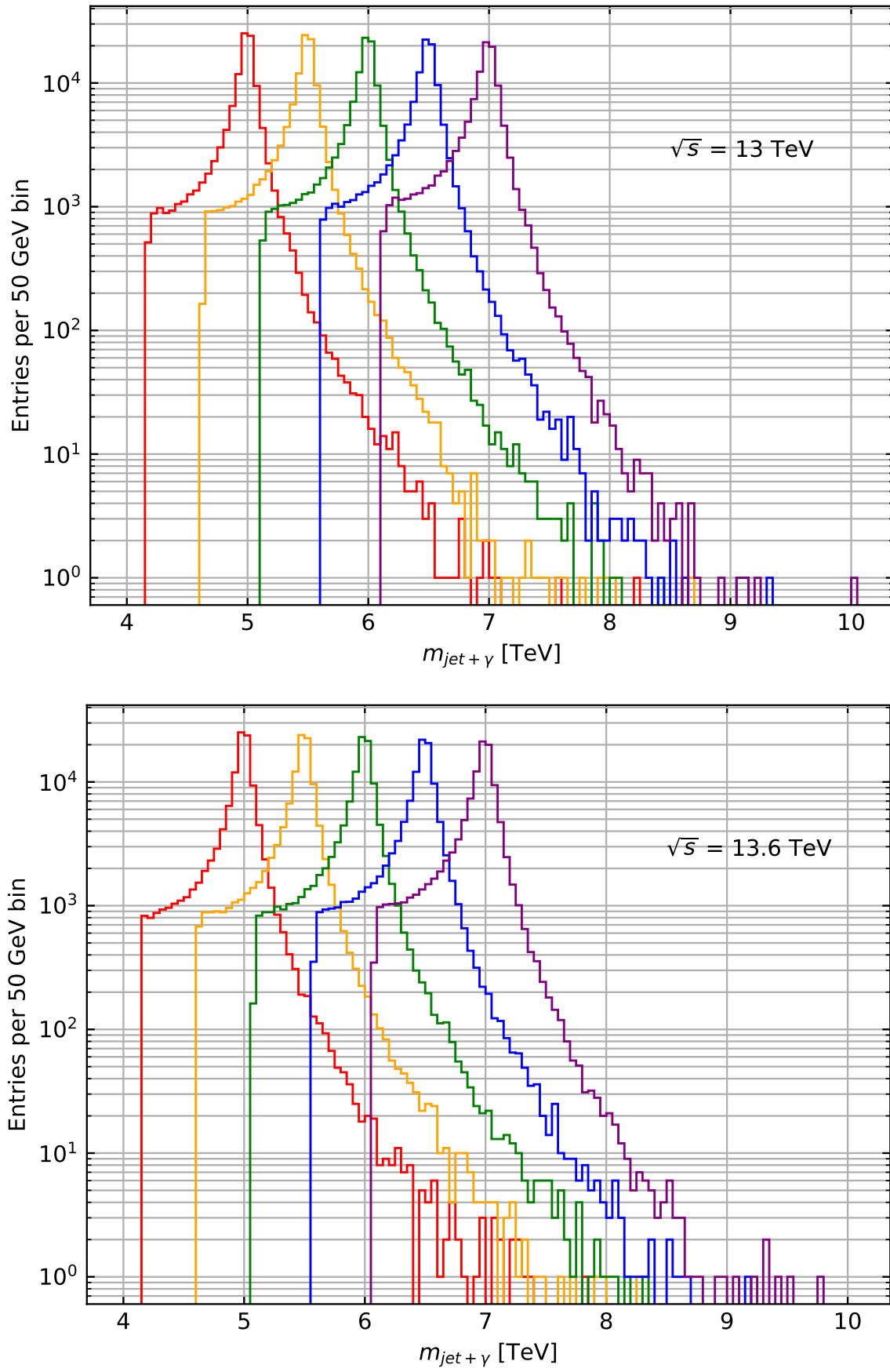


Figure 15: (Logarithmic Axis)

We can also superimpose the 13 TeV and 13.6 resonances onto each other:

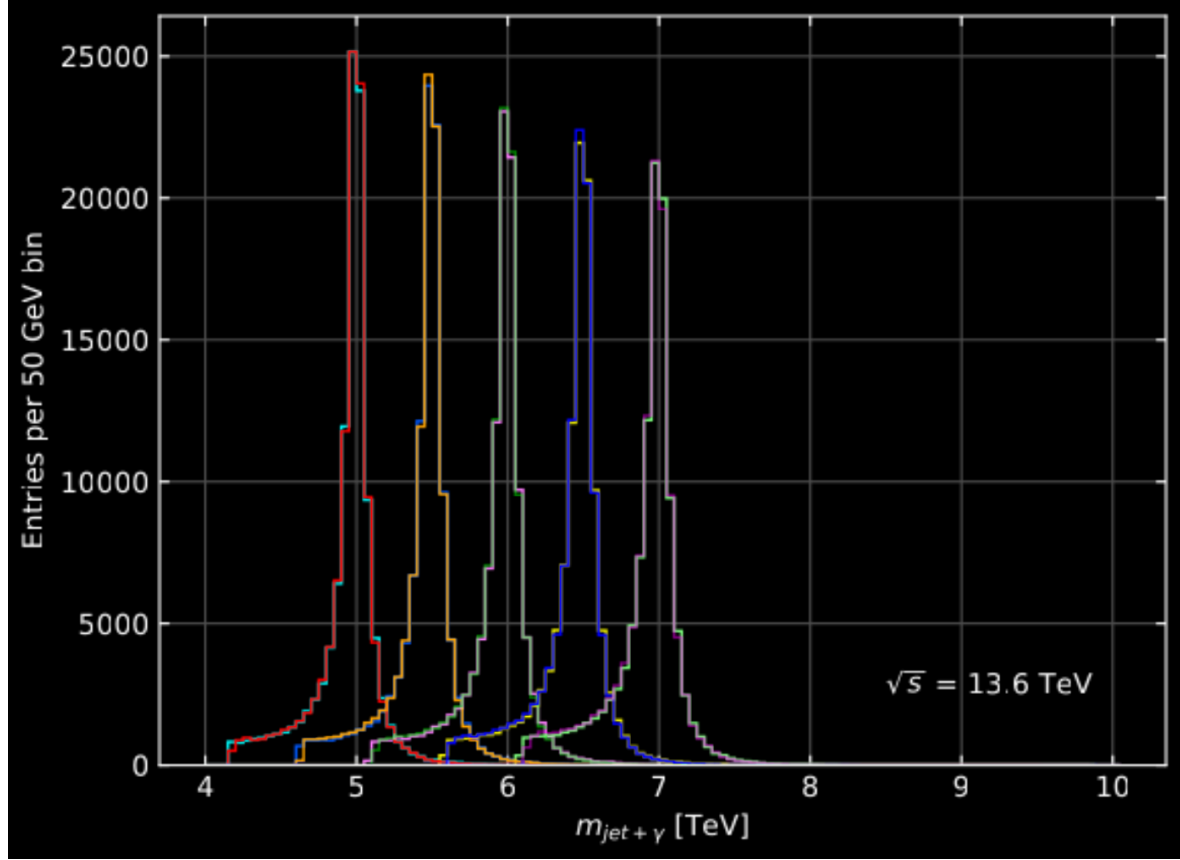


Figure 16: $\sqrt{s} = 13$ TeV & 13.6 TeV (inverted)

Here, the $\sqrt{s} = 13.6$ TeV plot has been inverted, with the $\sqrt{s} = 13$ TeV plot overlaid in regular color (red, orange, green, blue, violet). The 13.6 TeV distributions are slightly shorter in height and wider than the 13.0 TeV ones.

4.2 Angular Distribution Study

The radial angle θ changes depending on whether is being measured in the lab frame or the resonance frame, where the radial angle is defined as θ^* . In the resonance frame, the z momentum cancels out and the radial and azimuthal angles are opposite to each other for each outgoing parton.

The cosine of the radial angle is given by $\theta = \frac{p_z}{p}$. To convert p_z into the resonance frame, a Lorentz boost is applied along the z -axis:

$$p_z^* = \gamma(p_z - E\beta) \quad (4)$$

where

$$\gamma = \frac{E^s}{M^s} \quad \beta = \frac{p_z^s}{E^s} \quad (5)$$

The superscript s stands for 'string.' The distribution of the radial cosines is described by the curve $2 + 3x^2$ in the gg case, and $\frac{94}{25} + 6x^2 + x^4$, where $x = \cos \theta^*$.

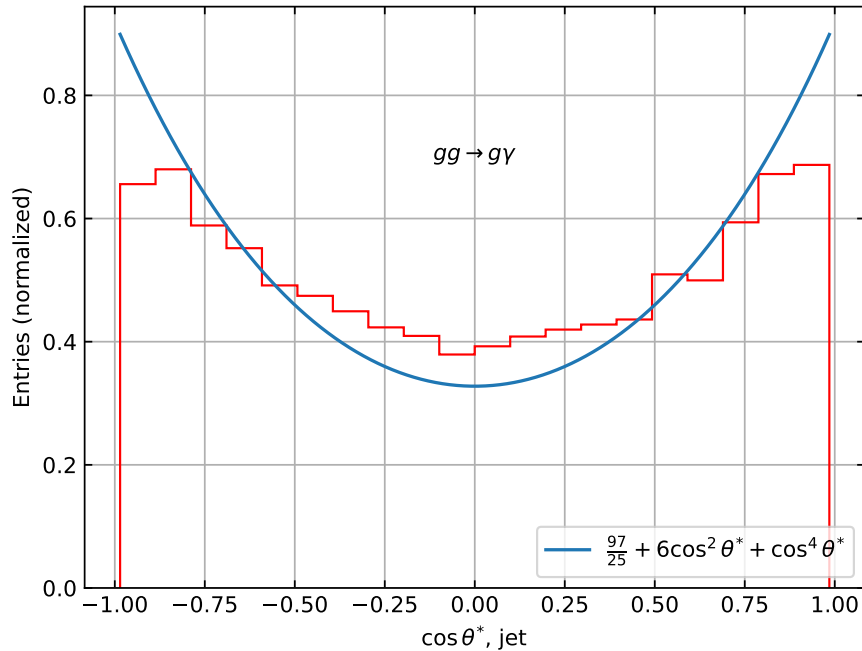


Figure 17: Angular distribution for $M_s = 5$ TeV

The recorded data does not match the theoretical distribution well; this could be because this theory is based on the assumption that all events are happening at $M = M_s$, but in reality, there is a distribution of events around M_s . In past trials studying dijet events, this theory has seemed to work well [6]:

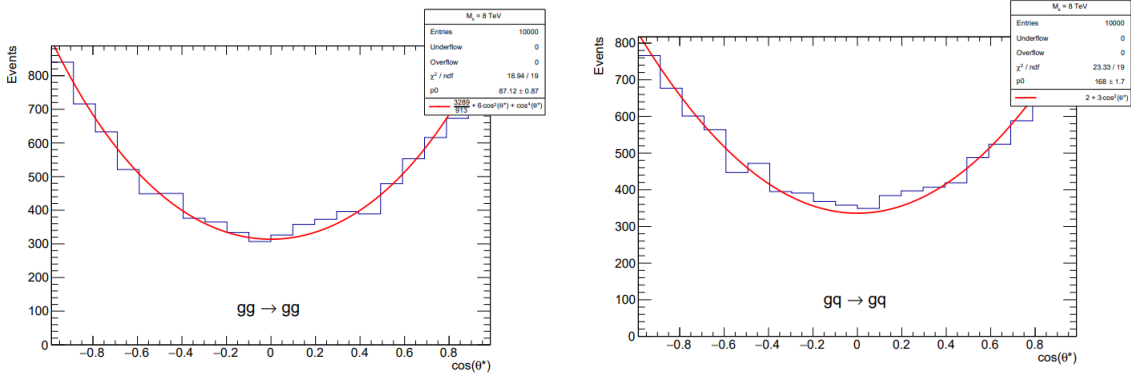


Figure 18: Angular distributions

It is possible that this old version of STRINGS was more accurate than it should have been. Referring to section 7.3, it also seems that as the string scale increases, the theory matches the data slightly better.

Furthermore, the maximum rapidity cut on the data generated was 2.5. This cut minimizes how close an outgoing parton's trajectory can be to the beam axis. With a higher rapidity cut, the distribution may be more closely matched by allowing more events to scatter partons close to the beam axis (such events would have a $\cos \theta^*$ close to ± 1).

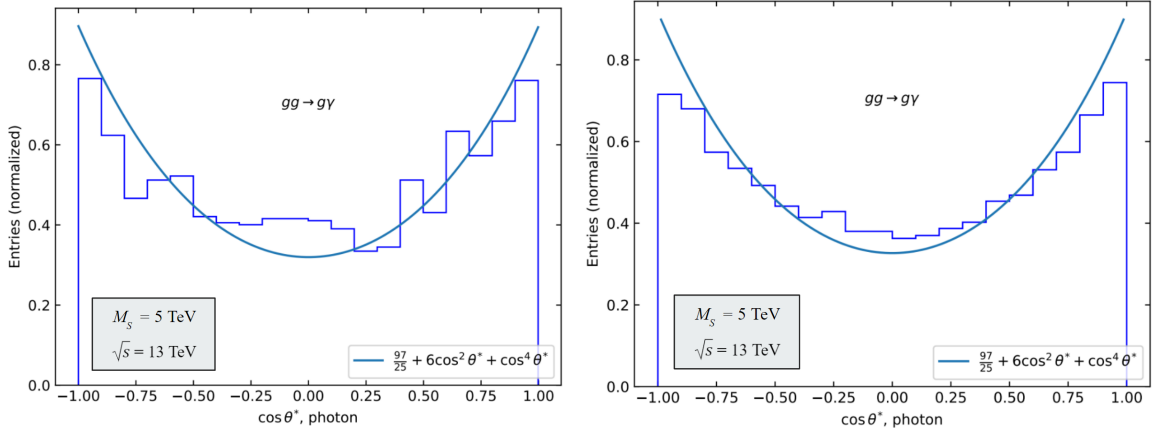


Figure 19: 11,000 events, $y_{cut} = 10$; 110,000 events, $y_{cut} = 6$

Given the data in the above figures, this seems to be the case. A cut of 6 gives a shape closer to the predicted distribution. A cut of 10 would likely be even better, but because imposing greater cuts vastly increases the time it takes for the generator to run, not many events were generated. It is likely that with more events, the distribution would be smoother. Based on the angular distributions from the appendices in 7.3, it seems that the theoretical distribution may be more valid for higher-TeV string scales.

4.3 Pythia Samples

Following the STRINGS simulations, LHE files are fed into the Pythia program, which is a much more sophisticated and realistic generator used for simulating scattering events. The histograms on the next page are generated using ROOT, and follow the same color scheme as the corresponding previous STRINGS histograms. Histograms presenting other kinematic variables like η , ϕ , and p_\perp are in appendix.

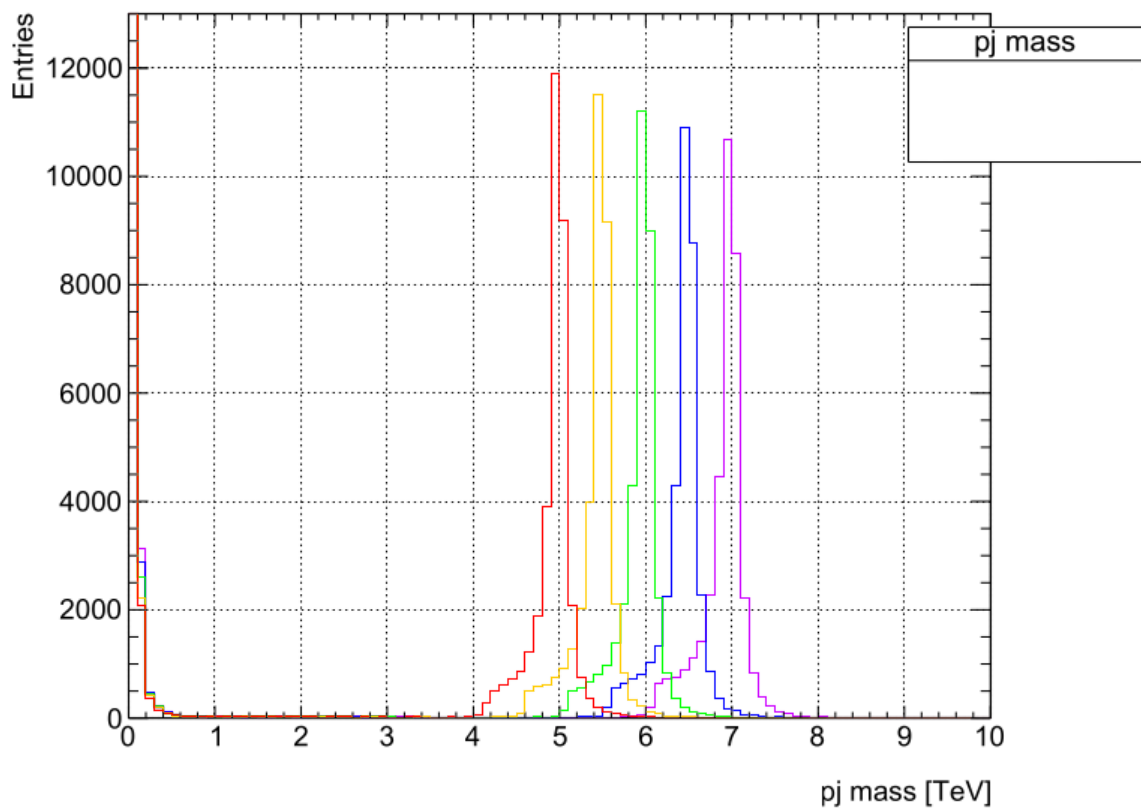
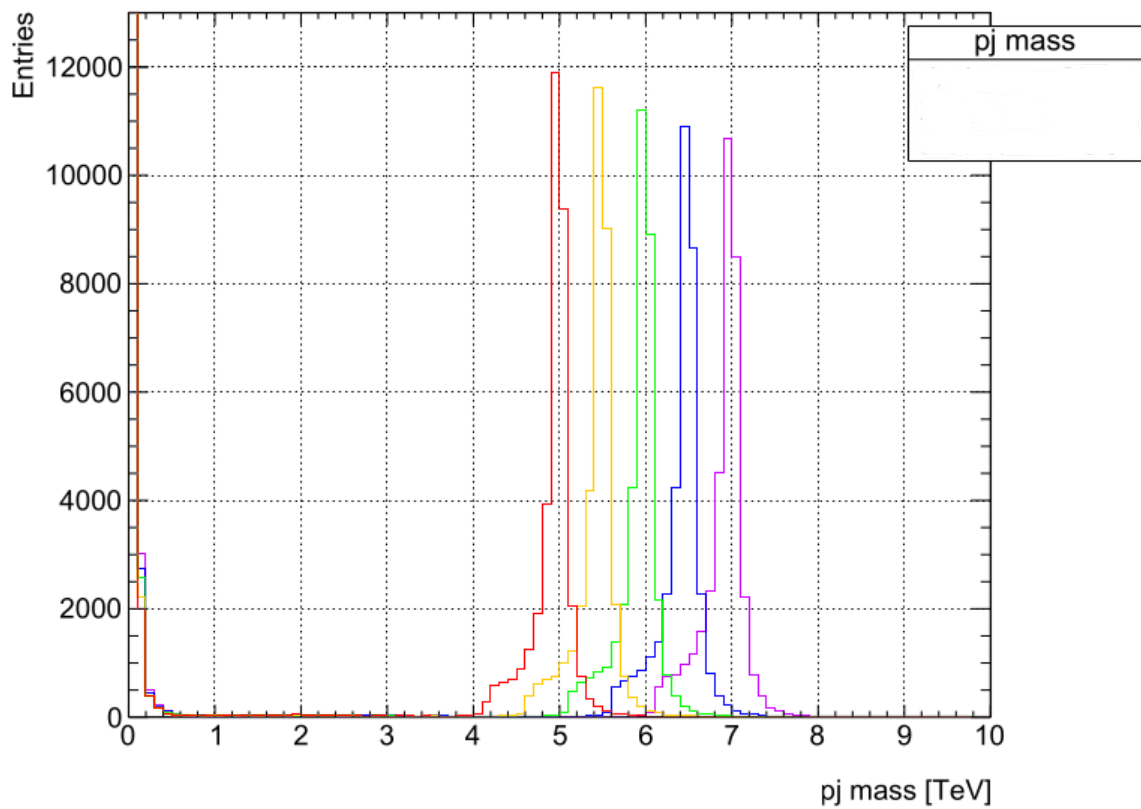


Figure 20: Linear Axis; $\sqrt{s} = 13$ TeV (top) and 13.6 TeV (bottom)

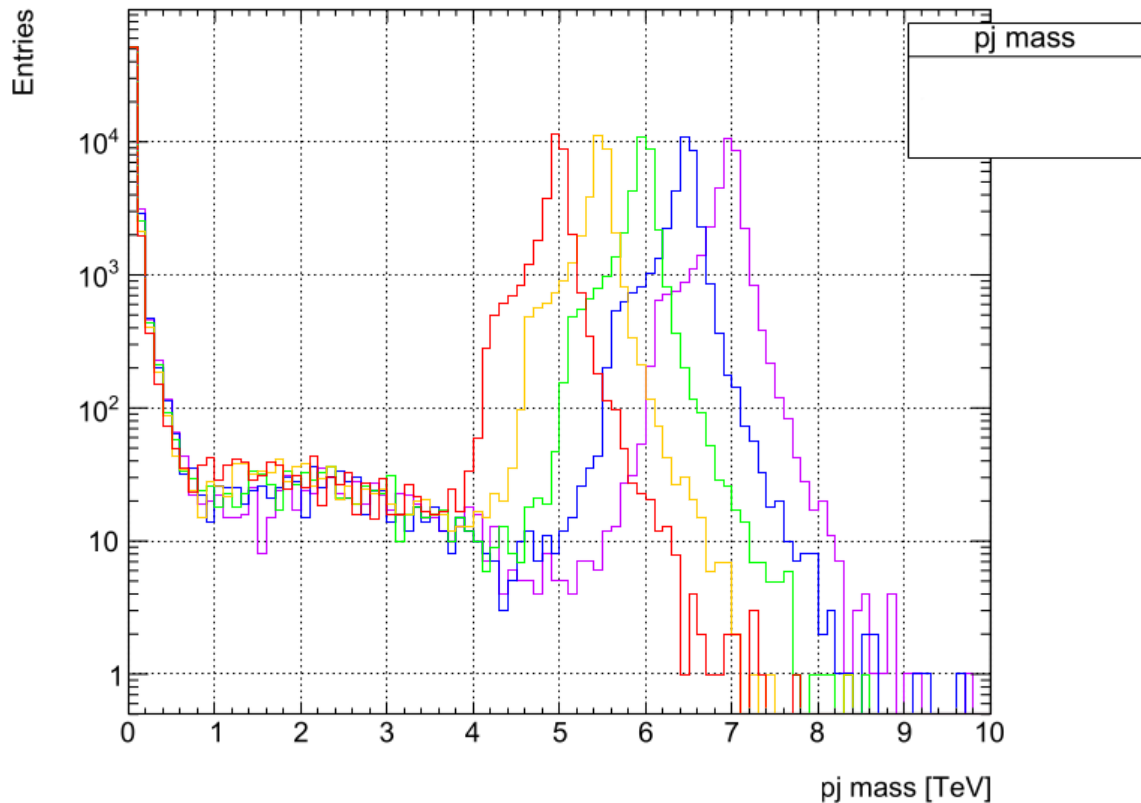
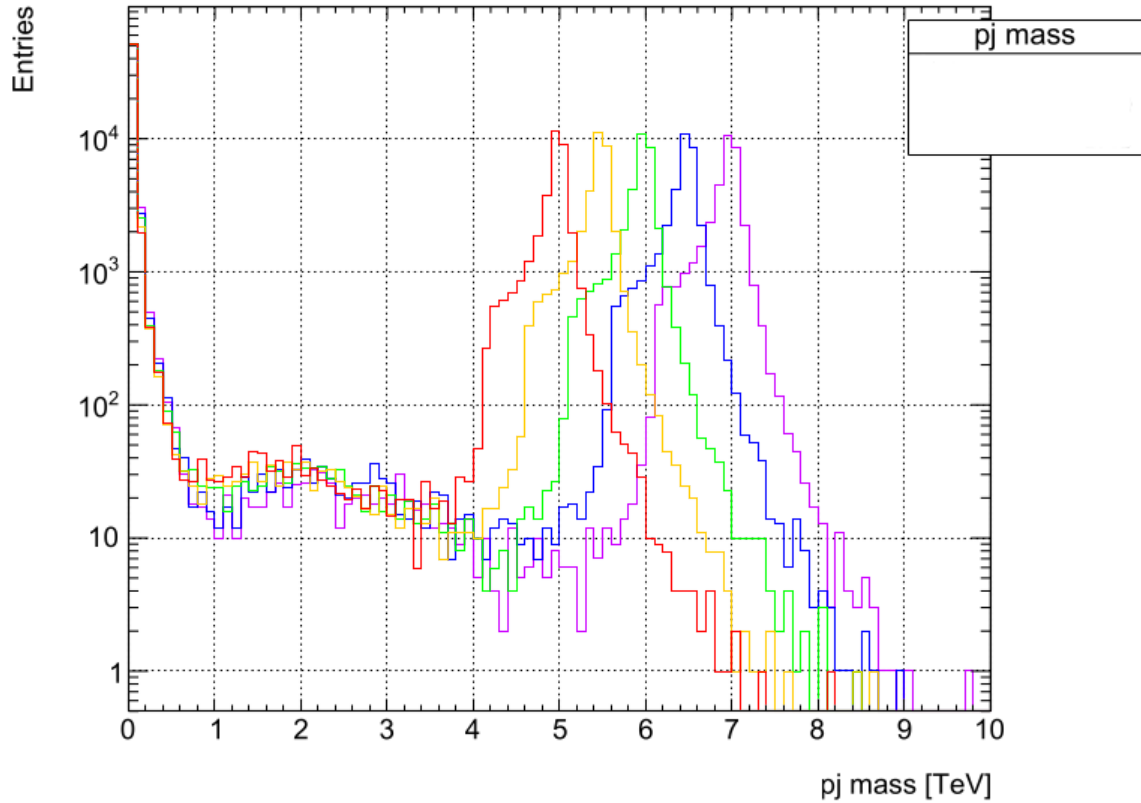


Figure 21: Logarithmic Axis; $\sqrt{s} = 13$ TeV (top) and 13.6 TeV (bottom)

Superimposing the 13 TeV and 13.6 resonances onto each other:

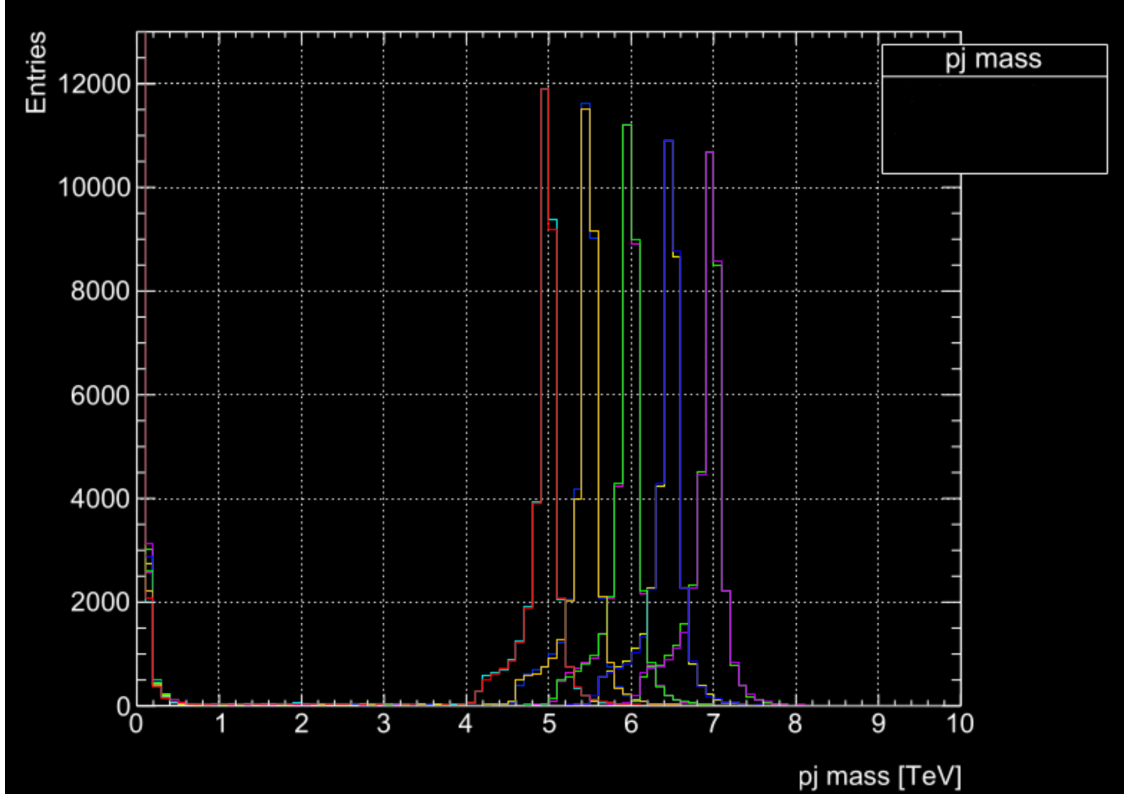


Figure 22: $\sqrt{s} = 13$ TeV & 13.6 TeV (inverted)

As observed in the STRINGS samples, the 13.6 TeV resonances are slightly wider than the 13 TeV ones. However, unlike the STRINGS samples, the peak height is virtually the same for all the resonances, except for $M_s = 5.5$ TeV, where the 13 TeV resonance is evidently shorter than the 13.6 one. This is unexpected, at cuts against the established trend of decreasing peak height with increasing \sqrt{s} .

5 Conclusions

After concluding our Monte Carlo resonance search, there are several conclusions that we may draw. Firstly, the Pythia events generated demonstrate the resonance peaks are remarkably similar for $\sqrt{s} = 13$ and 13.6 TeV, meaning that discovery potential at either \sqrt{s} is relatively consistent. The evolution of the resonance peak shape as M_s is consistent with our expectation; as M_s increases, the peak gets shorter and thicker at the base.

As evidenced in the initial attempt, the discovery potential for string scales on the interval [7,9] TeV is problematic because there is a significant decrease in the number of events as compared to [5,7] TeV. For studying photon jet scattering processes, discovery potential is much higher at scales lower than 7 TeV. We also observe a drastic low-mass tail in all of the invariant mass distributions generated with Pythia. These low-mass events are of little interest and could obscure events that we are interested in studying at the LHC.

Going into the future, for the purposes of resonance searches in photon jet scattering events with ATLAS at the LHC, the data acquired in this study will be especially useful, and is planned on being sent to ATLAS colleagues.

6 Sources

- 1 N. Wolchover, S. Velasco, L. Reading-Ikkanda. "A New Map of All the Particles and Forces." (22 October 2020) <https://www.quantamagazine.org/a-new-map-of-the-standard-model-of-particle-physics-20201022/>
- 2 N. Arkanihamed, S. Dimopoulos, and G. Dvali. "The hierarchy problem and new dimensions at a millimeter". In: Physics Letters B 429.3-4 (1998), pp. 263–272. issn: 0370-2693. doi: 10.1016/s0370-2693(98)00466-3. url: [http://dx.doi.org/10.1016/S0370-2693\(98\)00466-3](http://dx.doi.org/10.1016/S0370-2693(98)00466-3)
- 3 F. Lyons. "Search for Low-Scale String Resonances with ATLAS at the Large Hadron Collider." (2021)
- 4 L. Anchordoqui et al, String Resonances at Hadron Colliders, Phys. Rev. D 90 (2014) 066013, ArXiv:1407.8120 [hep-ph]
- 5 L. Anchordoqui, H. Goldberg, S. Nawata, T. Taylor. "Direct photons as probes of low mass strings at the LHC." (April 2008) <https://arxiv.org/abs/0804.2013>.
- 6 Gingrich et al. "Search for new phenomena in dijet events using 3 quark/gluon tagging based on track multiplicity." (draft version 0.3) 25 January 2022.

7 Appendices

7.1 Strong Coupling Testing

Plots for this validation are located in `kmdrury/figures/7.2`. For each strong coupling, there is a plot of the differential cross-section, an unscaled ratio plot, and a scaled ratio plot (three plots total). Each file begins with '`0065`, '`0070`, '`0075`, ... , '`0120`' to represent the strong coupling value, and ends with either '`_cross.pdf`', '`_unscaled.pdf`', or '`_scaled.pdf`' to indicate what plot it is.

7.2 Differential Cross-sections

7.2.1 $M_s = [1,4]$ TeV (gg scattering only)

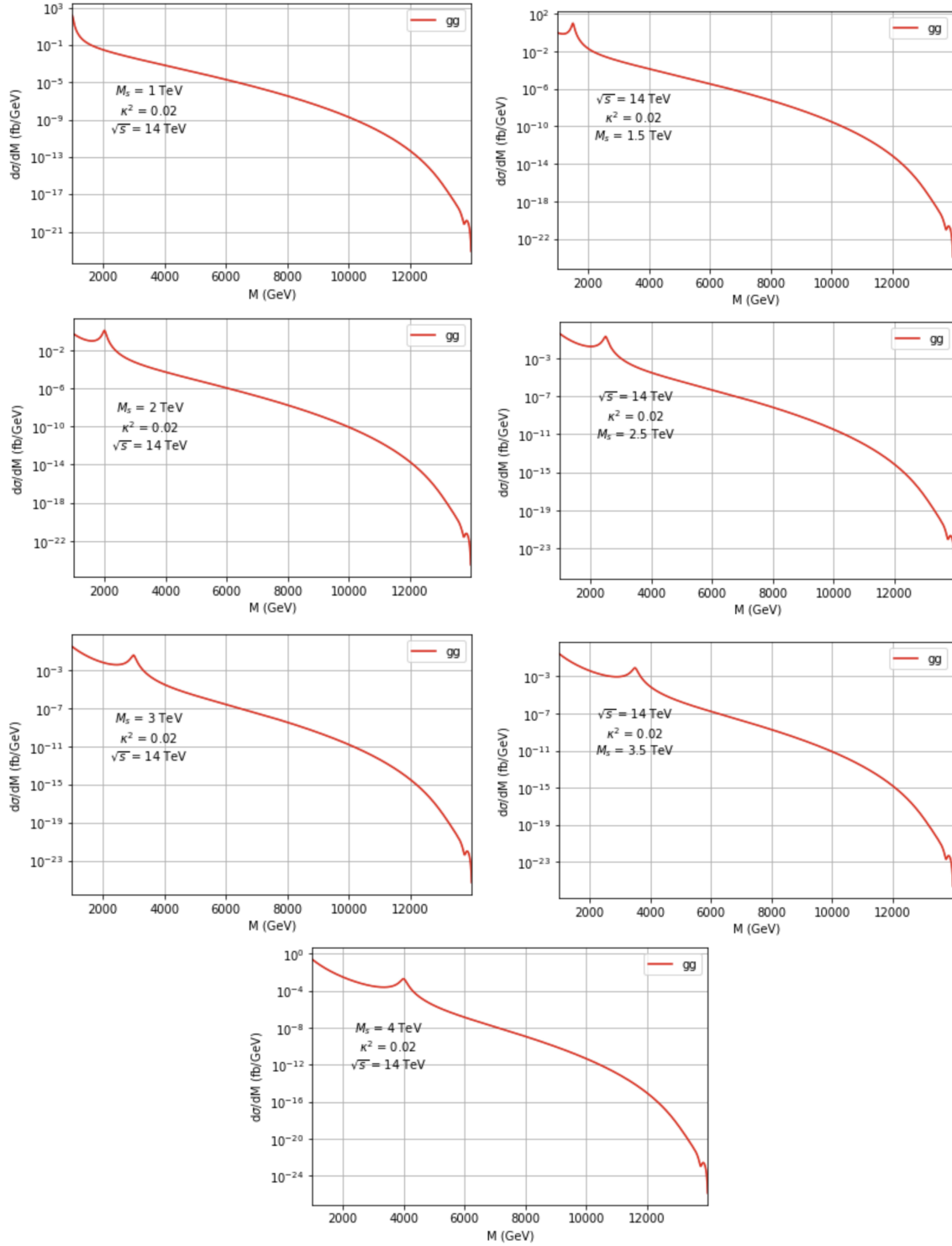


Figure 23: Differential cross-section curves for $M_s = [1, 4]$ TeV, $\sqrt{s} = 14$ TeV

String Scale M_s [TeV]	M_{cut} [GeV]
1	1000
1.5	1170
2	1590
2.5	2010
3	2450
3.5	2890
4	3350

Table 5: String scale vs M_{cut}

7.2.2 $M_s = [7, 9]$ TeV

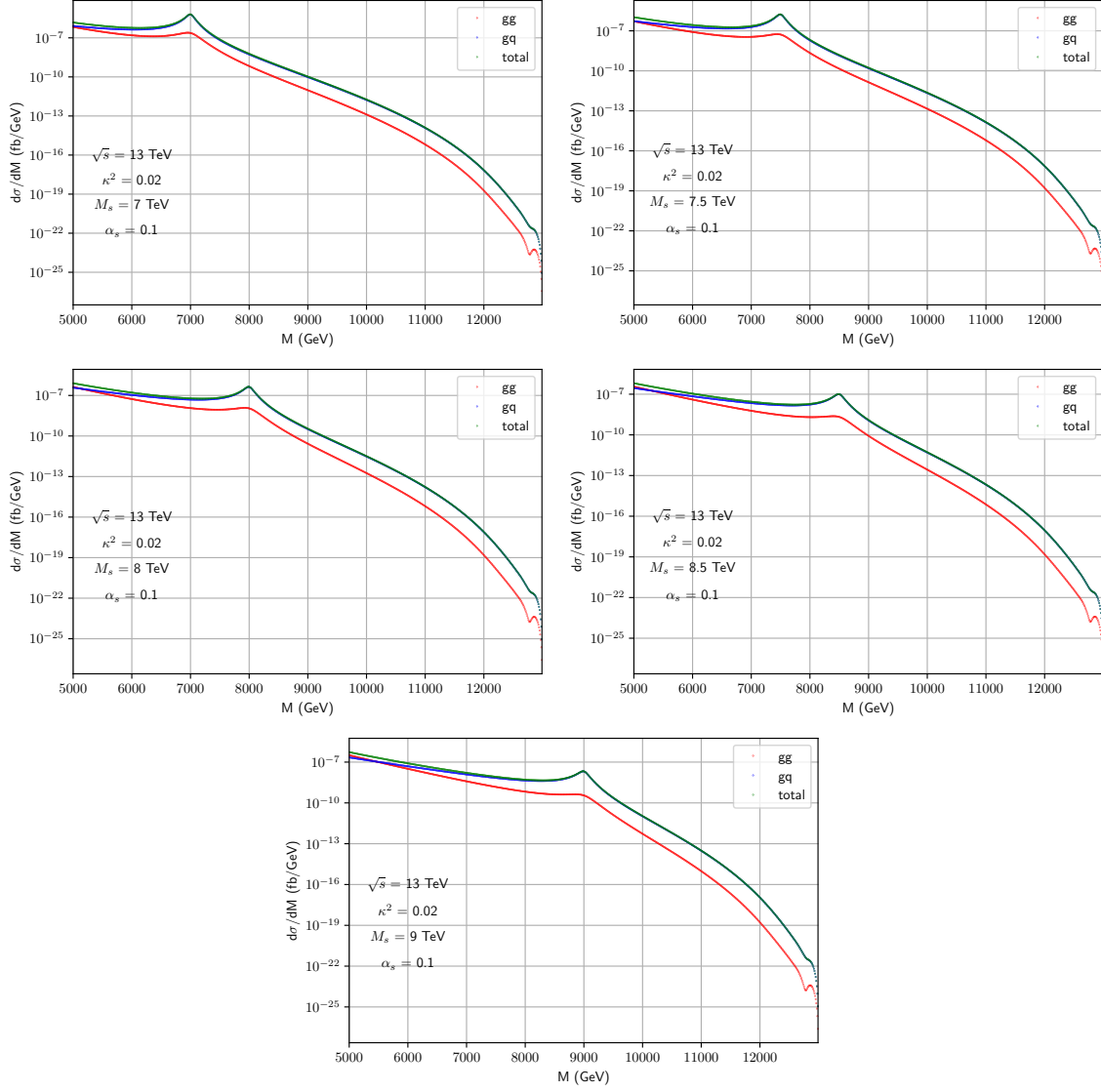


Figure 24: Differential cross-section curves for $M_s = [7, 9]$ TeV, $\sqrt{s} = 13$ TeV. Note that there is a typo in these plots: α_s is the running coupling, not 0.1.

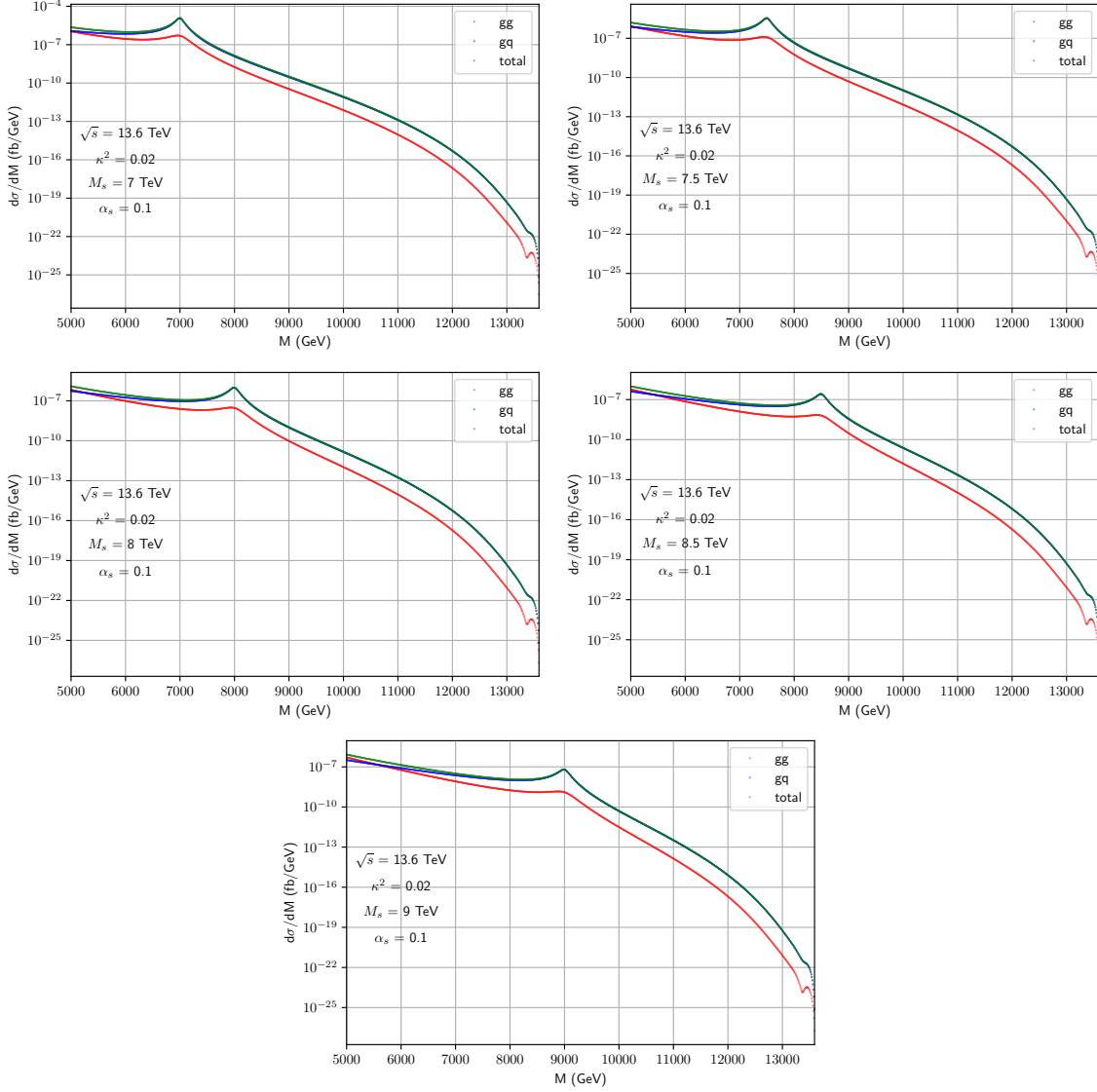


Figure 25: Differential cross-section curves for $M_s = [7, 9]$ TeV, $\sqrt{s} = 13.6$ TeV. Note that there is a typo in these plots: α_s is the running coupling, not 0.1.

String Scale M_s [TeV]	$M_{cut}, \sqrt{s} = 13$ TeV [TeV]	$M_{cut}, \sqrt{s} = 13.6$ TeV [TeV]
7	6.04	6.09
7.5	6.60	6.60
8	7.19	7.13
8.5	7.74	7.67
9	8.30	8.22

Table 6: Lower mass cuts for each M_s , \sqrt{s}

7.2.3 $M_s = [5, 7]$ TeV

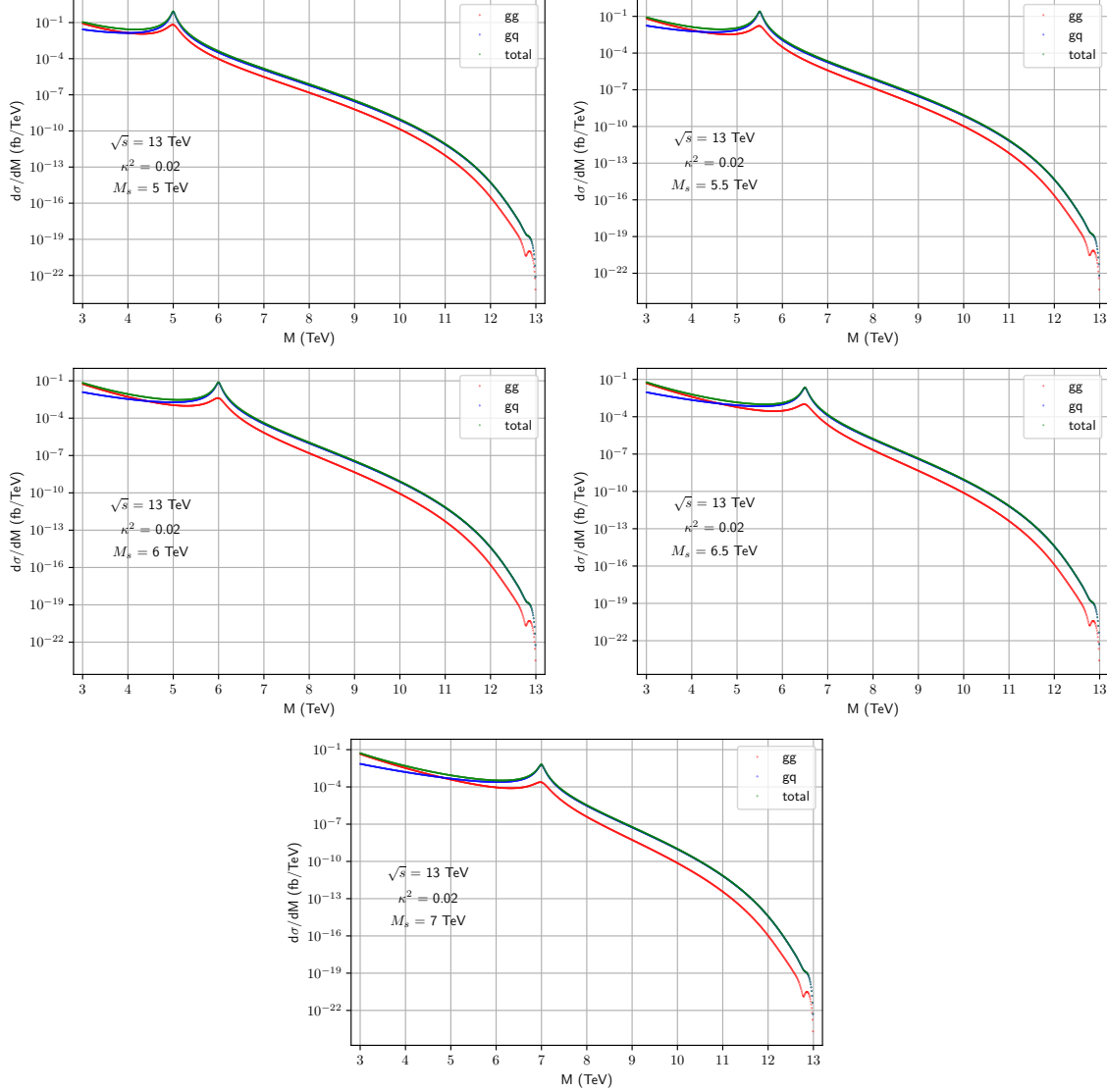


Figure 26: Differential cross-section curves for $M_s = [5, 7]$ TeV, $\sqrt{s} = 13$ TeV

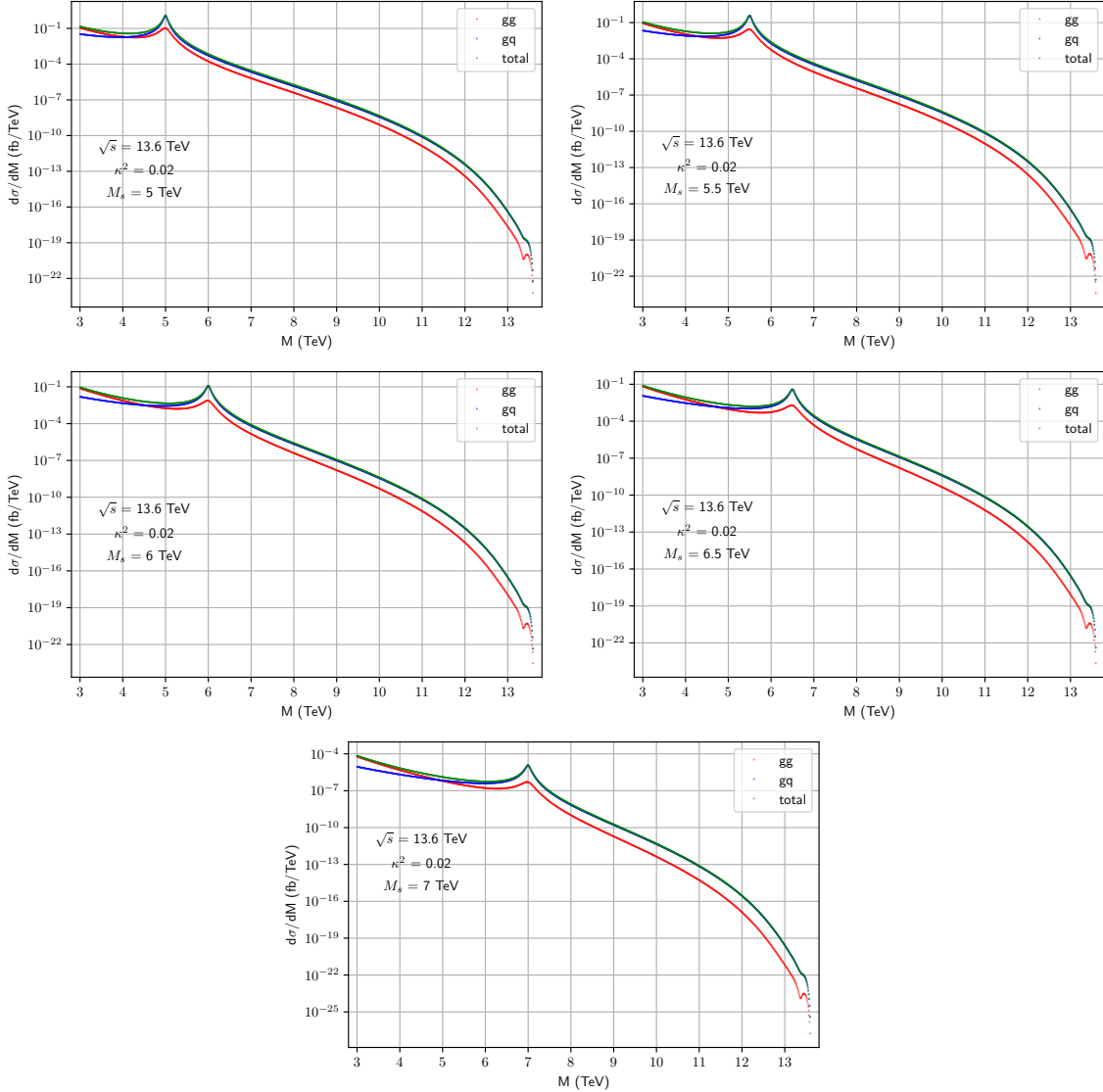


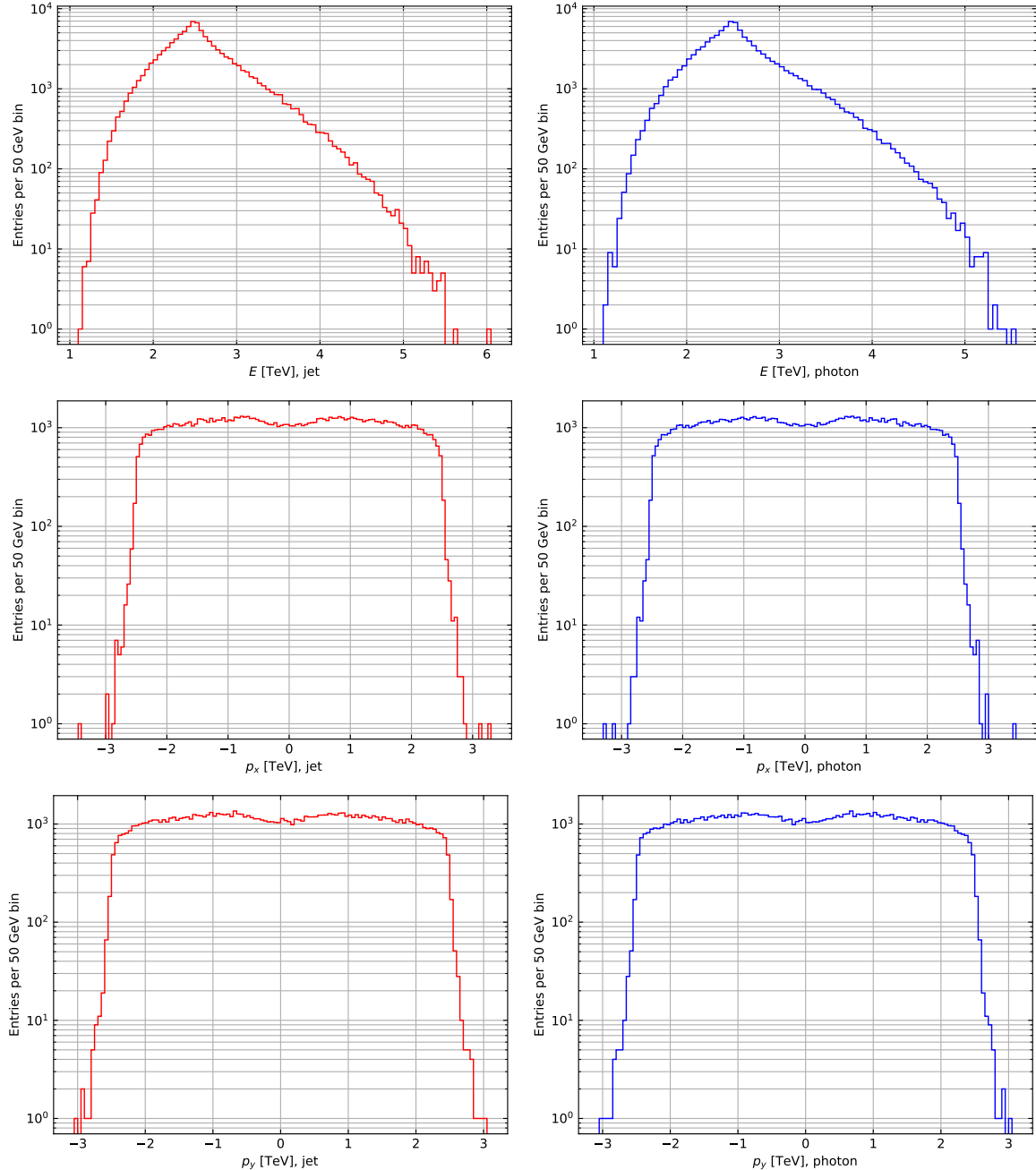
Figure 27: Differential cross-section curves for $M_s = [5, 7]$ TeV, $\sqrt{s} = 13.6$ TeV

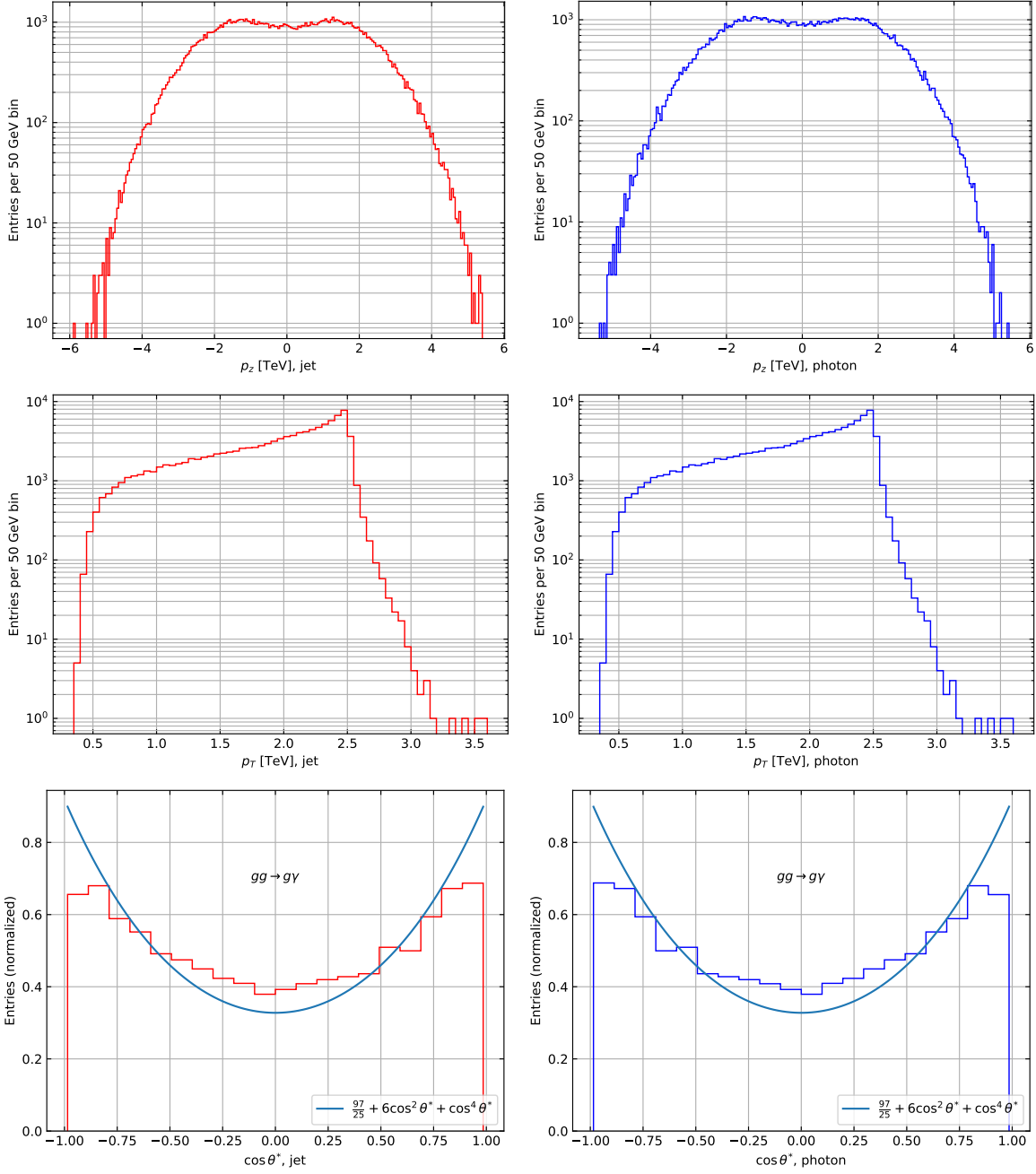
String Scale	M_{cut} for 13 TeV	M_{cut} for 13.6 TeV
5	4.17	4.15
5.5	4.64	4.61
6	5.12	5.09
6.5	5.61	5.58
7	6.12	6.08

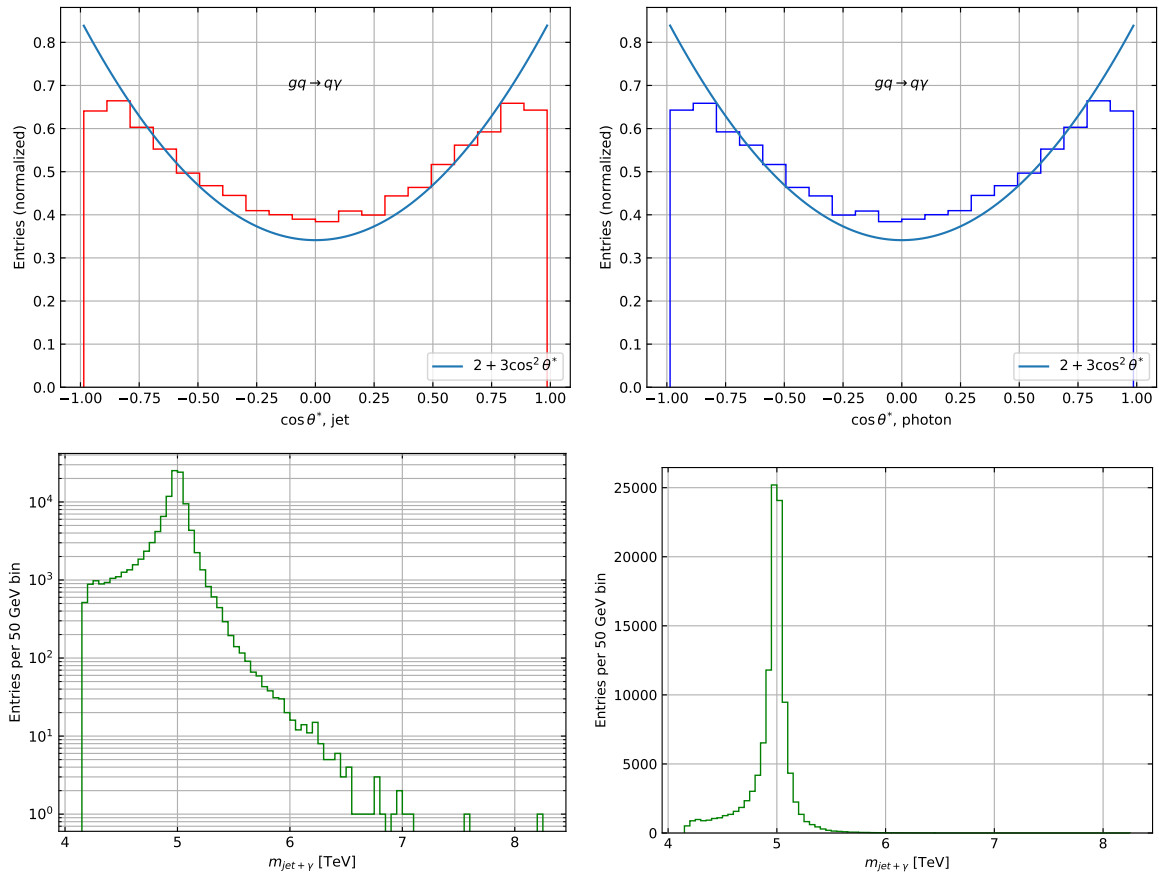
Table 7: Lower mass cuts for each M_s , \sqrt{s}

7.3 Kinematic Data Histograms

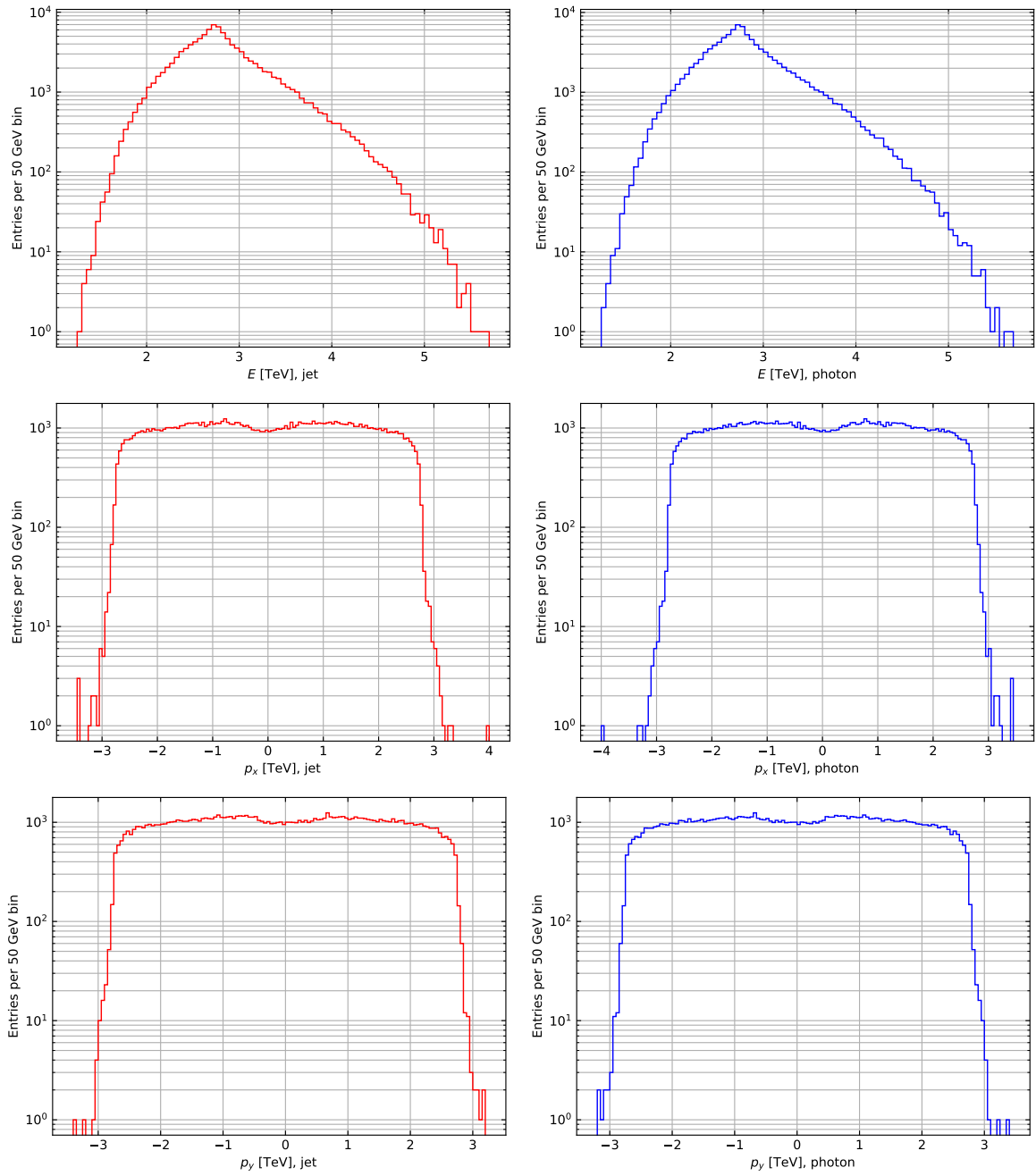
7.3.1 $\sqrt{s} = 13$ TeV, $M_s = 5$ TeV

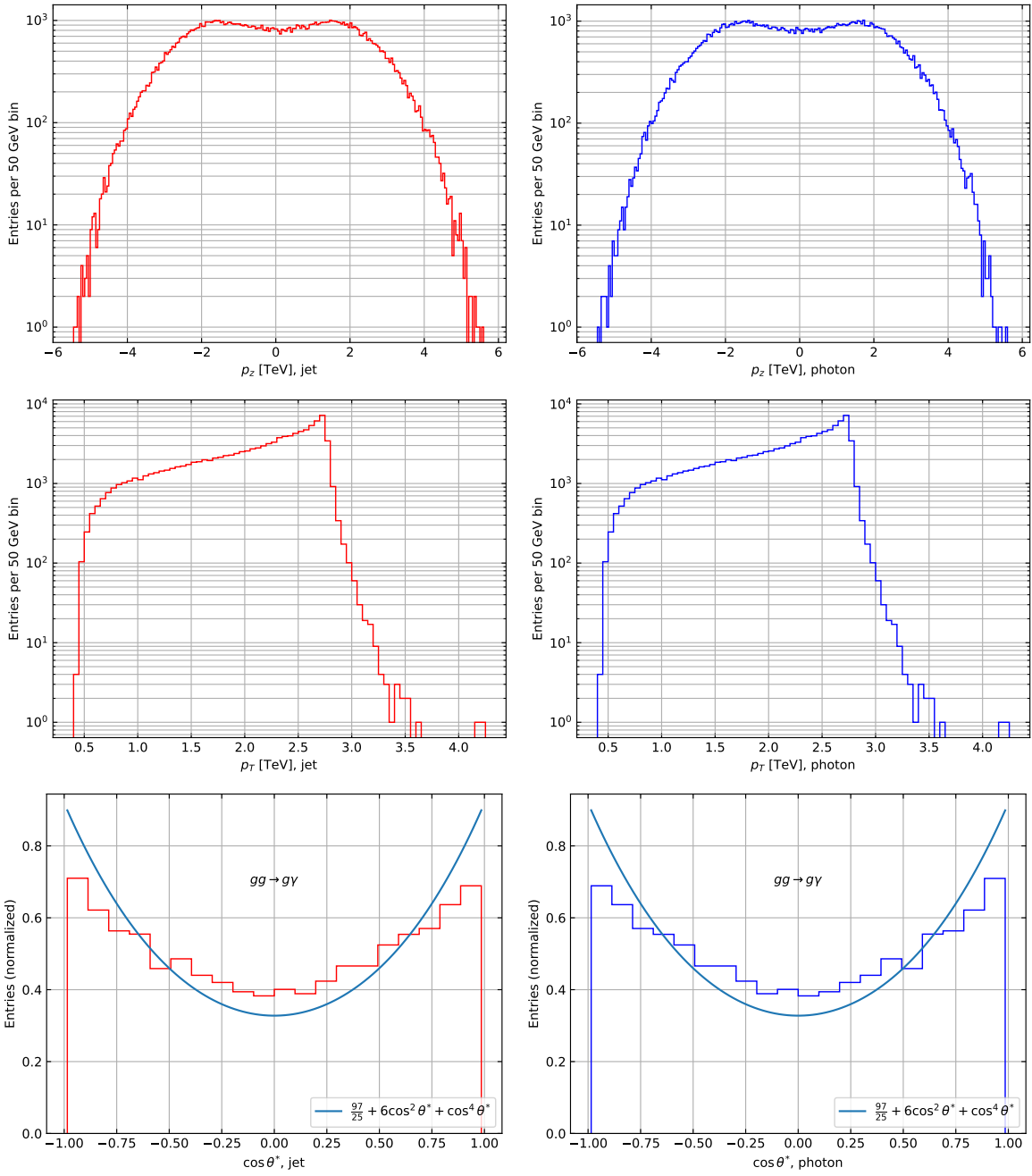


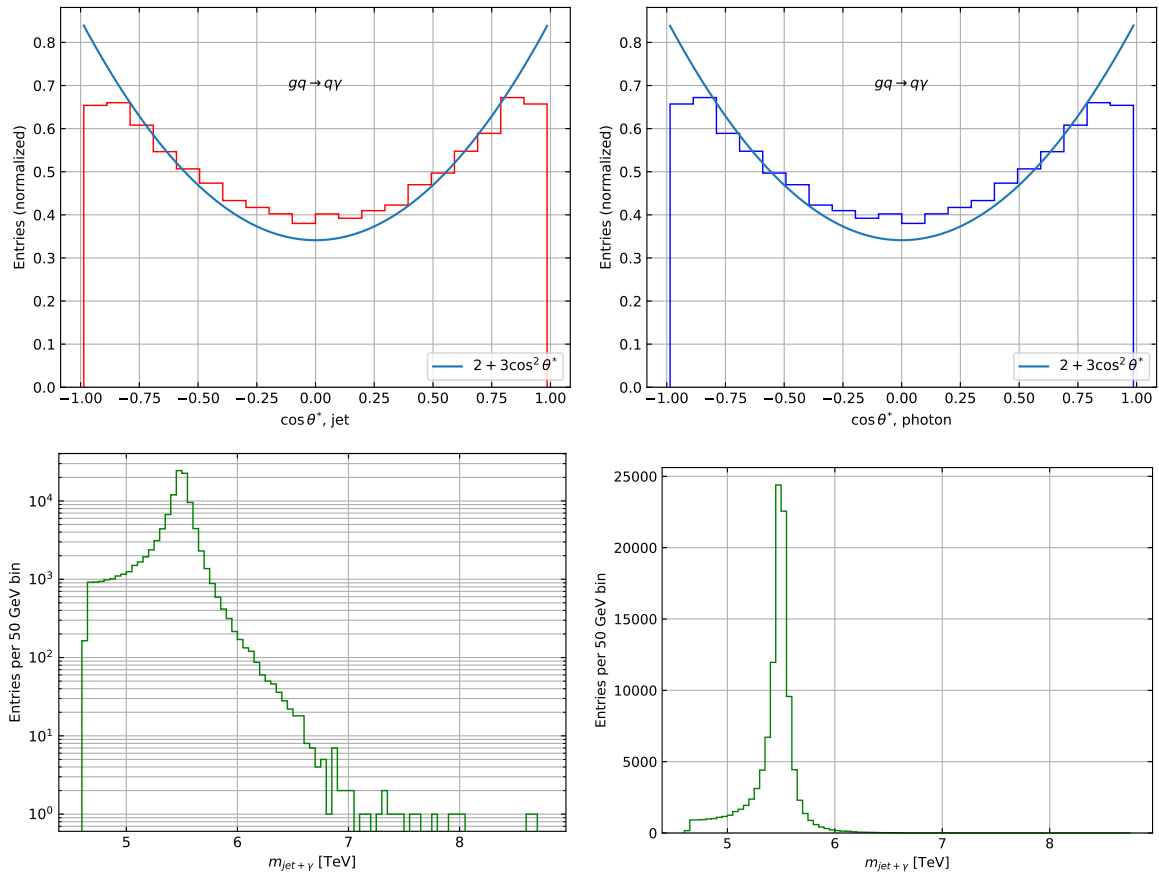




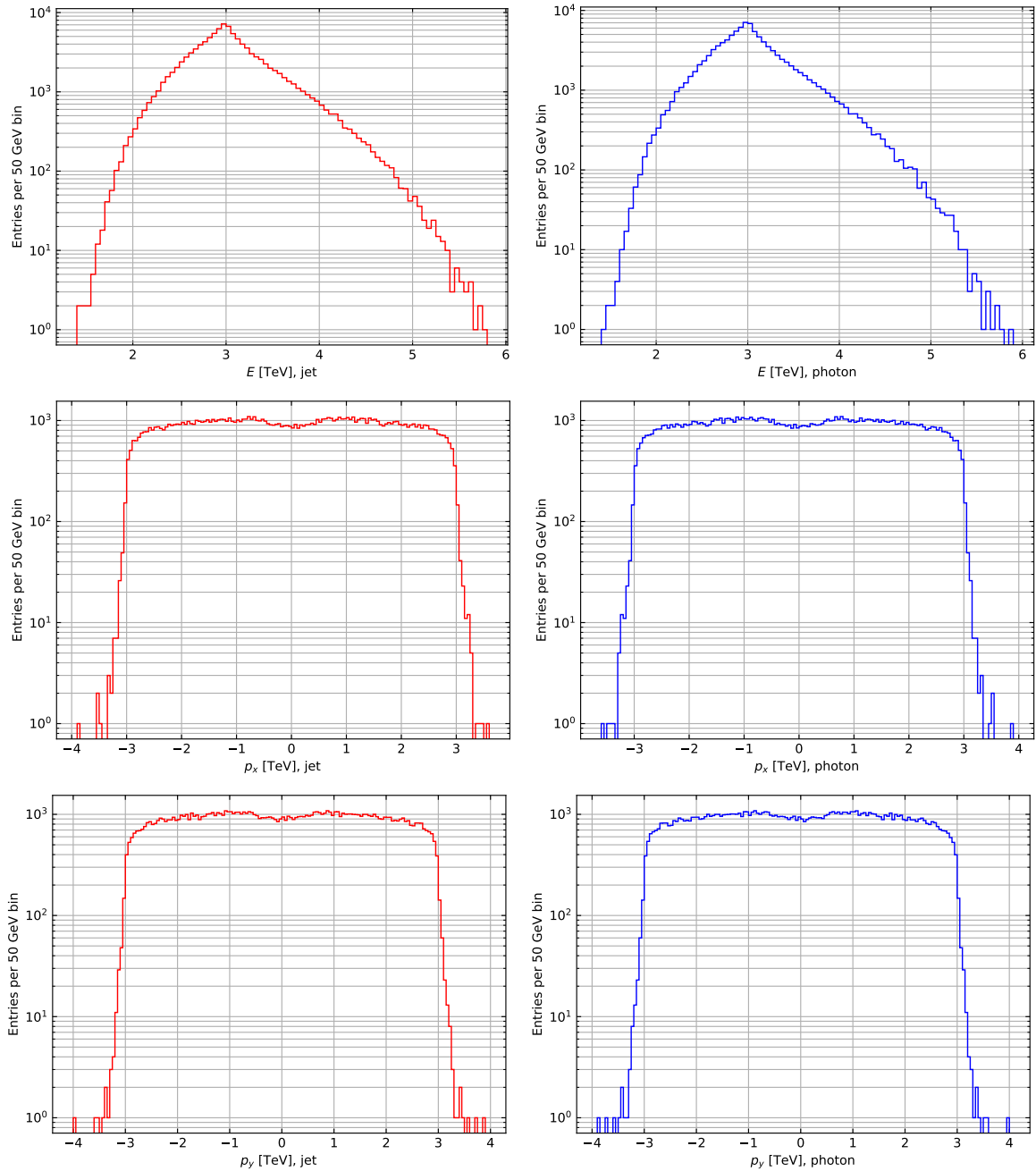
7.3.2 $\sqrt{s} = 13$ TeV, $M_s = 5.5$ TeV

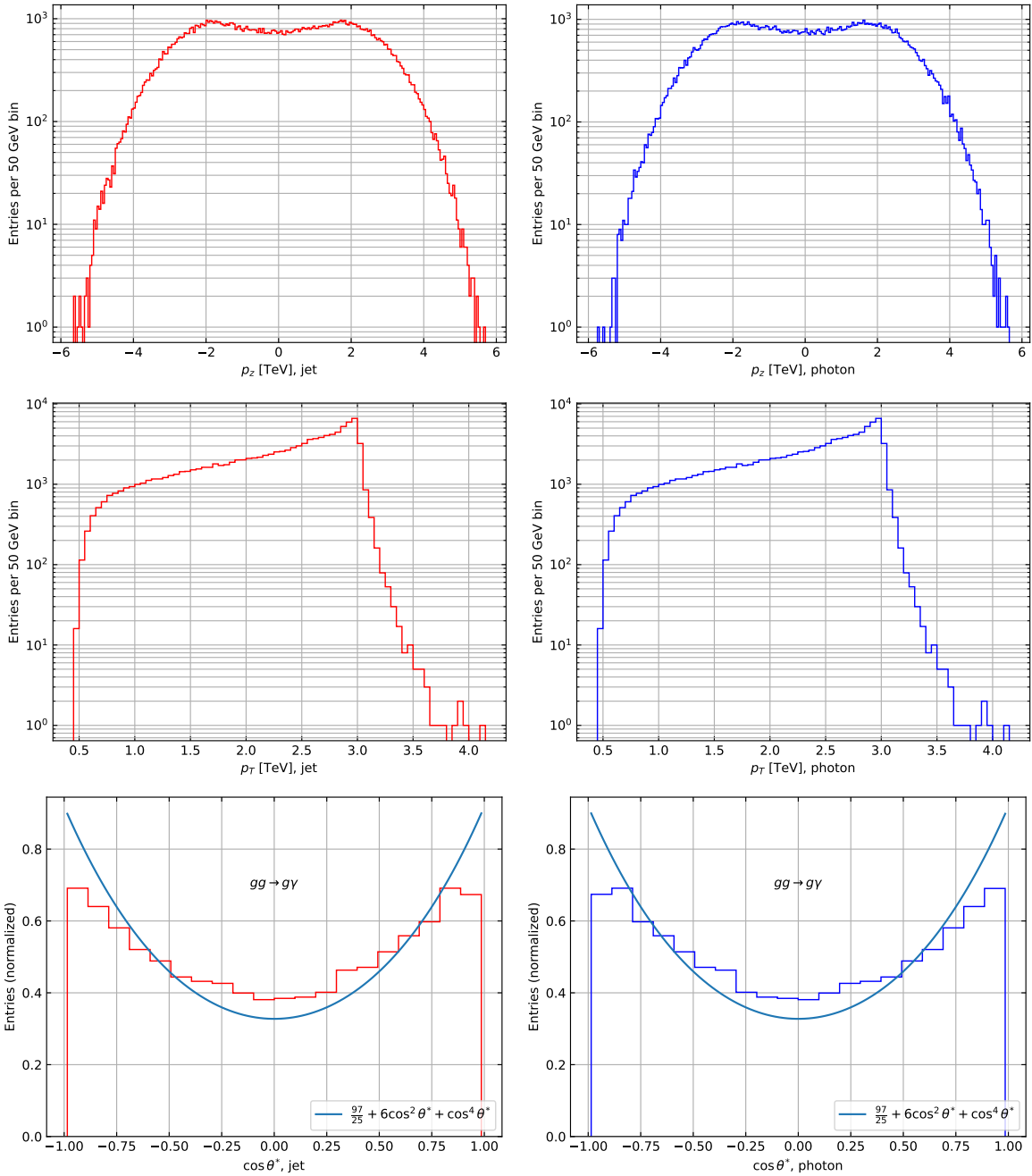


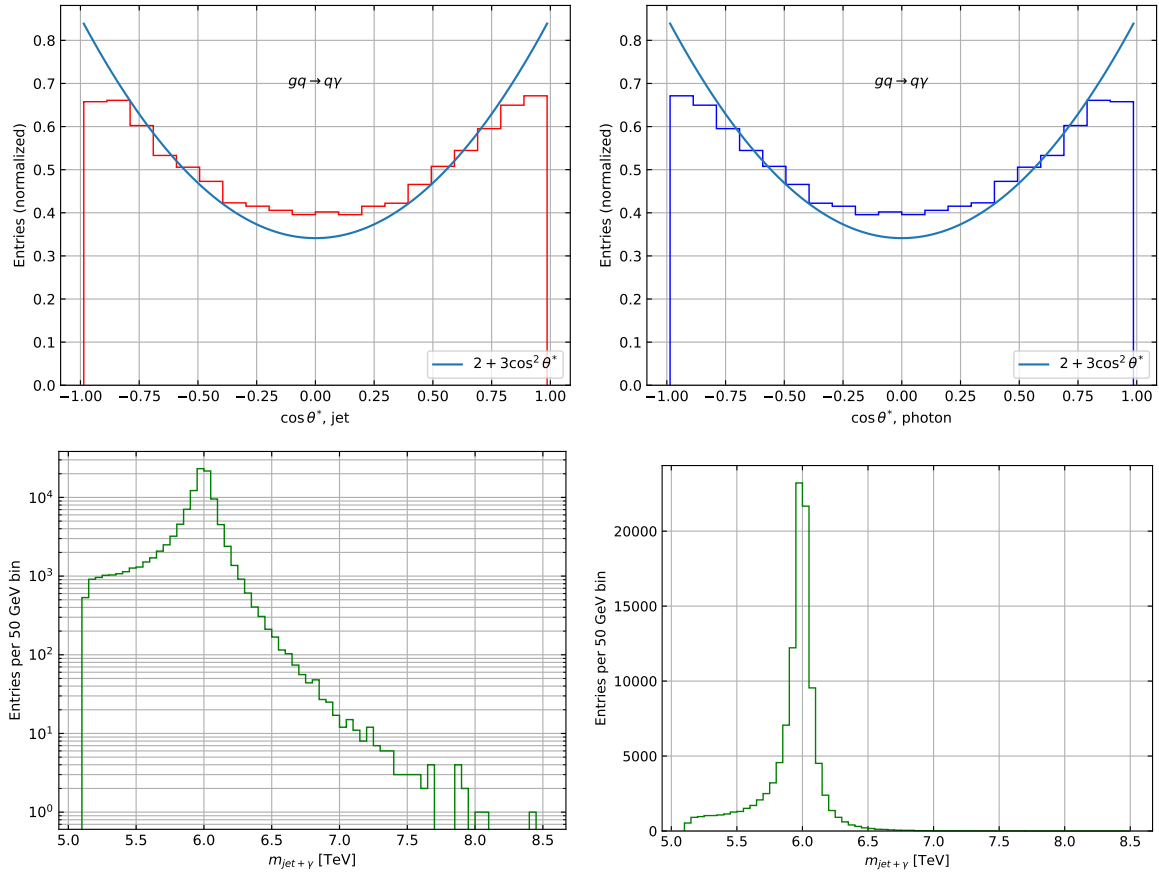




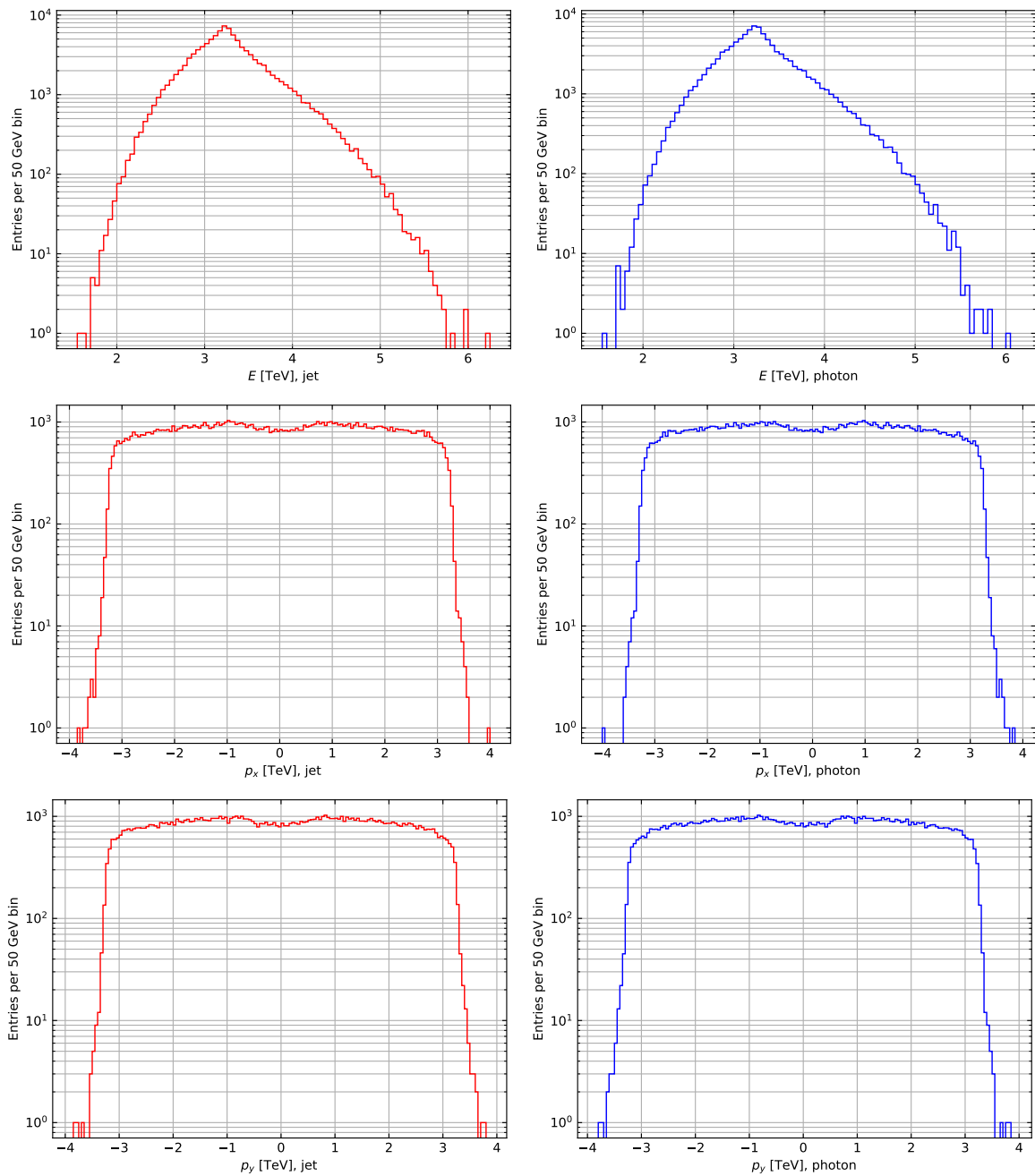
7.3.3 $\sqrt{s} = 13$ TeV, $M_s = 6.0$ TeV

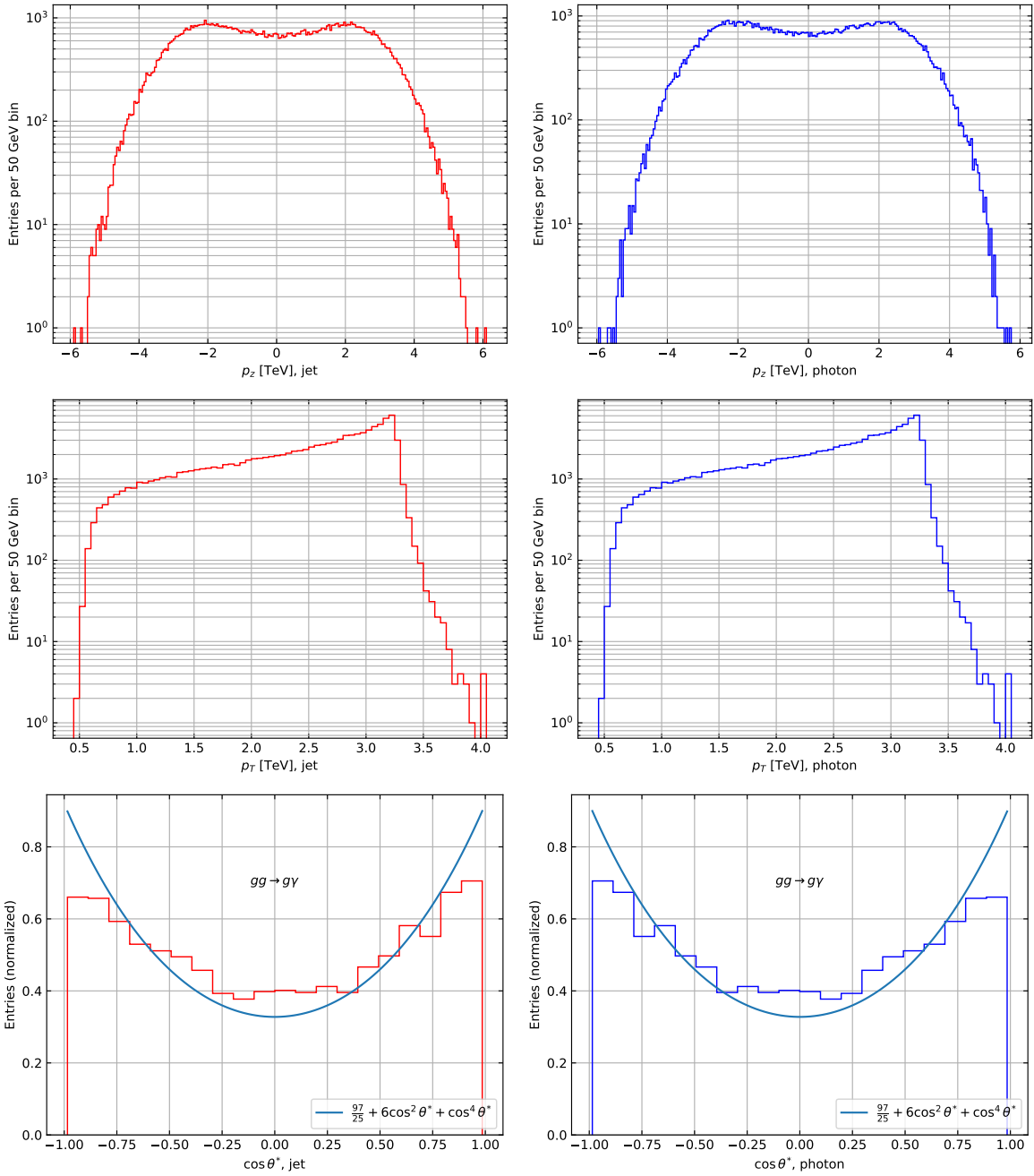


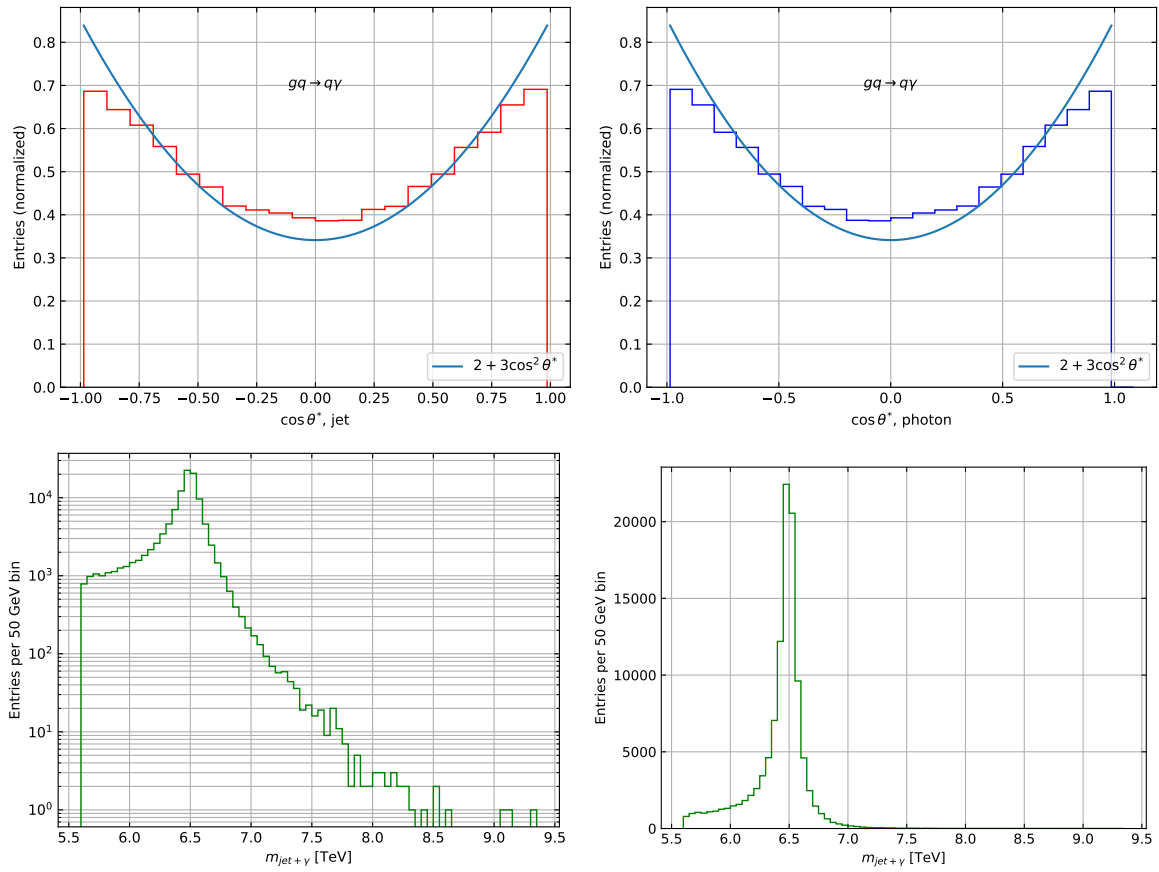




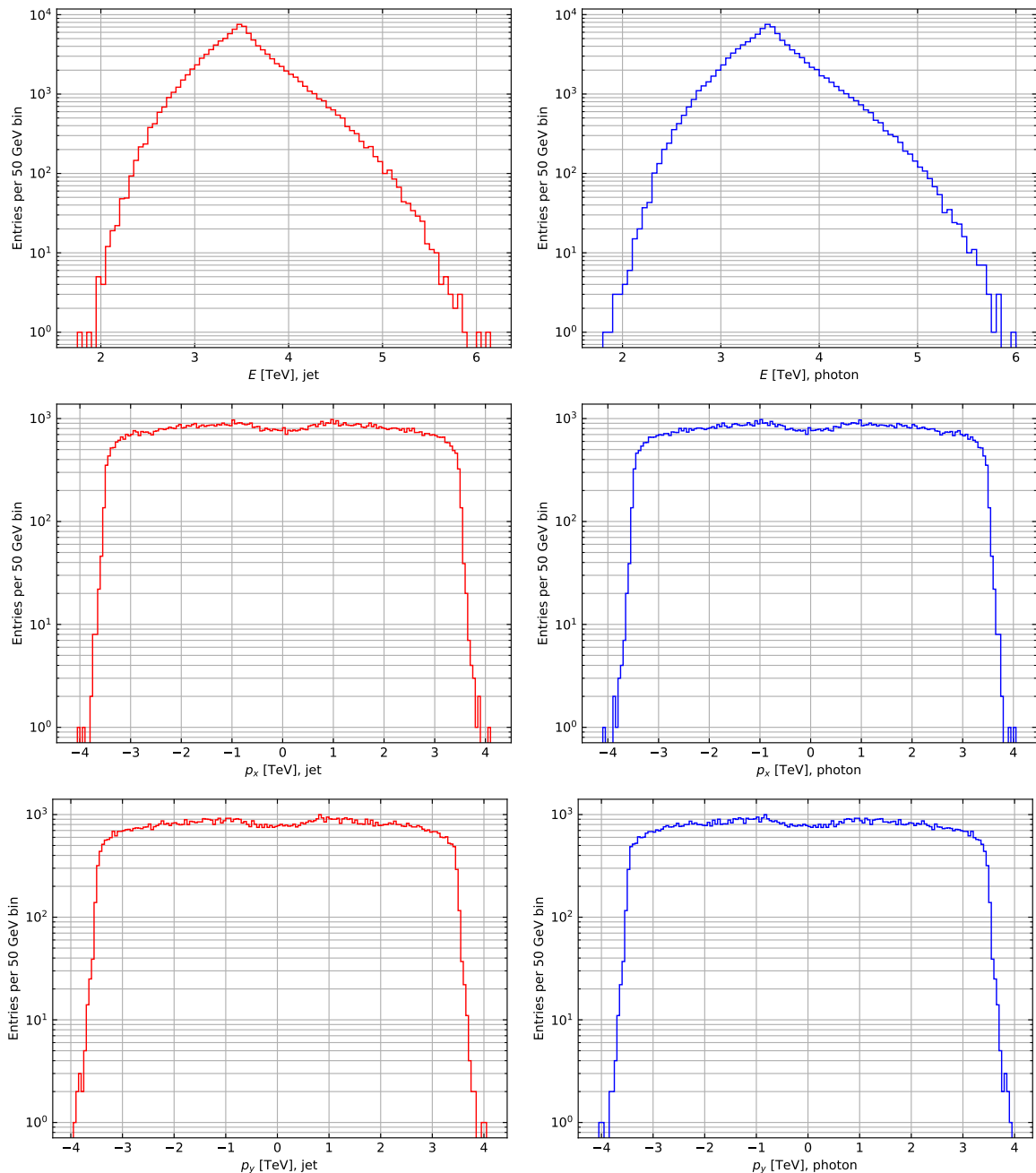
7.3.4 $\sqrt{s} = 13$ TeV, $M_s = 6.5$ TeV

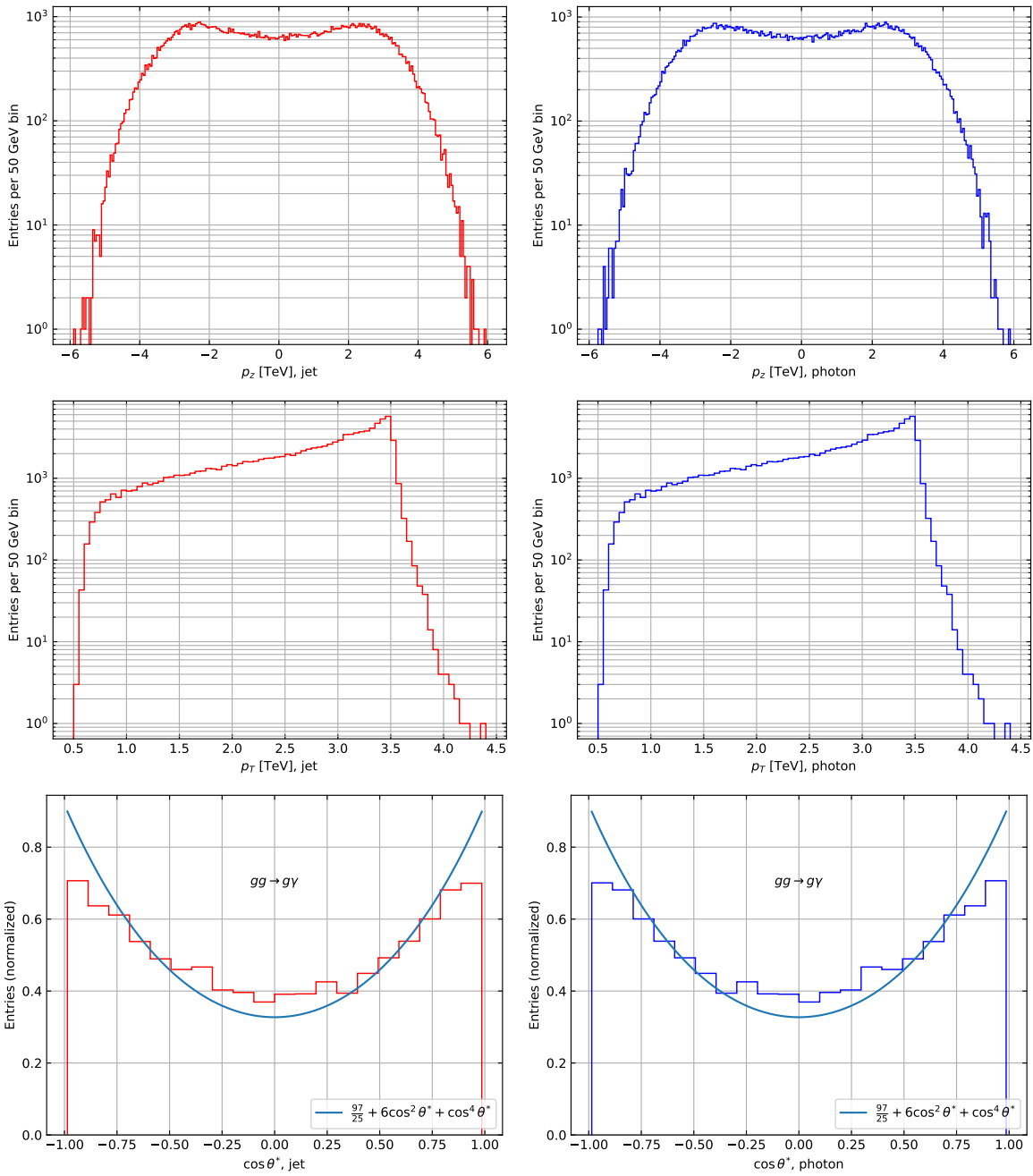


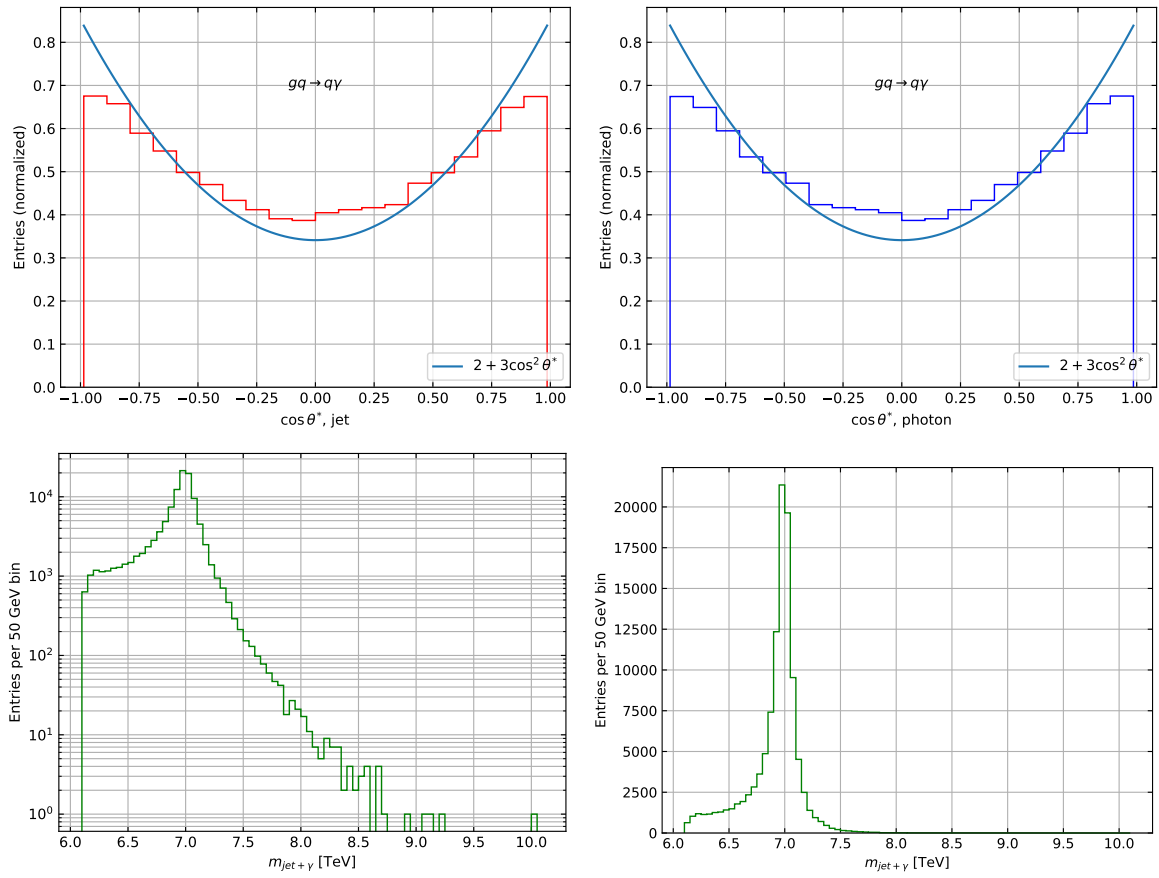




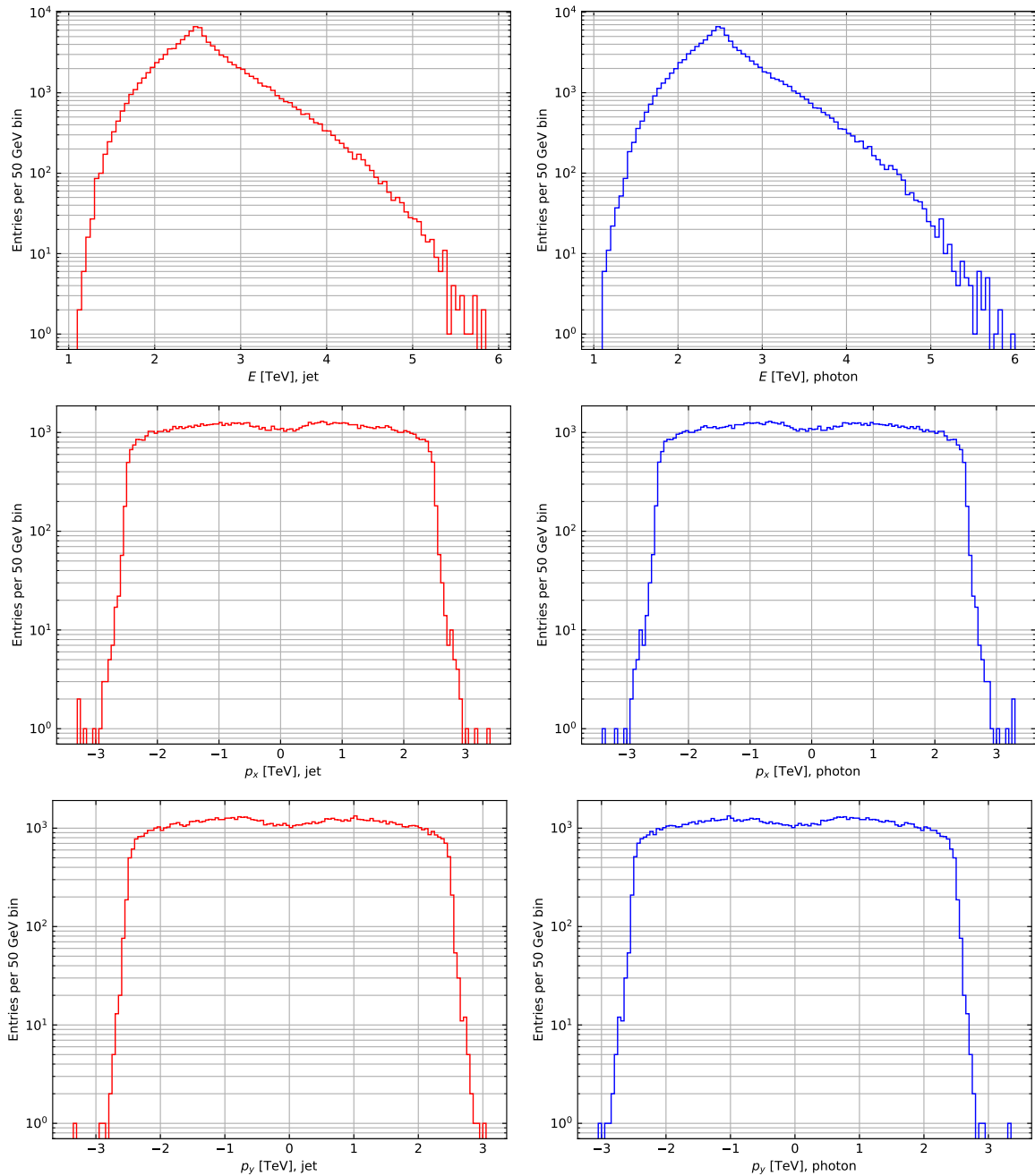
7.3.5 $\sqrt{s} = 13$ TeV, $M_s = 7.0$ TeV

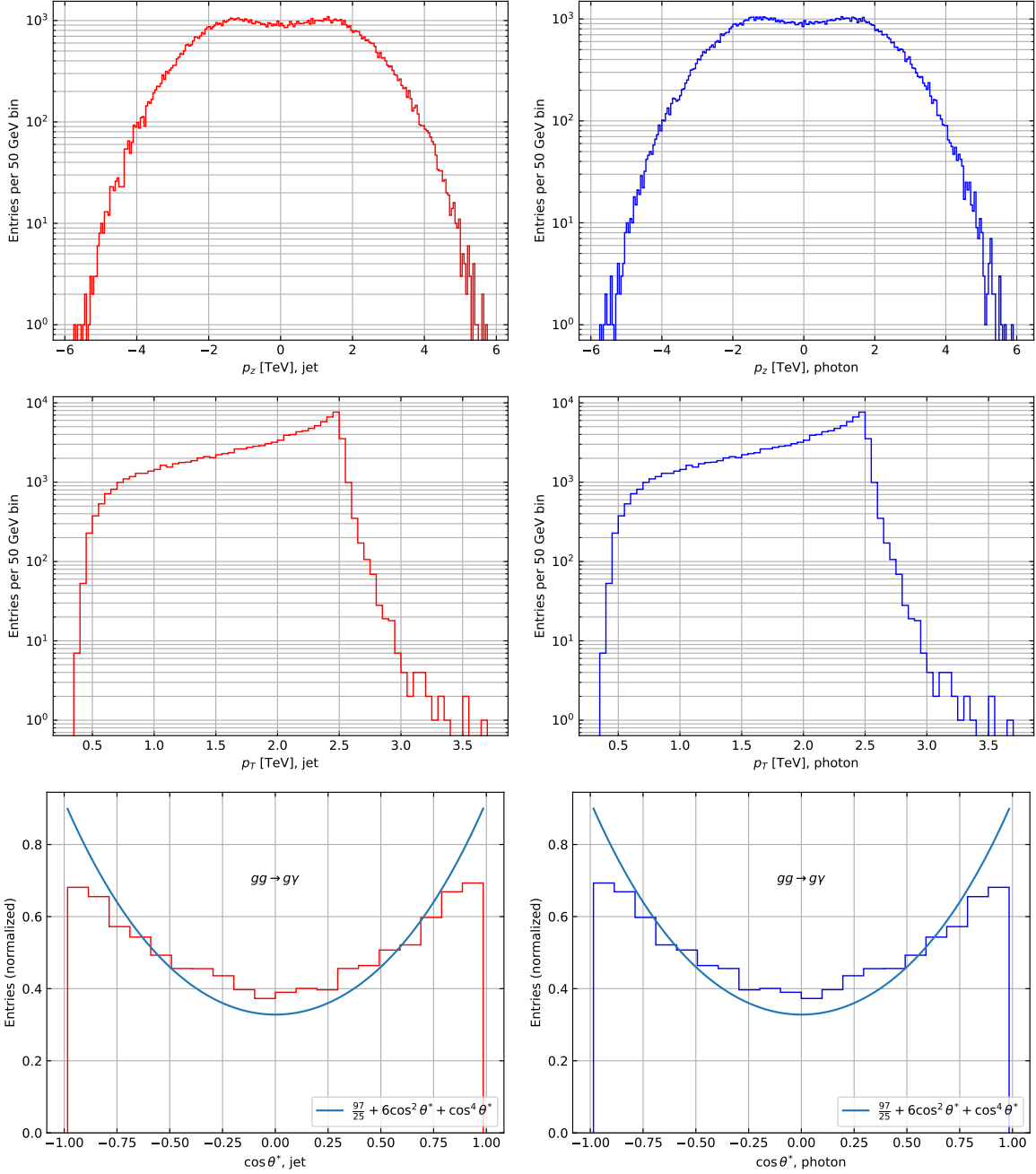


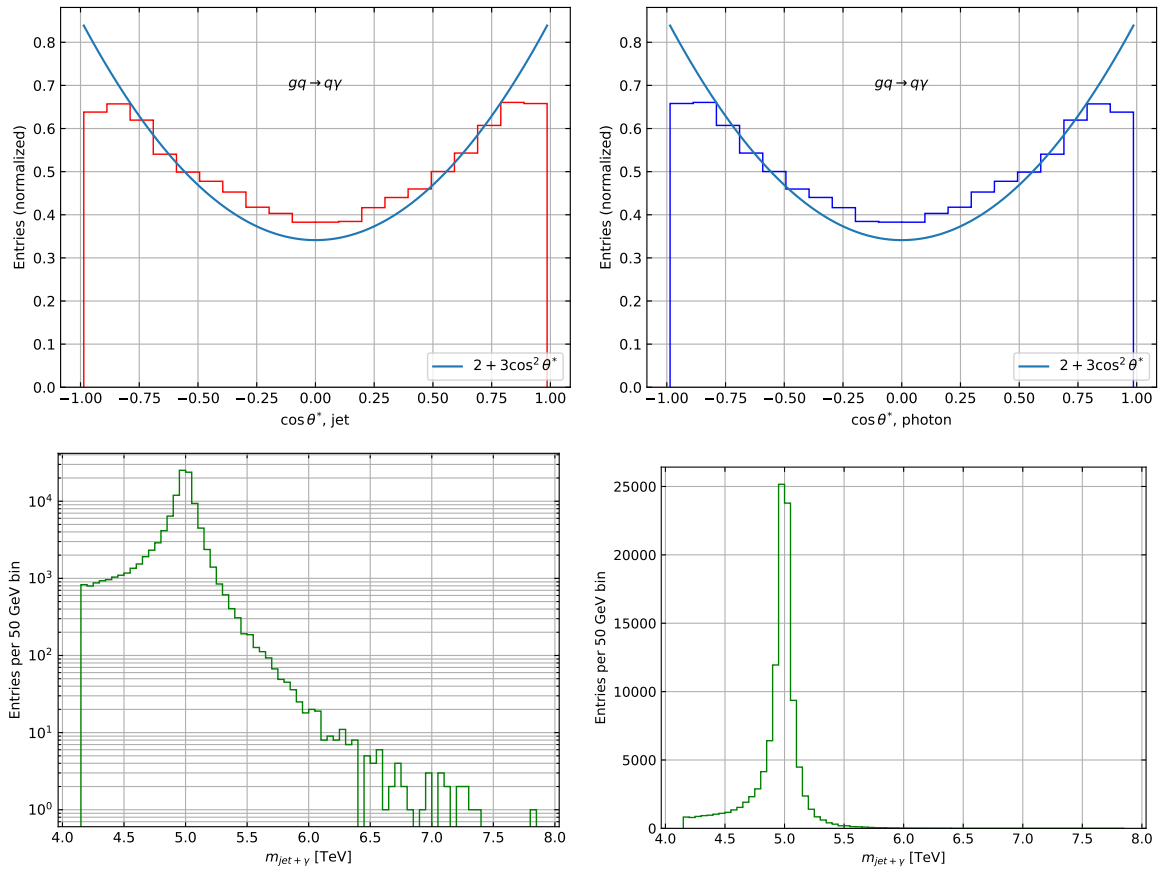




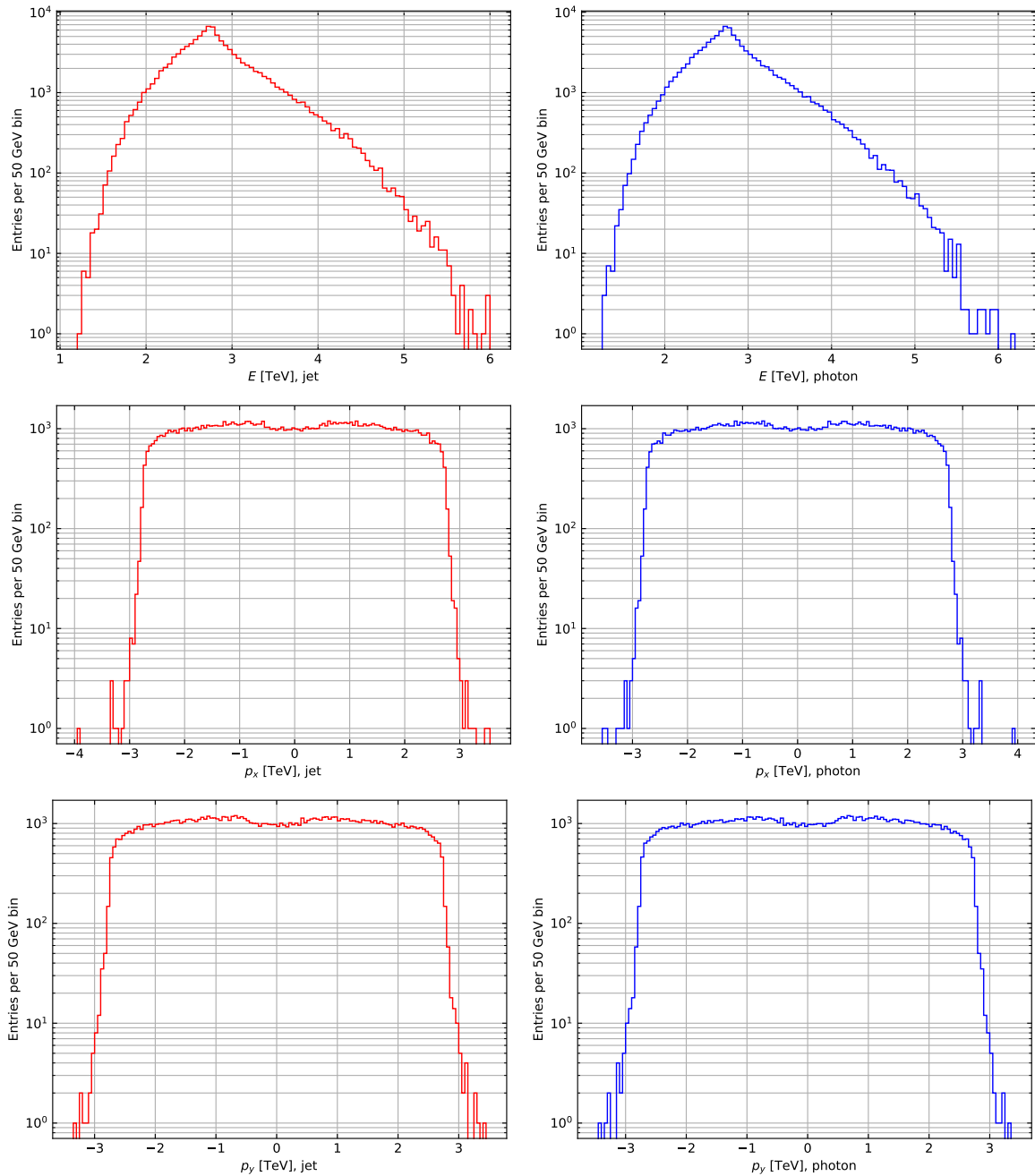
7.3.6 $\sqrt{s} = 13.6$ TeV, $M_s = 5.0$ TeV

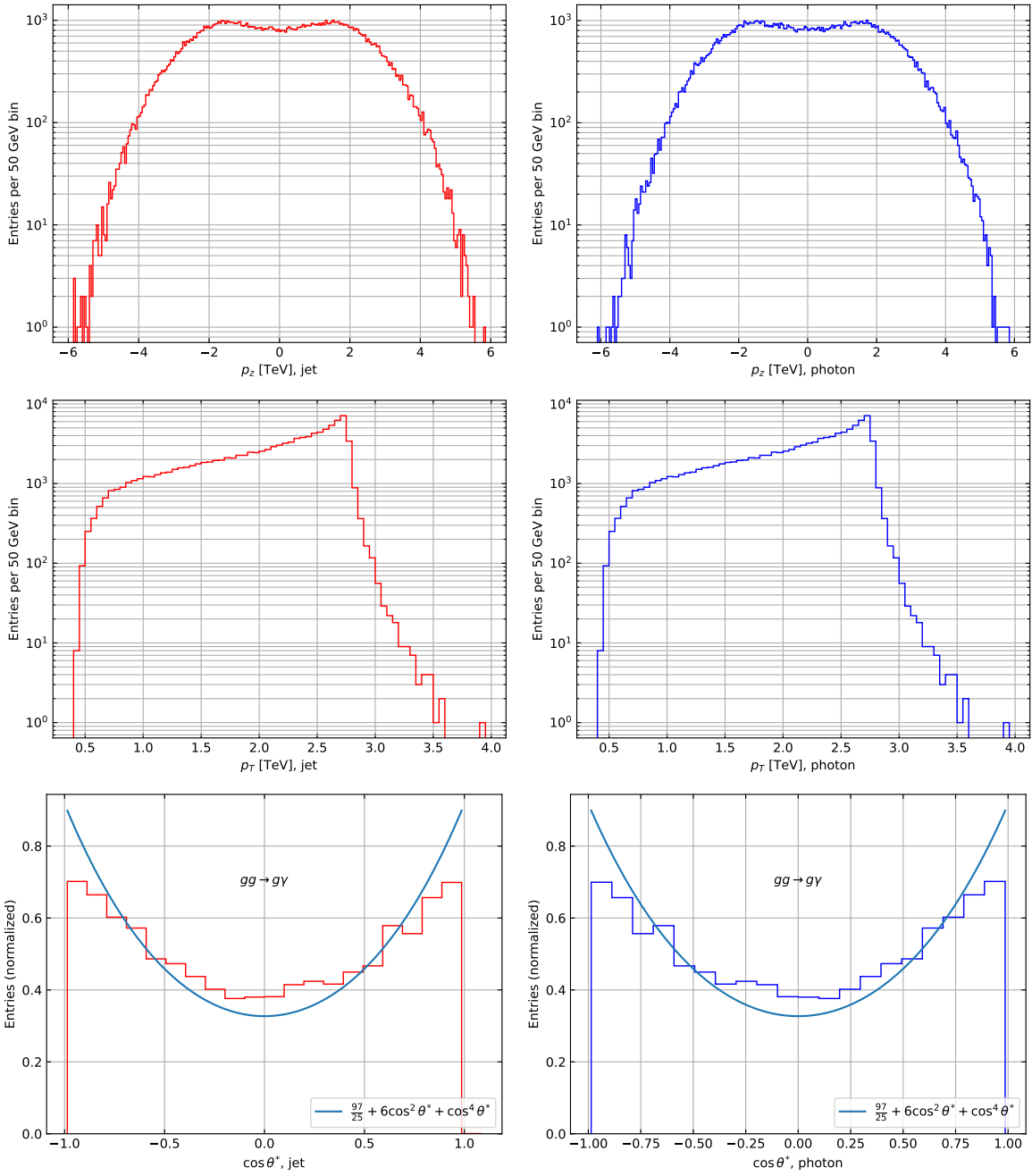


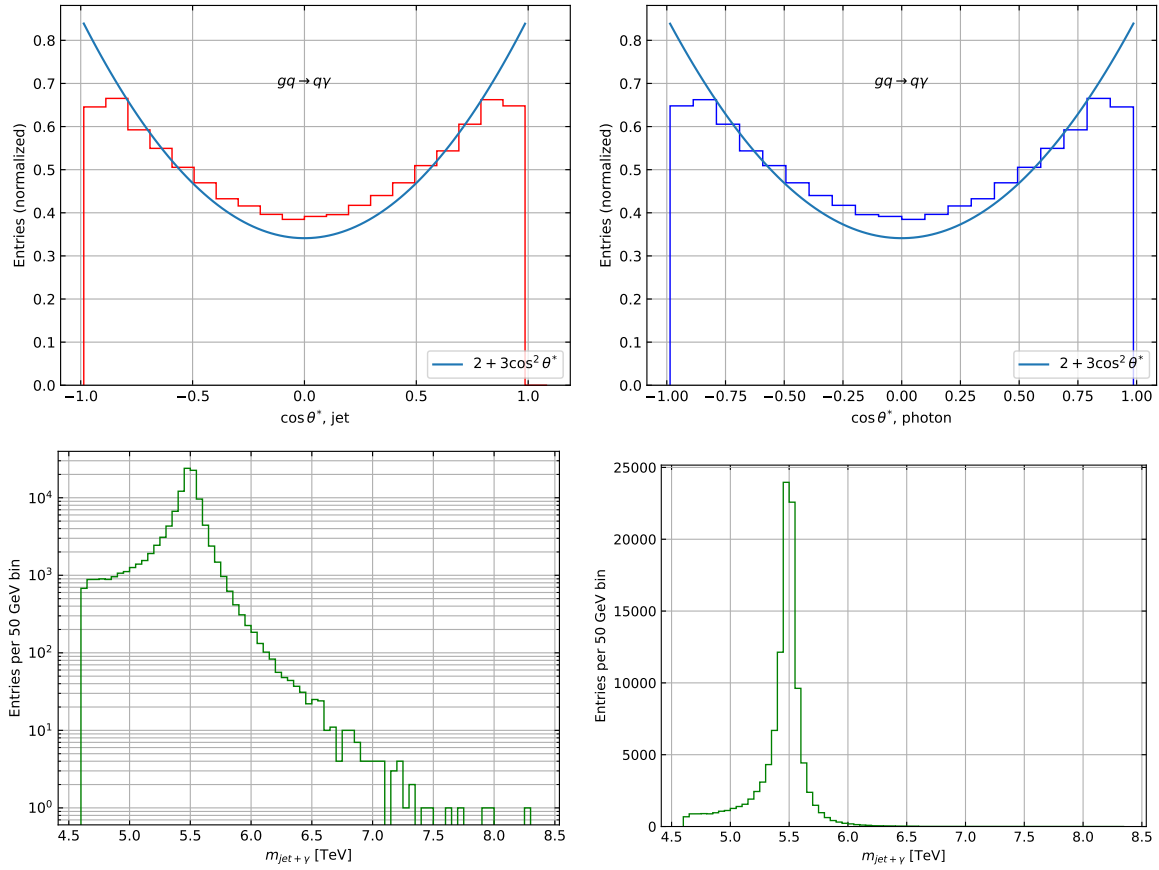




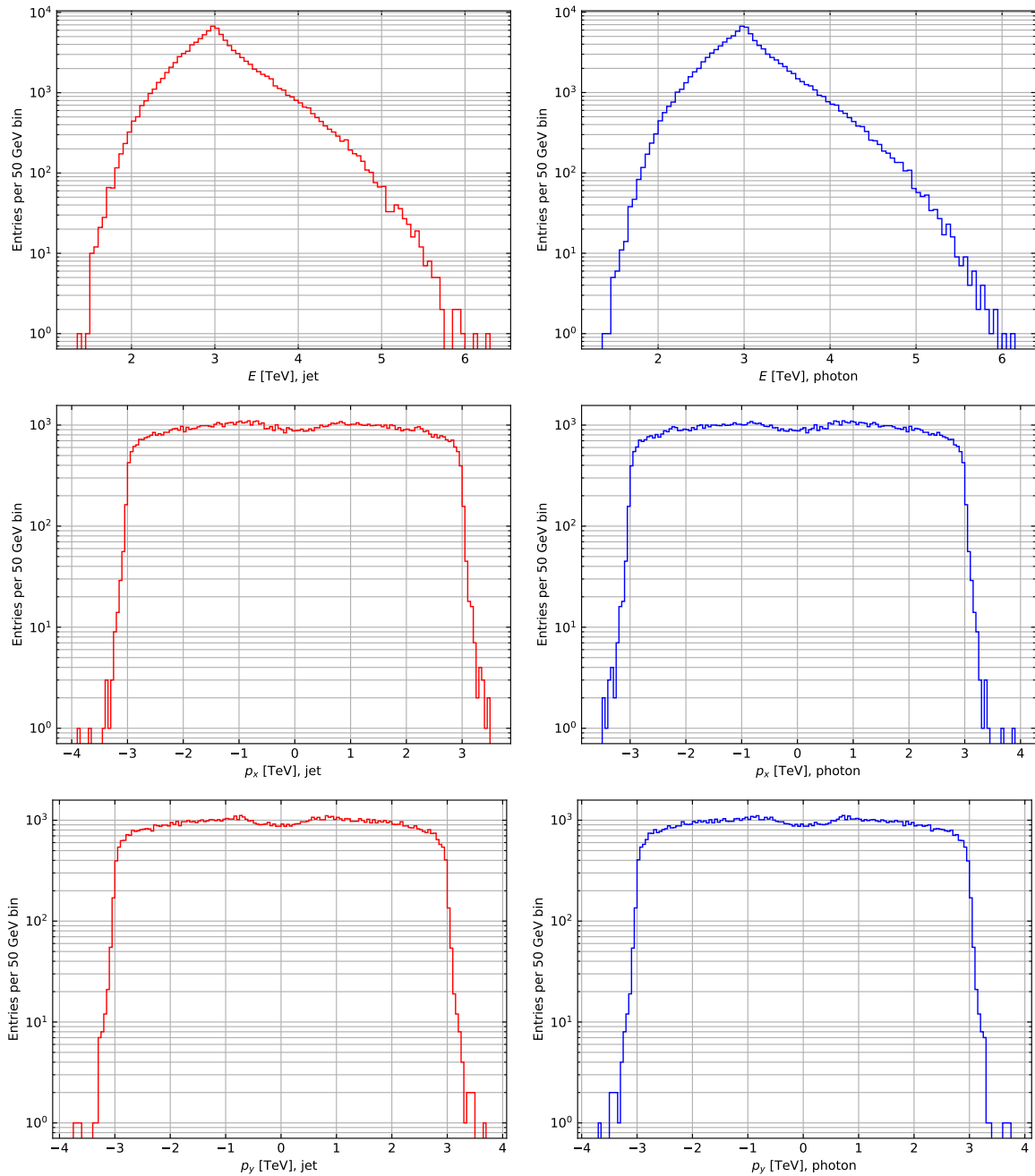
7.3.7 $\sqrt{s} = 13.6$ TeV, $M_s = 5.5$ TeV

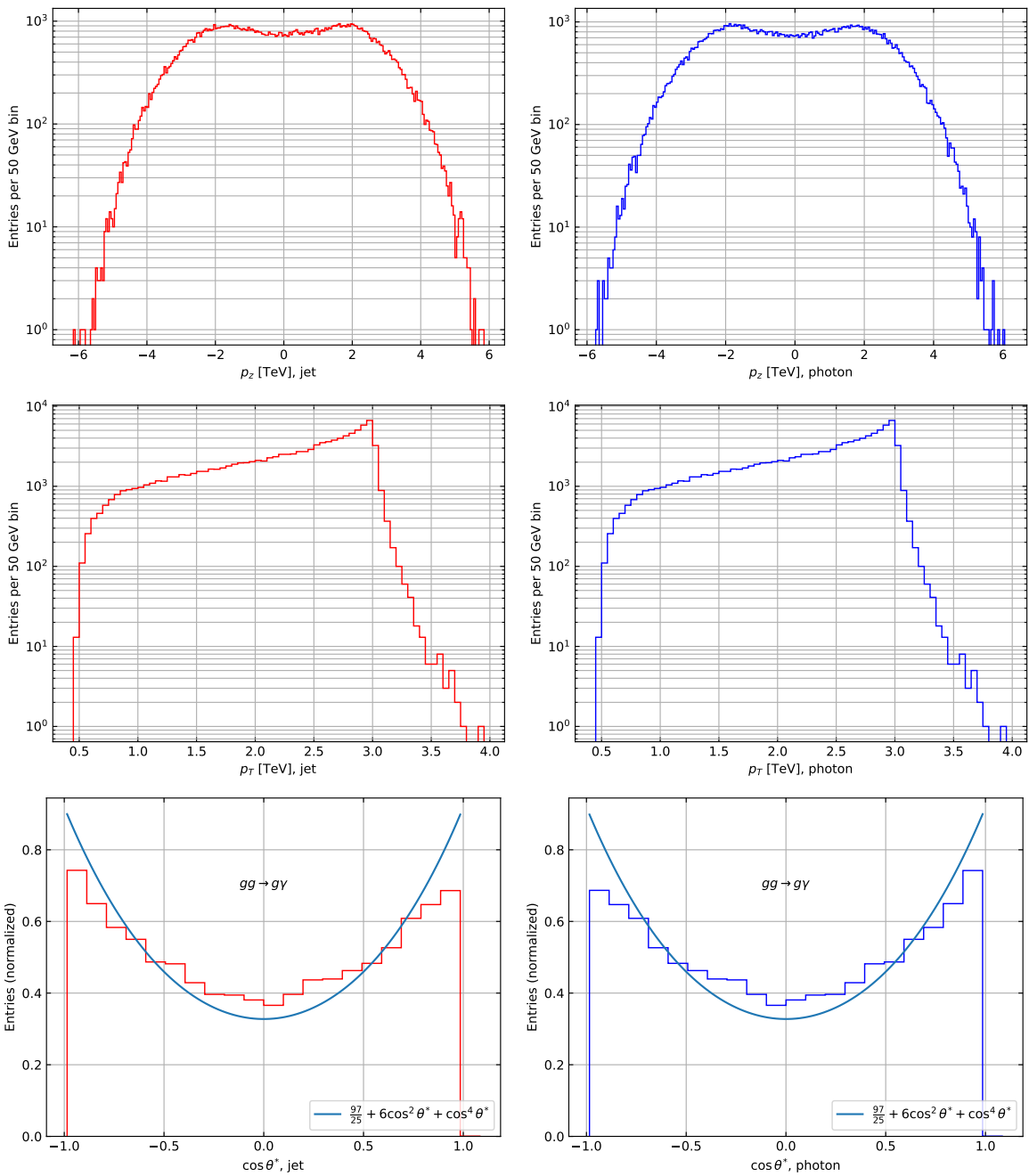


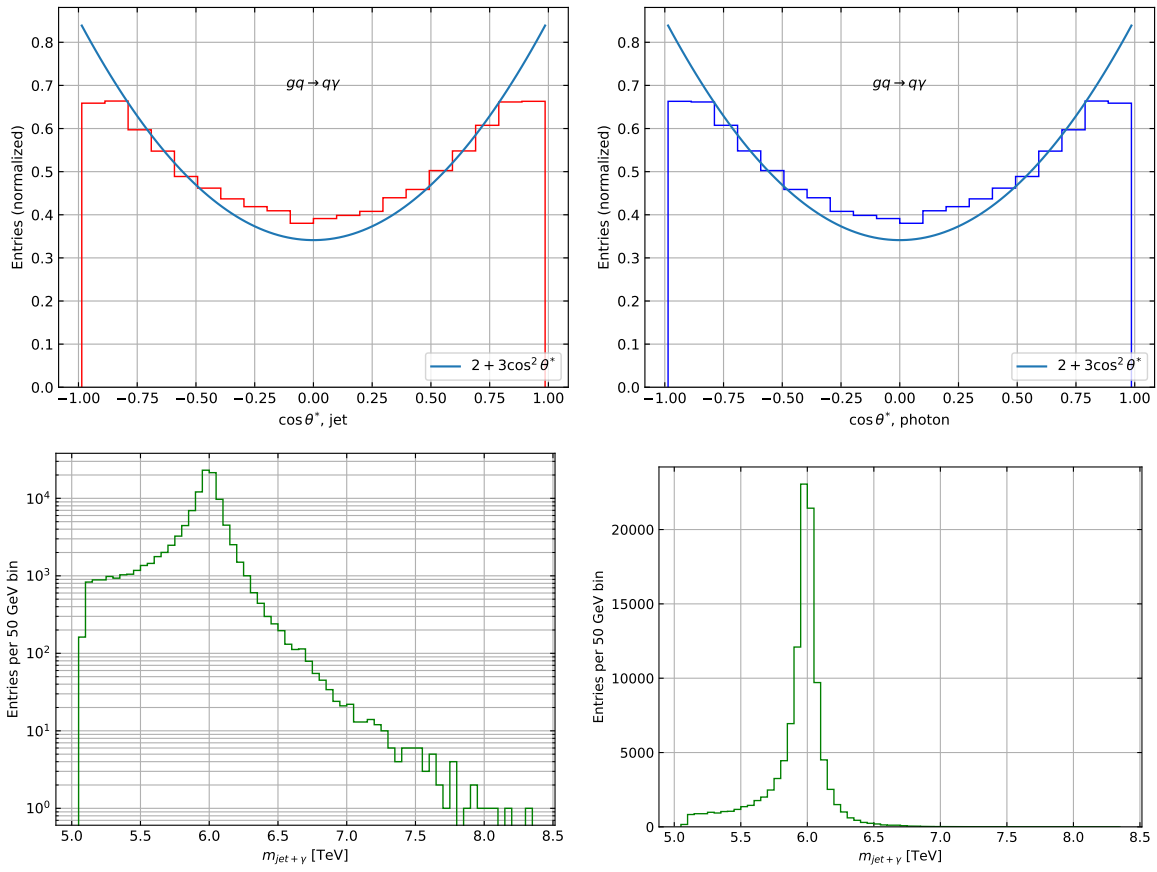




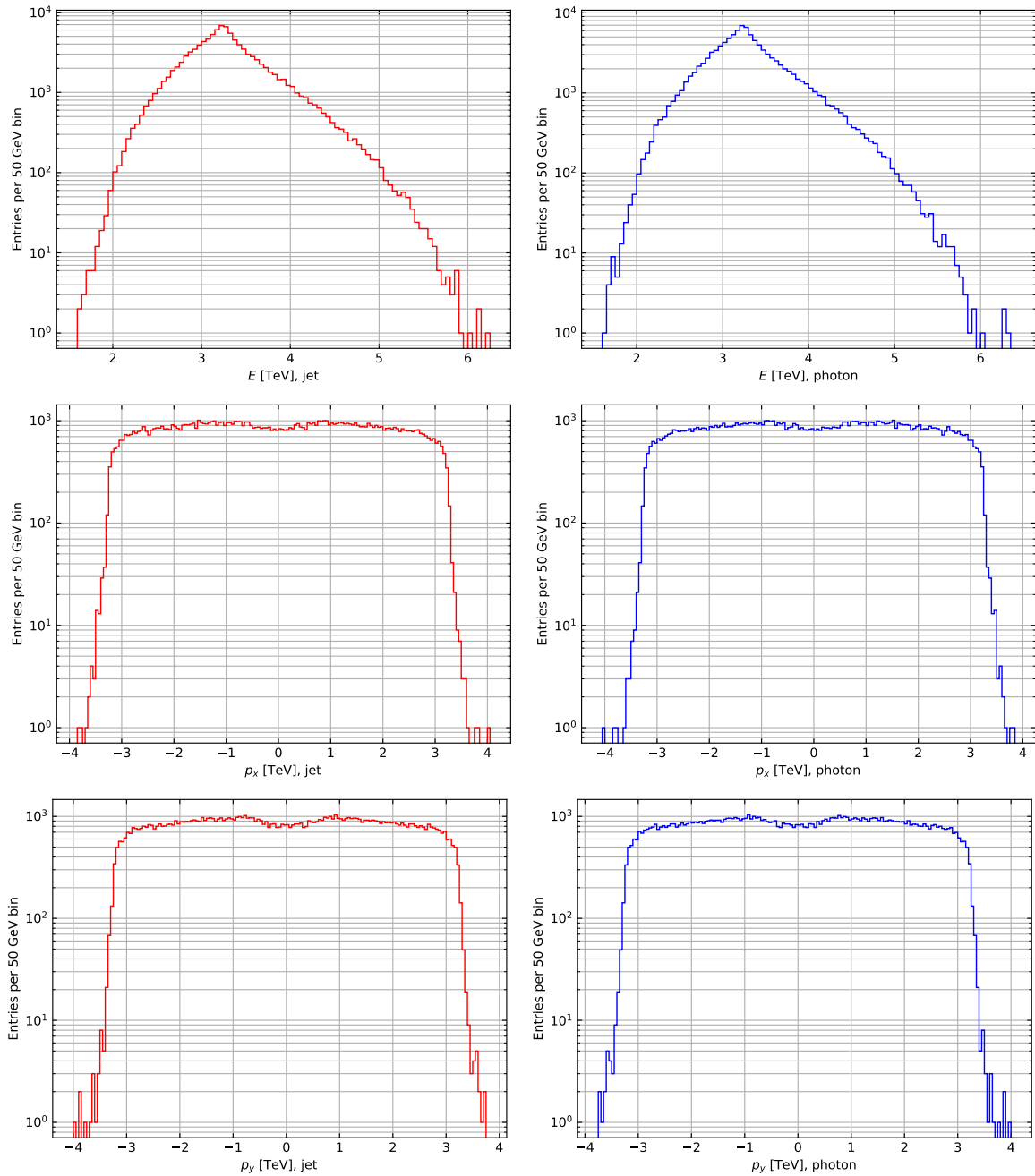
7.3.8 $\sqrt{s} = 13.6$ TeV, $M_s = 6.0$ TeV

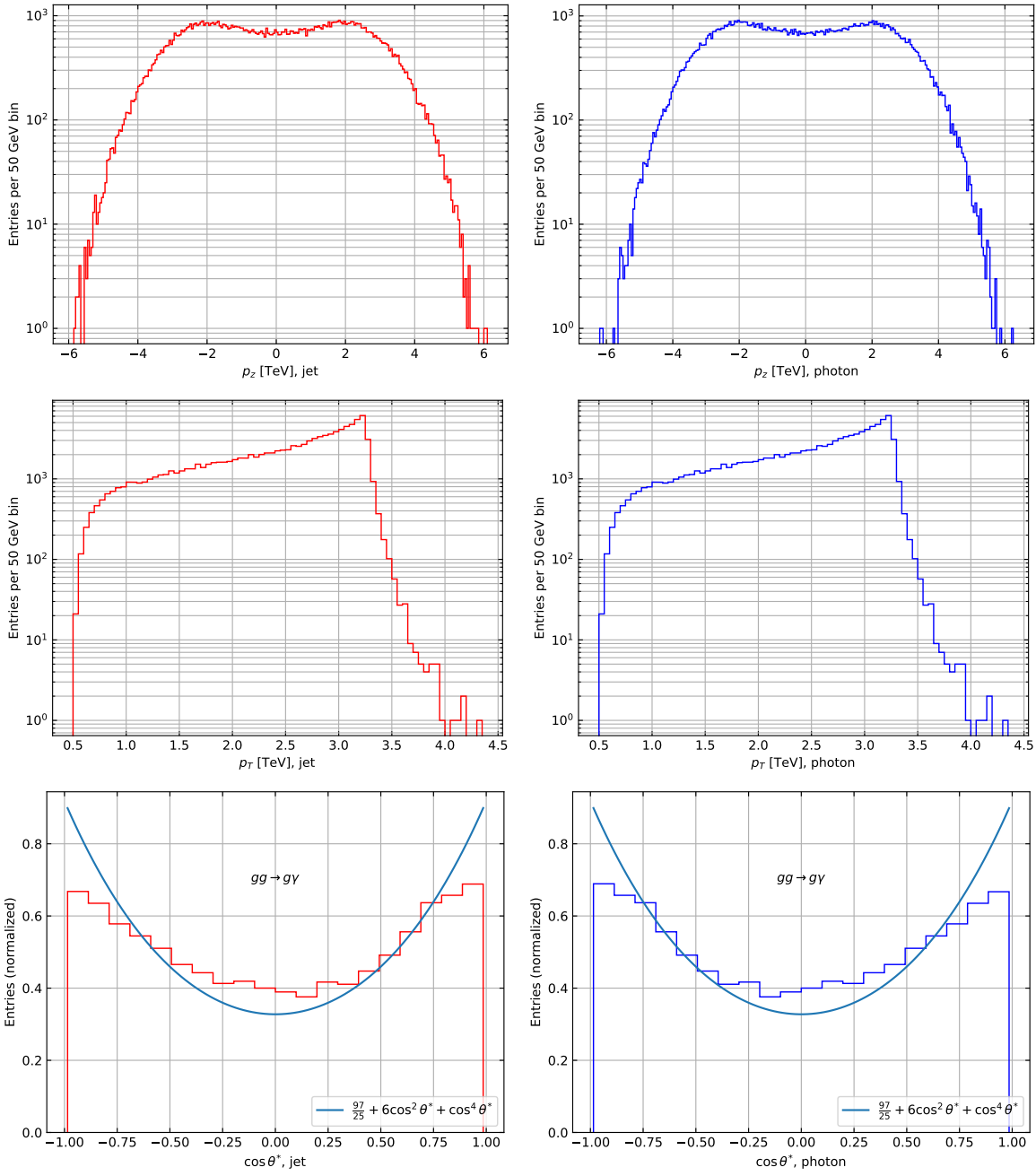


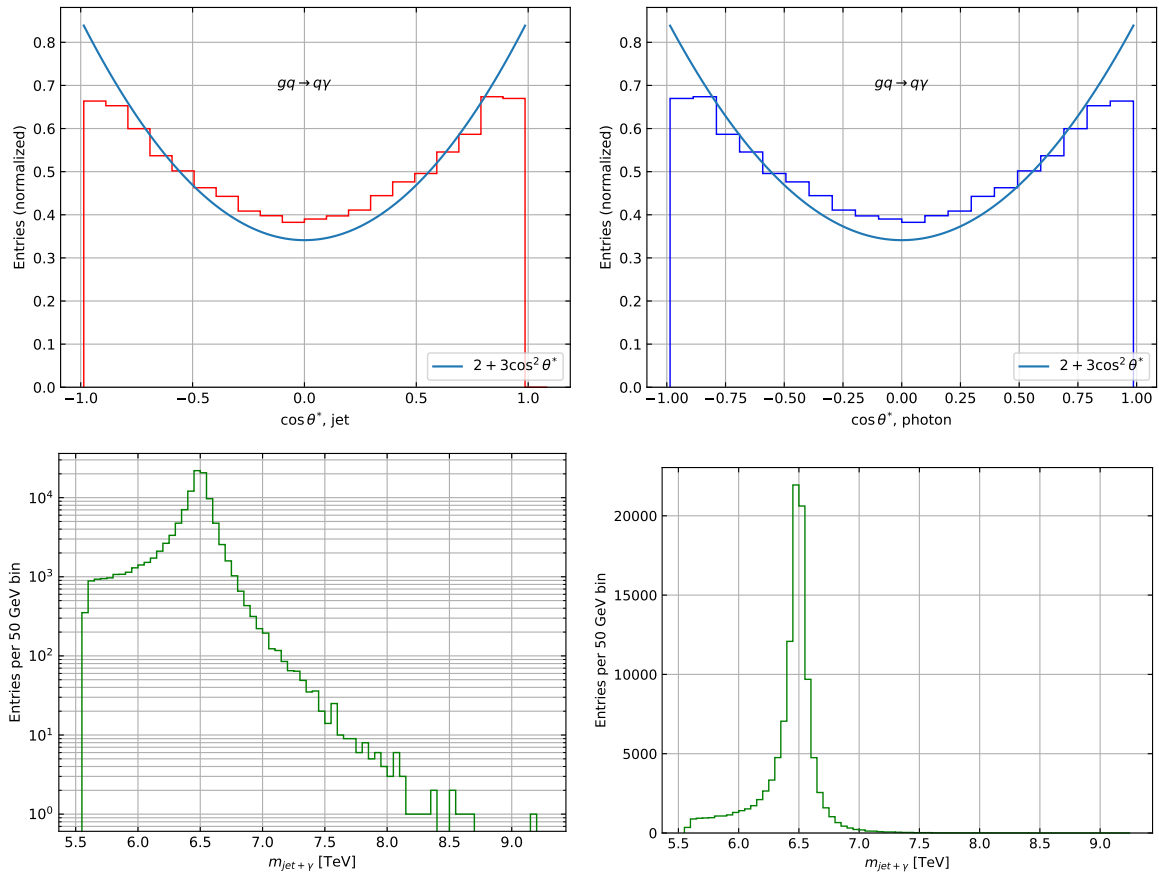




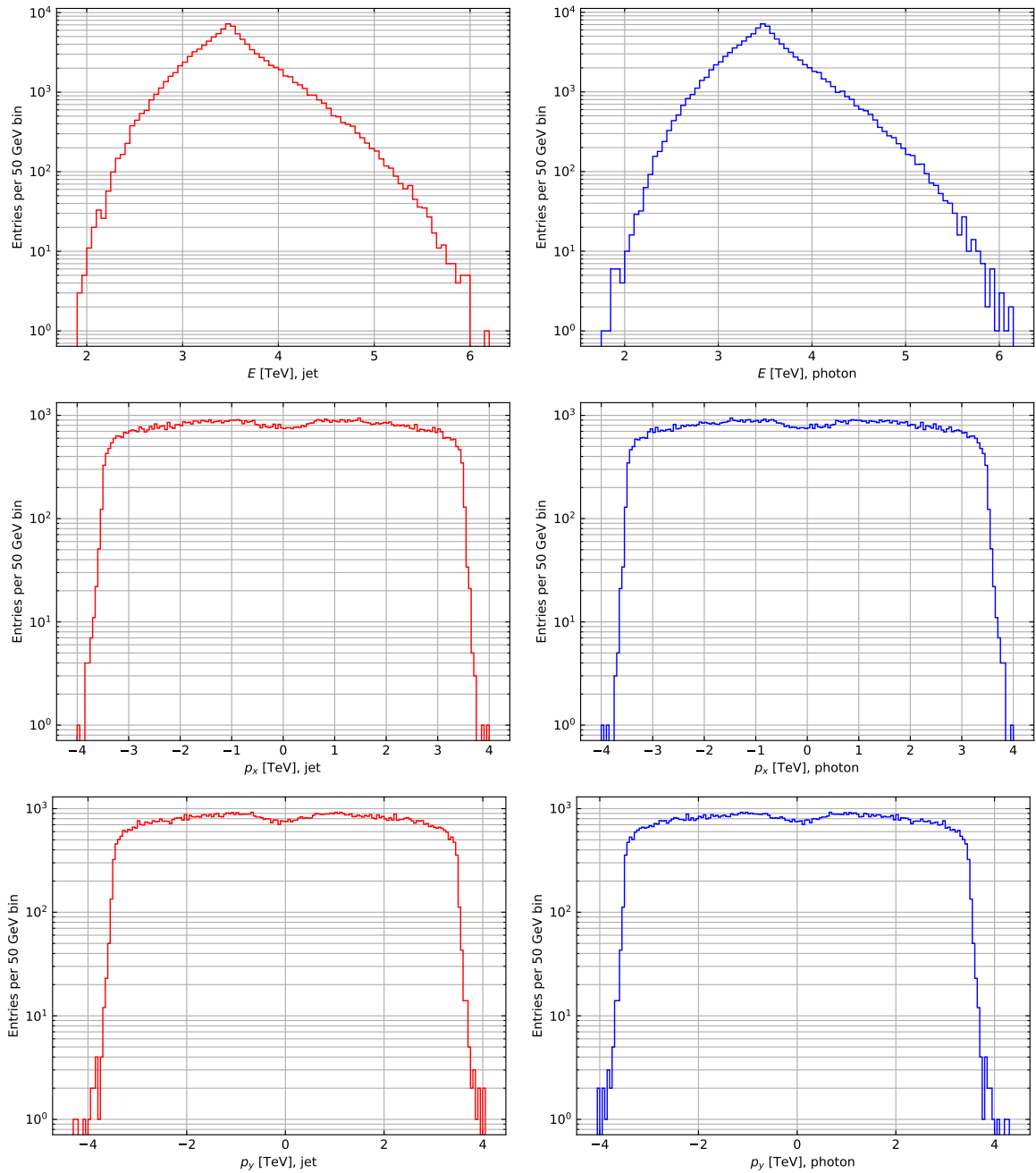
7.3.9 $\sqrt{s} = 13.6$ TeV, $M_s = 6.5$ TeV

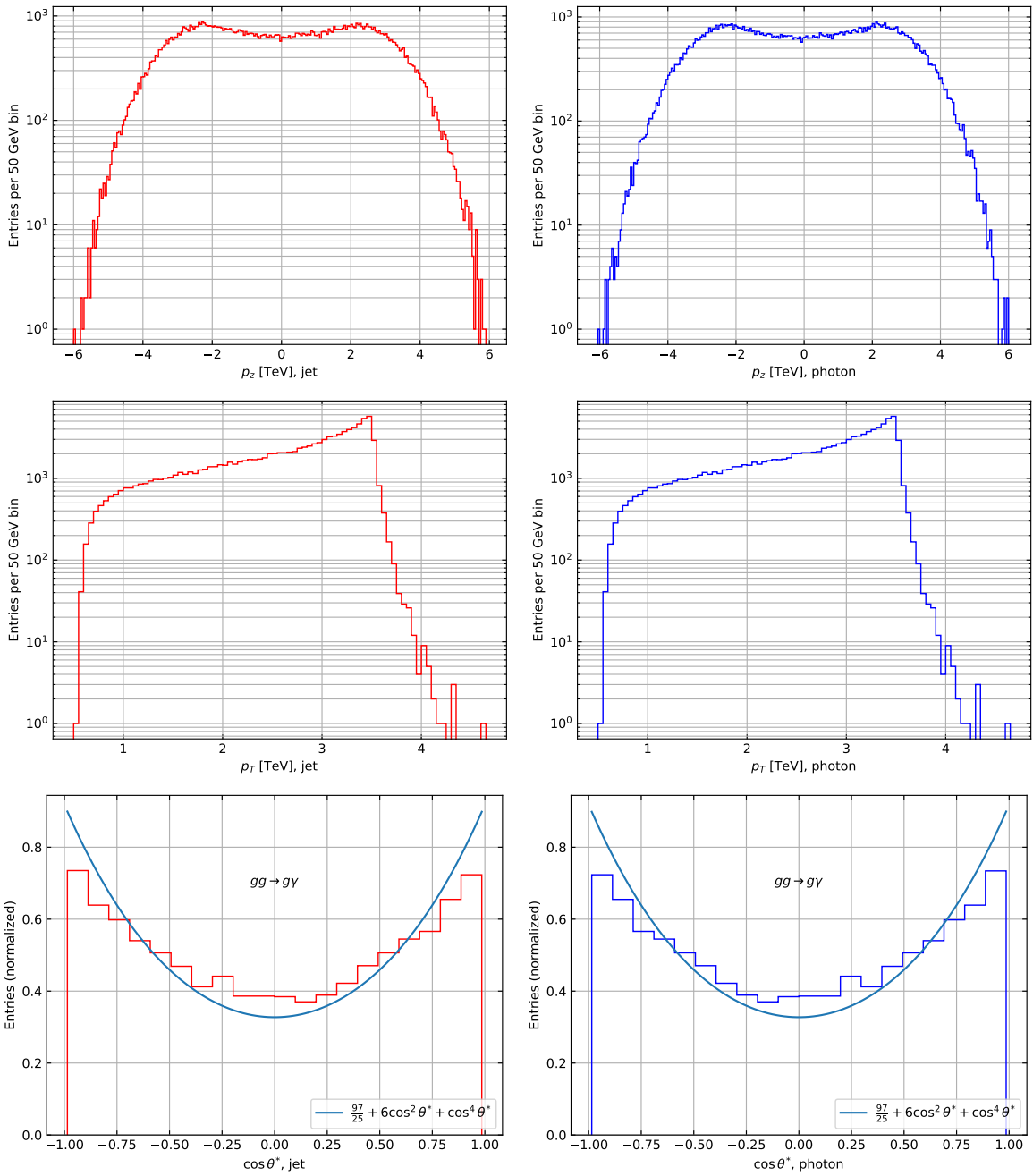


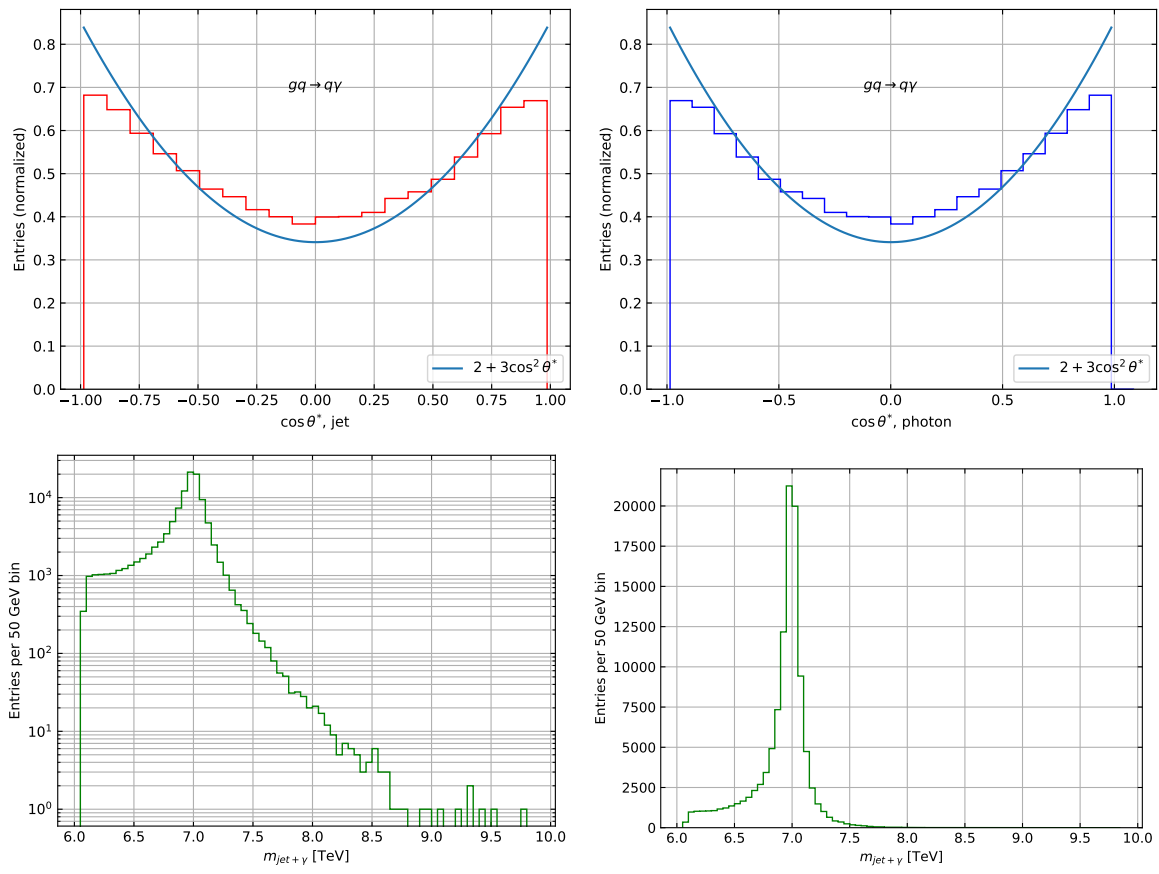




7.3.10 $\sqrt{s} = 13.6$ TeV, $M_s = 7.0$ TeV

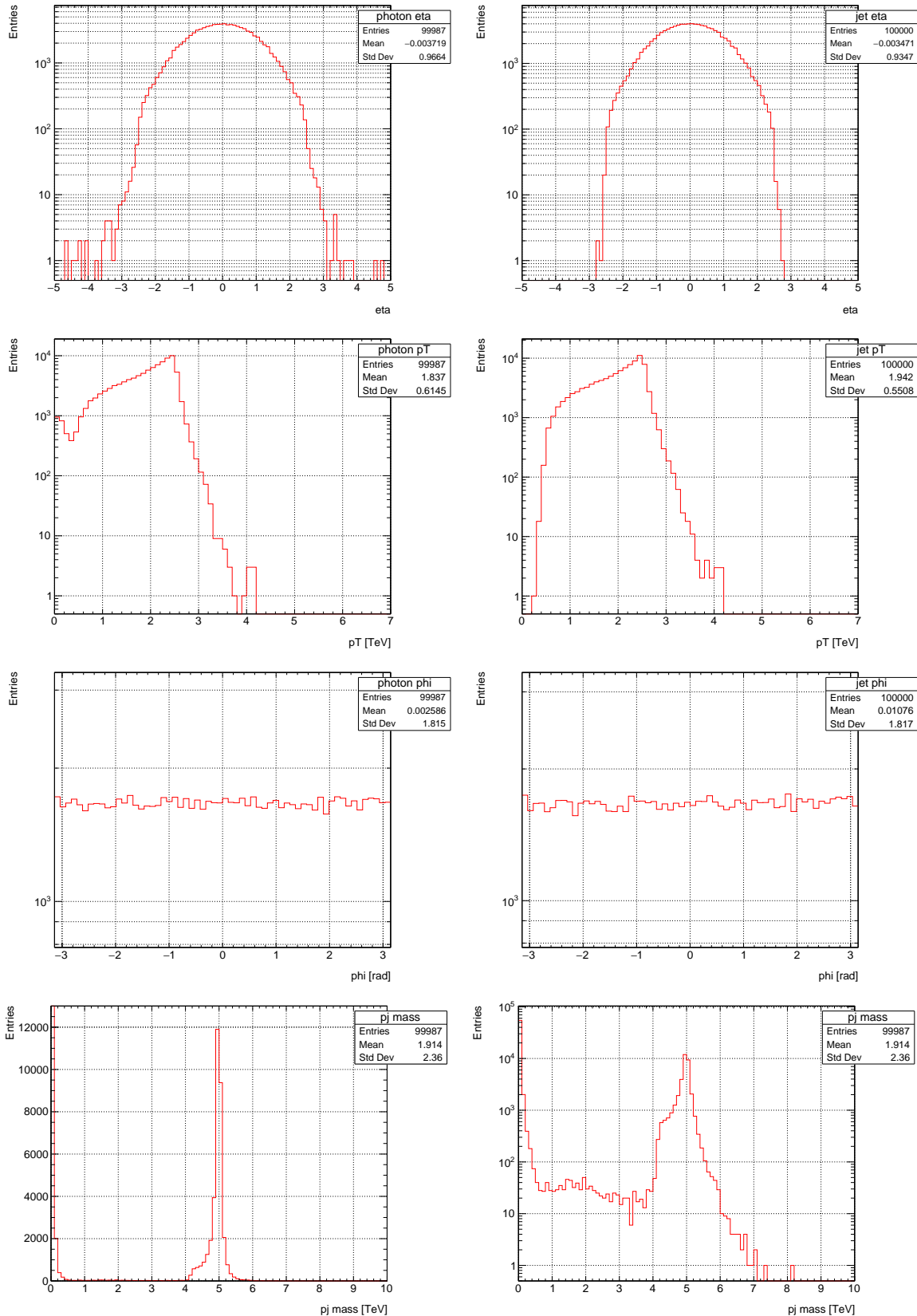




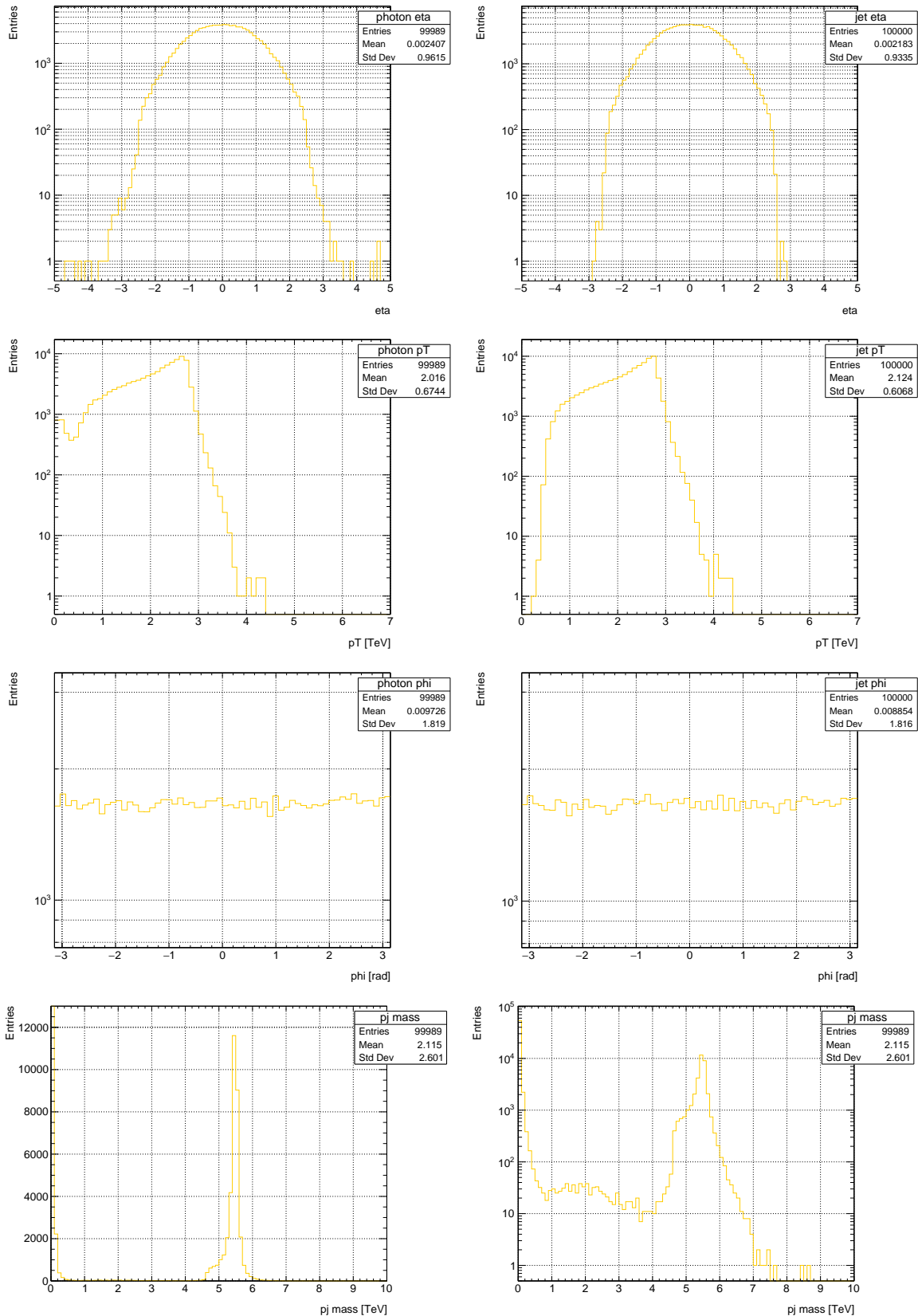


7.4 Pythia Kinematic Data

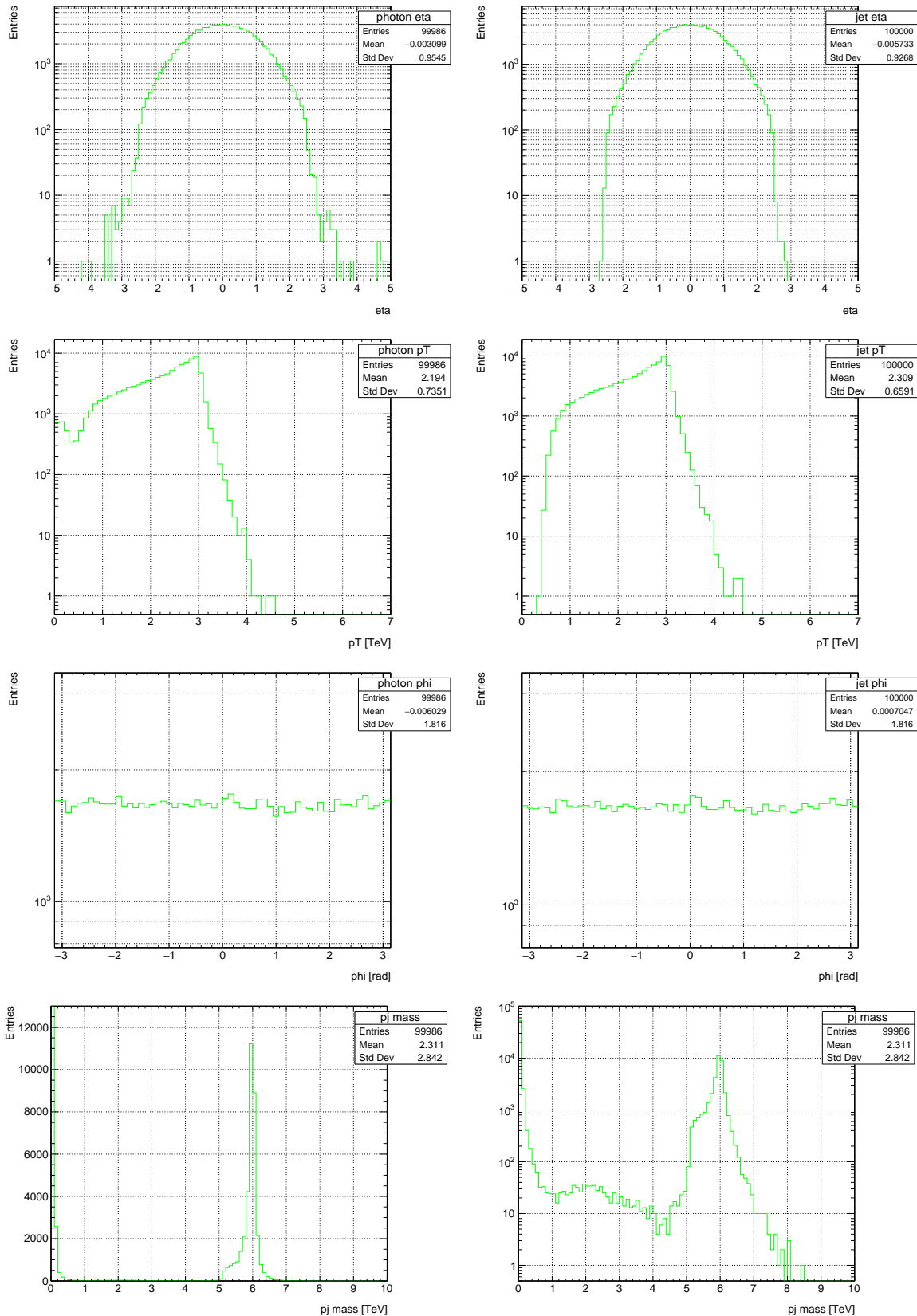
7.4.1 $M_s = 5 \text{ TeV}$, $\sqrt{s} = 13 \text{ TeV}$



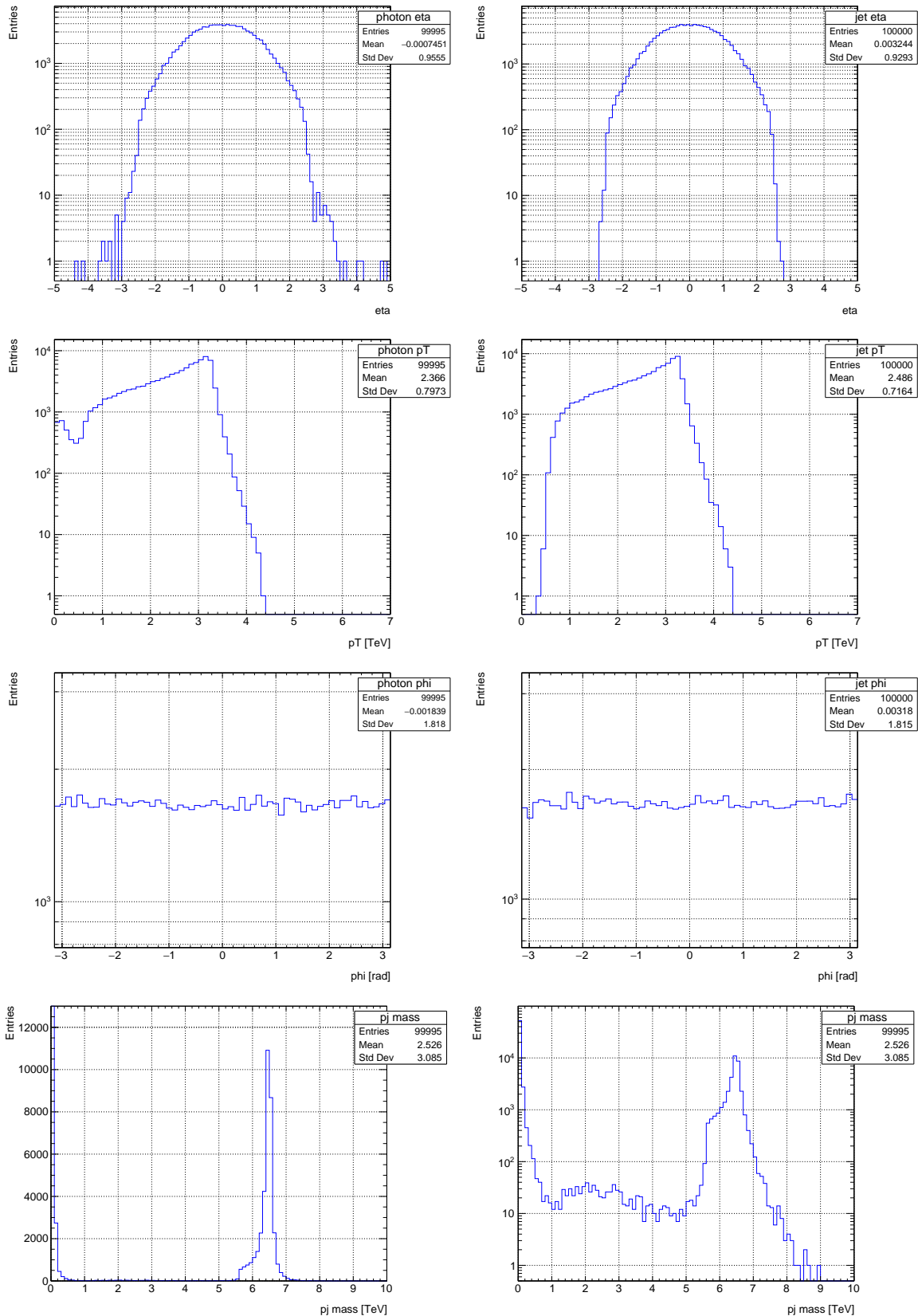
7.4.2 $M_s = 5.5$ TeV, $\sqrt{s} = 13$ TeV



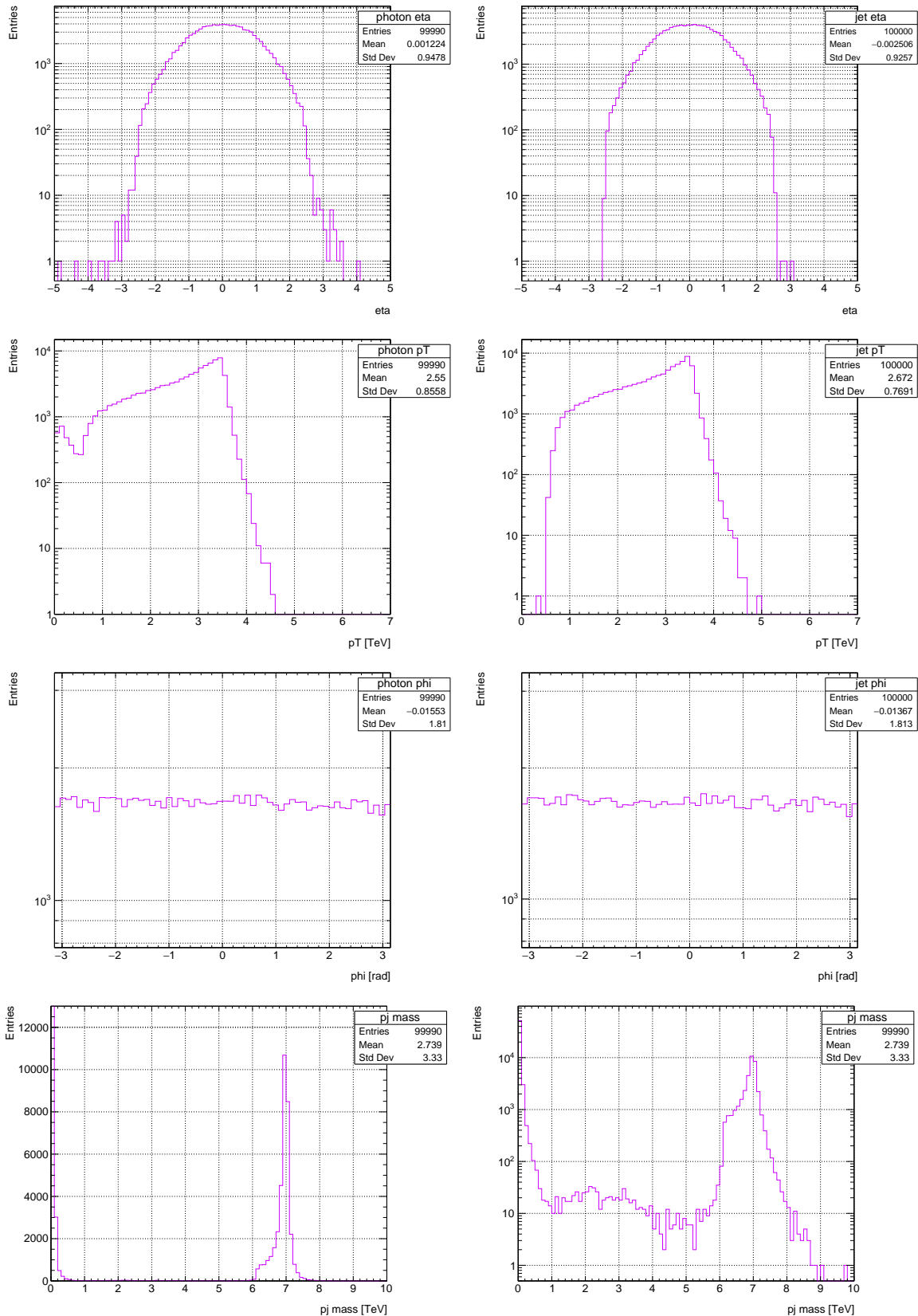
7.4.3 $M_s = 6$ TeV, $\sqrt{s} = 13$ TeV



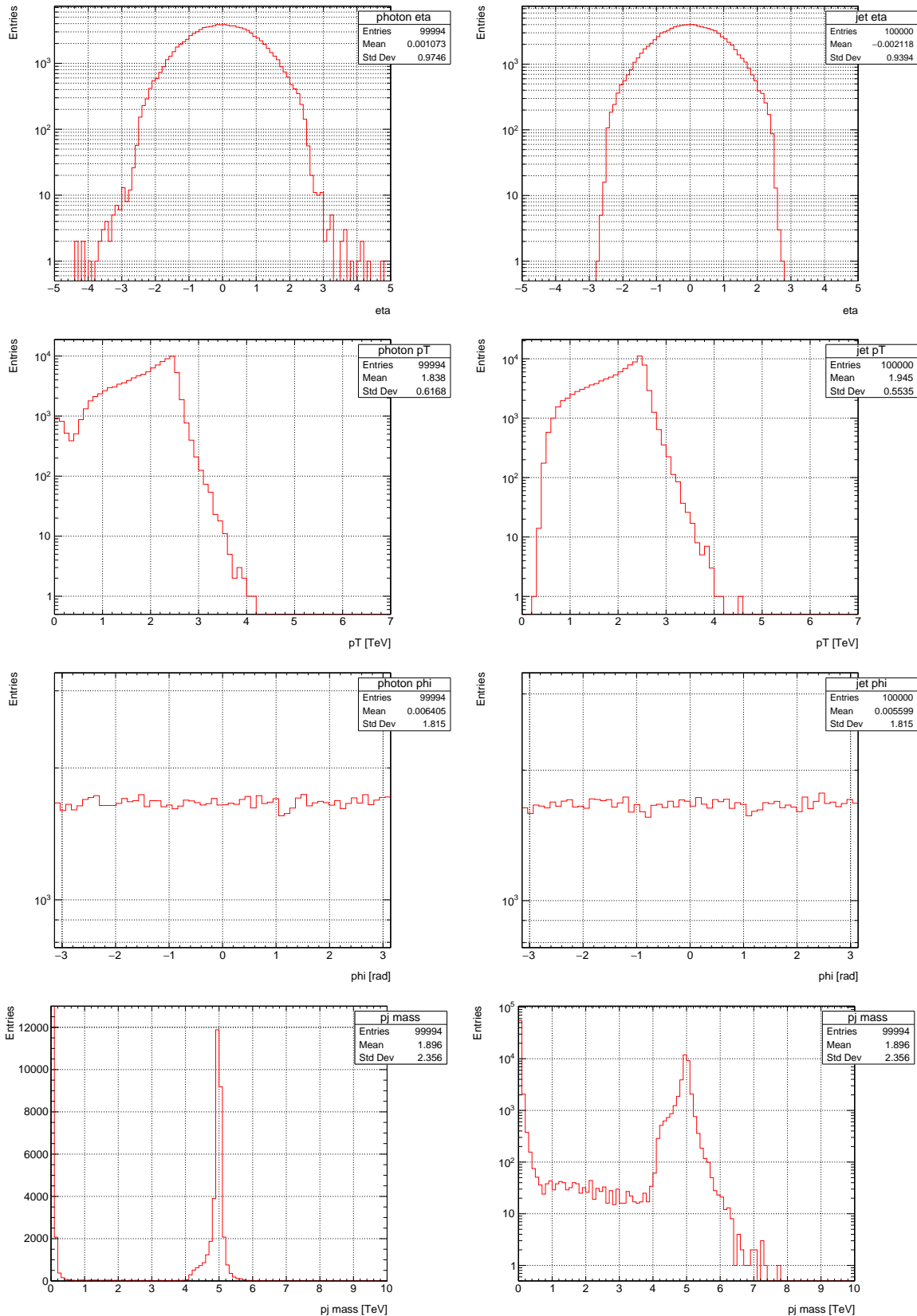
7.4.4 $M_s = 6.5$ TeV, $\sqrt{s} = 13$ TeV



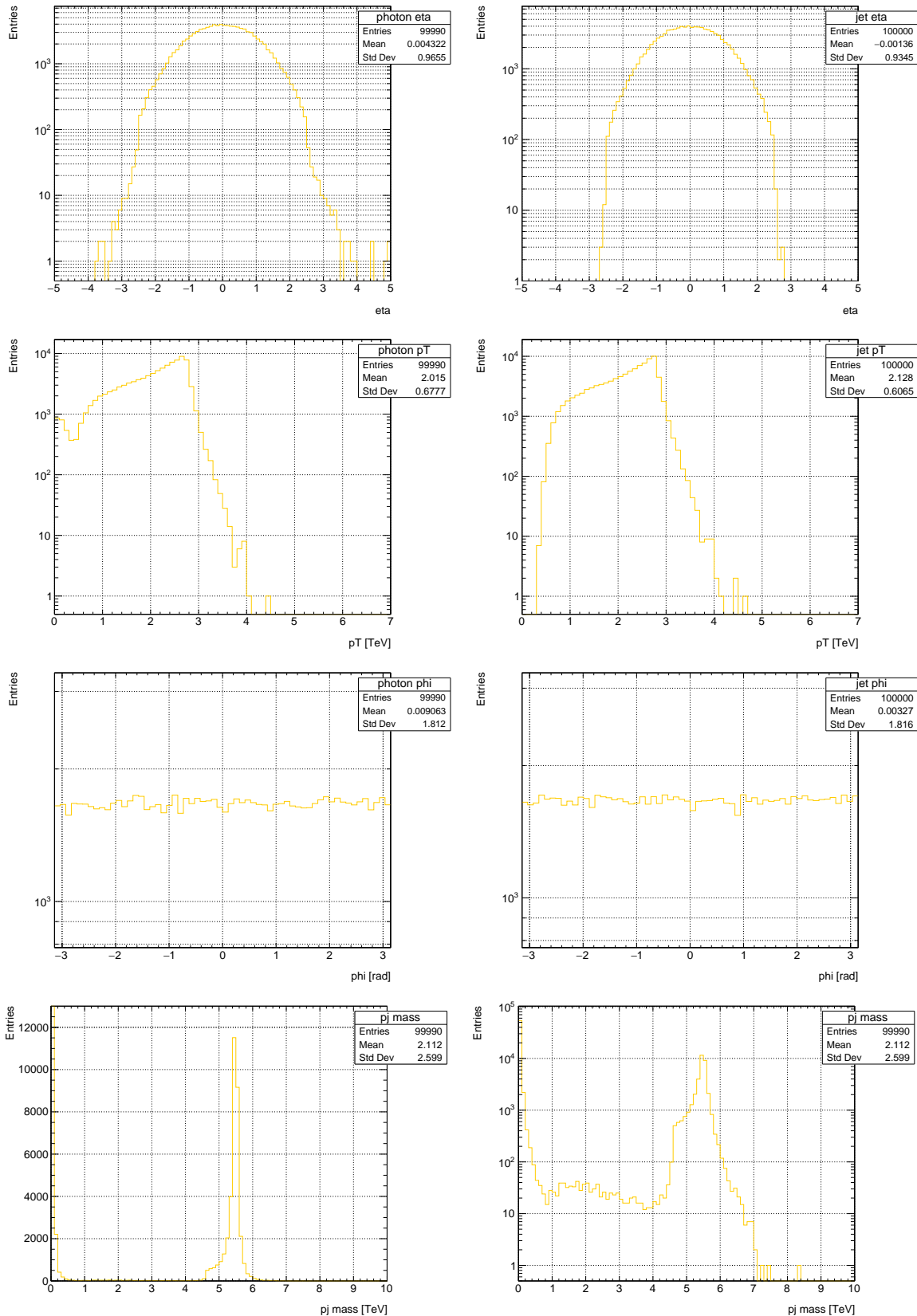
7.4.5 $M_s = 7$ TeV, $\sqrt{s} = 13$ TeV



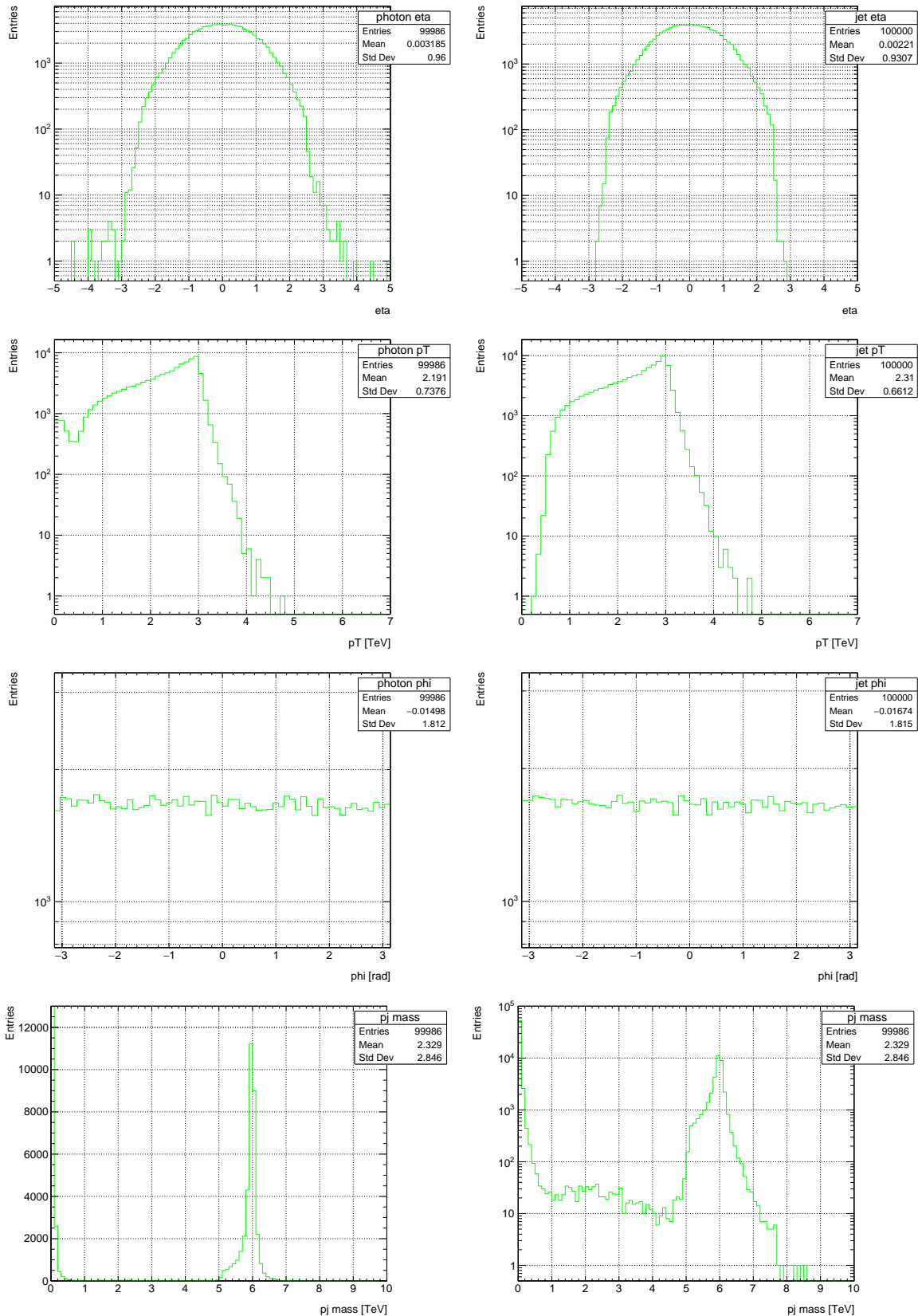
7.4.6 $M_s = 5$ TeV, $\sqrt{s} = 13.6$ TeV



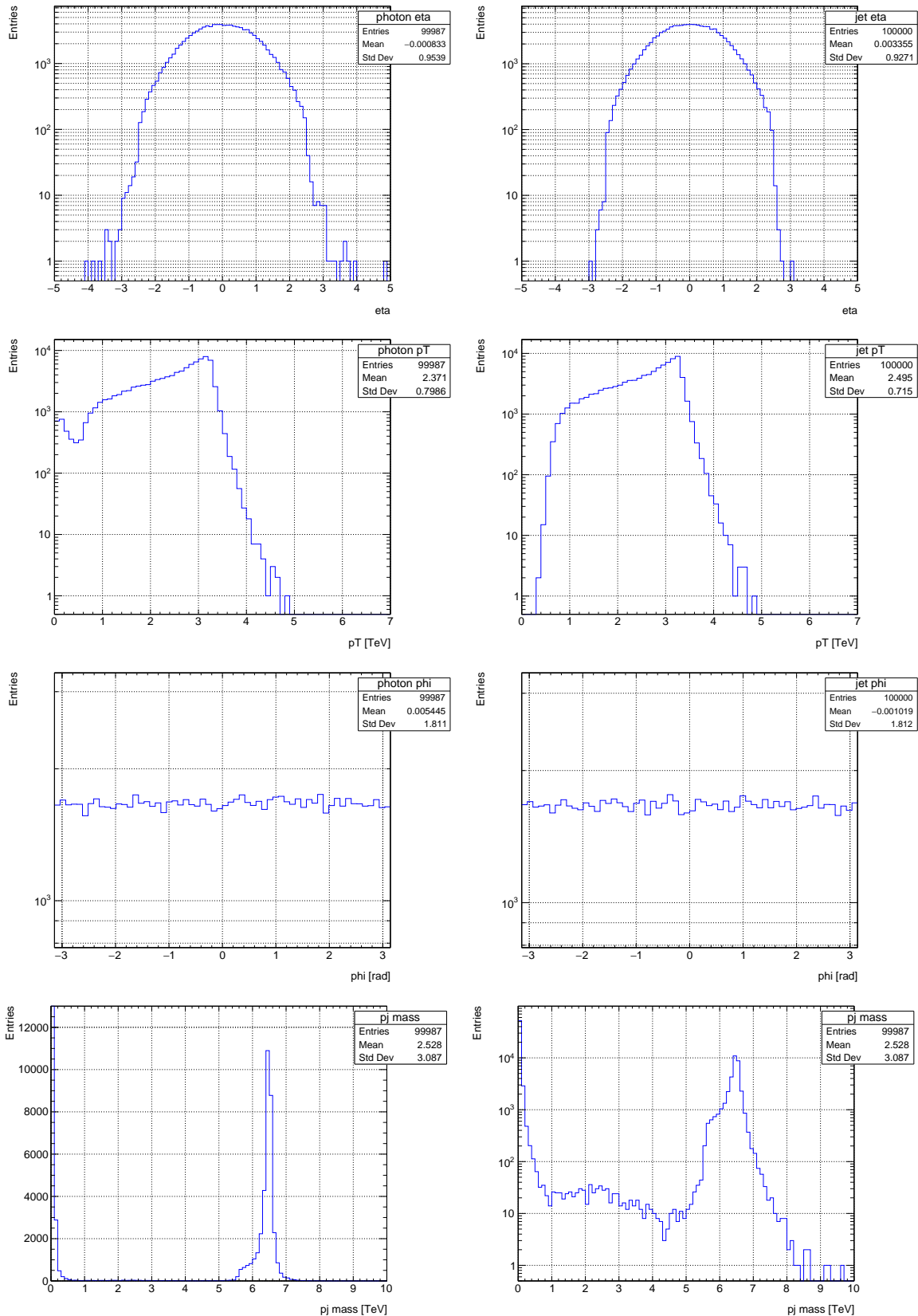
7.4.7 $M_s = 5.5$ TeV, $\sqrt{s} = 13.6$ TeV



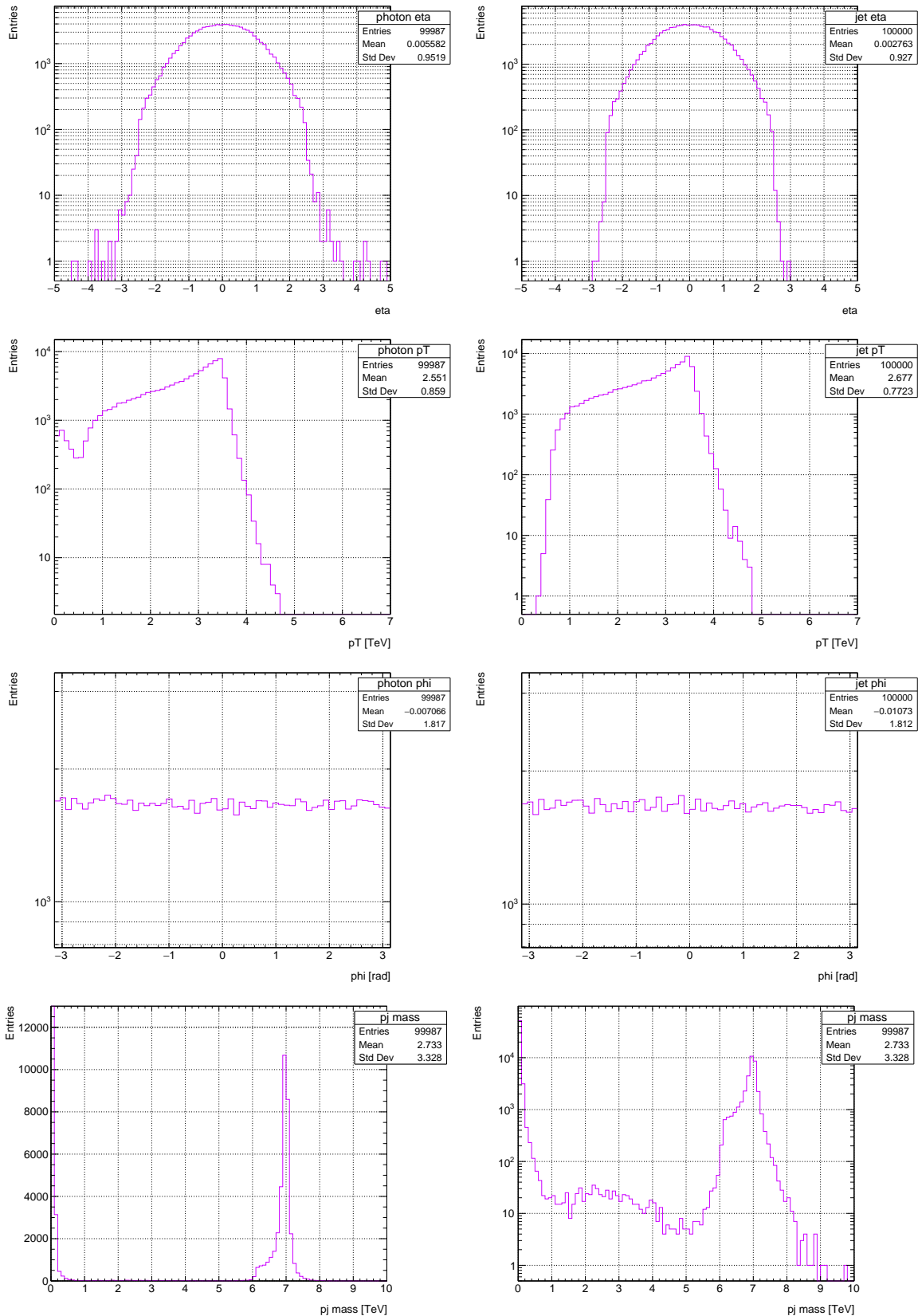
7.4.8 $M_s = 6$ TeV, $\sqrt{s} = 13.6$ TeV



7.4.9 $M_s = 6.5$ TeV, $\sqrt{s} = 13.6$ TeV



7.4.10 $M_s = 7$ TeV, $\sqrt{s} = 13.6$ TeV



7.5 Figures & File Organization on Local Cluster

Name	Size (KB)
..	1
.airb	22
.cache	16
.config	12
.emacs.d	2
__pycache__	16
athena	16
EVNTbackups	20
figures	1
july30	1
STRINGS_simulations	1
testFolder	1
testFolder2	1
testFolder3	1
.asetup	45
.bash_history	44
.cross.txt.swp	1
.data_sort.py.swp	1
.nfs0000000000f67dc00000034	1
.run.sh.swo	1
.run.sh.swp	1
.strings_v3.py.swp	1
.viminfo	1
.Xauthority	1
batch.sh	1
howToUseVi.txt	1
log	1
main.py	14
run.sh	3
setup.sh	1
strings.py	45
stringsold.py	44

`strings.py` and `main.py` are scripts used for the MC generator and `run.sh` and `setup.sh` are the run and setup shell scripts, respectively. `stringsold.py` is the old version of strings with the t -channel bug.

- The main STRINGS LHE files are contained in the `/STRINGS_simulations` directory.
- `/testFolder` contains two LHE files; `150000events.lhe` is the LHE file containing data for the 150,000-event run from section 6.2.1; `y10.lhe` is the LHE file for the 11,000 event running using $y_{cut} = 10$.
- `/testFolder2` contains the 10 LHE files used in the $y_{cut} = 6$ runs
- `/athena` is where Pythia simulations are stored, along with the associated root files and programs.

All figures *used* and *cited* that were *created* in this report can be found on the local cluster in `hepusers2/kmdrury/figures/`. In this directory, there are subdirectories named after the section whose figures they contain. Files are named after their figure number in this report, or the data they show. Note that for Appendix 7.3, there are many kinematic histograms for each string scale that were not included in this report but can be found on the local cluster.